



Politecnico  
di Torino



Master degree course in Nanotechnologies for ICTs

Master Degree Thesis

# Development and testing of an organ-on-a-chip system for brain organoid studies

## **Supervisors**

Senior Researcher Maria Dimaki  
Prof. Winnie Edith Svendsen  
Prof. Kristine Freude  
Prof. Carlo Ricciardi

## **Candidates**

Eleonora QUASSO

ANNO ACCADEMICO 2023-2024

This work is subject to the Creative Commons Licence

# Acknowledgements

My thanks go to DTU for hosting me for this academic year, making me meet new friends and giving me the means to explore my interests and deepen my knowledge in the field that I have found to be my passion. Especially, thank you to my supervisor Maria Dimaki for her continuous support and the kindness she has shown towards me in the time of need, both in personal relations and academic ones. I owe a lot of the success of this endeavor to her gentle and encouraging disposition in my regards. I am also grateful to the rest of the NaBIS group for always making me feel like part of the team and for teaching me a lot of new skills. Also I am grateful for the KU group that gave me the opportunity to try our devices on real organoids, despite everything.

I appreciate my italian supervisor Carlo Ricciardi for always answering any of my doubts and being very available throughout the whole duration of my year abroad.

I would like to thank Torino as the city that changed my life and made me the woman I am today. I am extremely grateful to my boyfriend and the friends I met there, that continue to be a strong foundation that always makes me miss the past years and this town.

Finally many thanks to my family and friends from Genova for supporting my journey and always lending a hand, or a call, whenever I needed it. With you in my life I never feel alone, anywhere I am in the world, even if I miss you every day.

## Abstract

Organ-on-a-chip systems are the new frontier of medicine and biotechnology, leading the research to an easier understanding of disorders' pathogenesis and a safer drug testing, which would eliminate the need for animal testing and allow for patient-specific prescriptions and unequivocal prognoses. Brain organoids are some of the most interesting organ-on-a-chip systems and they are currently grown starting from human pluripotent stem cells through a self-assembling process, carefully guided to get homogeneous results. The current state of the art for the culturing devices consists mostly of either simple culture chambers with a rocker system that simulates the brain environment or air/interface systems with a partial separation between the medium and the organoid, which is itself in contact with the air. The main difficulty with the latest designs is still a lack of vascularization established inside of the organoid, which in live brains is the main source of nutrients and oxygen, which then leads to apoptosis due to necrotic cores and hypoxia. Finding a way to circumvent this issue is the main objective of our thesis, one that we will make sure of addressing thoroughly and with different design ideas. The thesis work will begin with a series of COMSOL Multiphysics® simulations, starting from the analysis of a design close to the ones found in literature and then introducing the novelty of a flow inside of the nutrient reservoirs with the hope of automating the nutrients delivery. It will demonstrate that this solution completely outperforms the existing designs and that the introduction of flow of the perfusable nutrients medium stabilises their average concentration in the tissue in the span of one to a few days. This guarantees longer organoid survival and less human interaction with the device itself, leading to less chance of contamination and disruption of the operation. To test these simulations we will show how we attempted to fabricate a device for an experiment with real organoids, using laser ablation to carve the bottom channel and 3D printing to build the top chamber. After finding the correct settings for both steps we will perform some preliminary tests with some dyed Milli-Q water to get ready for the official experimental test that will take place at KU. Once these have been done, the real test with live organoids was set up with a syringe pump and an incubator and was to last two weeks, but, as it will be revealed, it was stopped after merely 2 days. The cause will be studied and searched for and it will finally be exposed to be a defect of the 3D printed piece, which would absorb most, if not all, of the inserted liquid, causing the sides to leak and the main chamber to overflow. This finding was extremely relevant in order to characterise the PLA in its relation to our device, leading us finally to fabricate a last one entirely made of PMMA with laser ablation, which worked perfectly, at least for what concerns the microfluidics behaviour. The experiments of this new device with the live organoids are left to future research, however this seems like an extremely fruitful starting point where many of the fabrication settings and processes are known and the results are positively promising.

## Danish abstract

Organ-on-a-chip-systemer er avancerede værktøjer inden for medicin og bioteknologi. De hjælper forskere med at forstå sygdomsudvikling bedre og muliggør sikrere lægemiddeltestning. Ved at bruge disse systemer kan vi undgå dyreforsøg og tilpasse behandlinger til individuelle patienter. Hjerneorganoider er nogle af de mest interessante organ-on-a-chip-systemer, og de dyrkes i øjeblikket ud fra humane pluripotente stamceller gennem protokoller, der sikrer ensartede resultater. Den nuværende state-of-the-art for dyrkningsudstyr består primært af enten enkle kulturkamre med et vippe-system, der simulerer hjernemiljøet, eller luft/væske-interface-systemer med en delvis adskillelse mellem mediet og organoiden, som selv er i kontakt med luften. Den største udfordring med de nyeste designs er stadig manglende vaskularisering inde i organoiden, hvilket i levende hjerner er hovedkilden til næringsstoffer og ilt. Den manglende vaskularisering kan føre til apoptose på grund af nekrotiske kerner og hypoxi. Hovedmålet med vores afhandling er at finde en måde at undgå celledød i kernen af organoiderne. Vi udførte en række COMSOL Multiphysics®-simulationer, der tog udgangspunkt i et design tæt på dem, der findes i litteraturen. Vores simuleringer viser, at vi kan opnå bedre resultater ved at tilføje en konstant strøm af medium omkring organoiderne, hvilket stabiliserer koncentrationen af næringsstoffer i organoiderne i løbet af få dage. Dette garanterer længere overlevelse af organoider og mindre menneskelig interaktion med selve enheden, hvilket fører til mindre risiko for forurening og forstyrrelse af driften. For at teste disse simulationer fremstillede vi en enhed til et eksperiment med rigtige organoider ved hjælp af laserablation til at udskære bundkanalen og 3D-printning til at bygge det øverste kammer. Efter at have fundet de korrekte indstillinger for begge processer udførte vi nogle foreløbige tests med farvet Milli-Q-vand for at sikre os, at vores enhed fungerede uden lækager. Eksperimenter med rigtige organoider blev udført på KU, men endte med alvorlige lækproblemer efter blot to dage. Årsagen til disse problemer blev undersøgt og afslørede nogle væsentlige problemer med de 3D-printede komponenter, som absorberede det meste af mediet. Denne opdagelse førte os til at fremstille en sidste enhed helt lavet af PMMA med laserablation, som fungerede perfekt, i det mindste hvad angår mikrofluidikadfærd. Eksperimenterne med denne nye enhed med de levende organoider overlades til fremtidig forskning, men dette synes at være et ekstremt frugtbart udgangspunkt, hvor mange af fabrikationens indstillinger og processer er kendt, og resultaterne er positivt lovende.

# Contents

List of Tables	9
List of Figures	10
<b>I Introduction</b>	<b>17</b>
<b>1 Brain organoids</b>	<b>19</b>
1.1 Classification and applications	19
1.2 Microfluidic approaches and challenges	21
1.3 Thesis aim and structure	24
<b>2 Materials and methods</b>	<b>27</b>
2.1 COMSOL Multiphysics®	27
2.2 Desktop laser cutter	28
2.3 Filament 3D printer	29
2.4 Bonding method	30
<b>II COMSOL Multiphysics® simulations</b>	<b>31</b>
<b>3 Static simulations</b>	<b>35</b>
3.1 1 plate design	35
3.1.1 Holes design	39
3.1.2 Membrane design	41
3.2 5 plates design	43
3.2.1 Holes design	44
3.2.2 Membrane design	46
3.2.3 5 plates design with complete geometry	49
<b>4 Dynamic simulations</b>	<b>51</b>
4.1 1 plate design	52
4.1.1 Holes design	52

4.1.2	Membrane design . . . . .	53
4.2	5 plates design . . . . .	55
4.2.1	Holes design . . . . .	56
4.2.2	Membrane design . . . . .	57
4.3	Study on the porosity of the membrane . . . . .	58
4.3.1	1 plate design . . . . .	59
4.3.2	5 plates design . . . . .	59
4.4	Concentration analysis . . . . .	61
4.4.1	1 plate design . . . . .	61
4.4.2	5 plates design . . . . .	62
4.5	Needle and tubing simulations . . . . .	63
4.6	Bottom plate channel . . . . .	69
4.6.1	First configuration . . . . .	71
4.6.2	Second configuration . . . . .	72
4.6.3	Third configuration . . . . .	73
4.6.4	Fourth configuration . . . . .	74
4.7	Simulations summary . . . . .	75
 <b>III Fabrication tests</b>		 <b>77</b>
<b>5</b>	<b>Laser ablation</b>	<b>79</b>
5.1	Stylus profilometer characterisation . . . . .	82
5.1.1	5 millimeters long lines . . . . .	83
5.1.2	Rotated "T" structures . . . . .	85
5.1.3	5mm×5mm squares . . . . .	88
5.1.4	Bottom channels . . . . .	90
5.2	Bottom channel fabrication . . . . .	91
<b>6</b>	<b>3D printer fabrication</b>	<b>93</b>
6.1	Initial experiments . . . . .	95
6.2	Dynamic 1 plate membrane design . . . . .	97
6.3	Needle and tubing wall . . . . .	97
<b>7</b>	<b>Assembling, testing and sterilizing the device</b>	<b>99</b>
7.1	Step by step chip construction . . . . .	100
7.1.1	Chip bonding . . . . .	100
7.1.2	Tubings and flow splitting . . . . .	102
7.1.3	Chamber sealing . . . . .	104
7.2	Preliminary tests . . . . .	105
7.3	Sterilisation . . . . .	106
7.4	Fabrication summary . . . . .	107

<b>IV</b>	<b>Real organoid experiment and results</b>	<b>109</b>
<b>8</b>	<b>Final setup and outcome</b>	<b>111</b>
8.1	Setup . . . . .	111
8.2	Results . . . . .	114
<b>9</b>	<b>Troubleshooting</b>	<b>117</b>
9.1	Devices' tests . . . . .	117
9.2	Problems and possible solutions . . . . .	117
9.3	Fully PMMA device . . . . .	121
<b>10</b>	<b>Conclusions</b>	<b>125</b>
<b>V</b>	<b>Project plan and self-evaluation</b>	<b>127</b>
	<b>Bibliography</b>	<b>131</b>

# List of Tables

2.1	Summary of all the designs simulated in COMSOL with the section number where they are situated and a brief description. . . . .	33
5.1	Laser power and speed settings for each section of the test PMMA piece. . . . .	81
5.2	Measurement values of average depth, average roughness height and relative roughness in the square structures in each section. . . . .	90
5.3	Measurement values of average depth, average roughness height and relative roughness in the channel structures in sections 2 and 6. . . . .	91
9.1	Laser power, speed and cuts repetitions settings for the new PMMA piece for the top element of the device. . . . .	122

# List of Figures

1.1	Two possible techniques to aid the development and the growth of the cytoarchitectures.[4]	21
1.2	Schematic representation of the three main types of microfluidic devices used for brain organoid-on-chip systems. (i) Microfluidic device with 3D-culture areas and channels; (ii) Microfluidic device with micropillar array; (iii) microfluidic device with air-liquid interface.[5]	22
1.3	Design of a pump-free microfluidic device with a rocker system-driven medium flow in the chamber.[6]	22
1.4	Simulation of glucose diffusion in a simplified version of microfluidic devices having different numbers of channels using COMSOL Multiphysics® .[6]	23
1.5	(a) Prenatal cannabis (e.g., cannabinoids such as THC) exposure may impact fetal brain development. (b) Schematics of a microfluidic brain organoid assembly device that compacts with well plates. (c) Schematics of brain organoid fabrication and cannabis exposure within the microfluidic device.[7]	24
3.1	Two designs for the 1 plate static simulations.	36
3.2	Sugar concentration diffusion in the system from the bottom of the plate to slightly above the holes/membrane layer in circa 20.8 minutes with diffusivity $D = 2.0 \times 10^{-10} \text{m}^2/\text{s}$ .	37
3.3	Sugar concentration diffusion in the system from the bottom of the plate to slightly above the holes/membrane layer in circa 43.6 minutes with diffusivity $D = 9.56 \times 10^{-11} \text{m}^2/\text{s}$ .	37
3.4	Two designs for the 1 plate static simulations with the tissue on top.	38
3.5	Plots of the two cutlines taken to analyse the concentration inside of the organoid.	38
3.6	Concentration in the cutlines of the 1 plate holes design in the span of 4 days.	39
3.7	Average concentration in the organoid in the 1 plate holes design in 4 days.	39
3.8	Concentration in the cutlines of the 1 plate holes design in the span of 4 days during maturation.	40

3.9	Chosen cutplane to measure the concentration in the cross section of the 1 plate holes design in the span of 2 days during maturation and result. . . . .	40
3.10	Average concentration in the organoid in the 1 plate holes design during maturation in 4 days. . . . .	41
3.11	Concentration in the cutlines of the 1 plate membrane design in the span of 4 days. . . . .	42
3.12	Average concentration in the organoid in the 1 plate membrane design in 4 days. . . . .	42
3.13	Concentration in the cutlines of the 1 plate membrane design in the span of 4 days during maturation. . . . .	43
3.14	Cutplane surface concentration and average concentration in the tissue in the 1 plate membrane design during maturation. . . . .	43
3.15	Two quarters of the designs for the 5 plates static simulations with the tissue inside. . . . .	44
3.16	Concentration in the cutlines of the 5 plates holes design in the span of 4 days. . . . .	45
3.17	Average concentration in the organoid in the 5 plates holes design in 4 days. . . . .	45
3.18	Concentration in the cutlines of the 5 plates holes design in the span of 4 days during maturation. . . . .	46
3.19	Surface concentration and average concentration in the tissue in the 5 plates holes design during maturation. . . . .	46
3.20	Concentration in the cutlines of the 5 plates membrane design in the span of 4 days. . . . .	47
3.21	Average concentration in the organoid in the 5 plates membrane design in 4 days. . . . .	47
3.22	Concentration in the cutlines of the 5 plates membrane design in the span of 4 days during maturation. . . . .	48
3.23	Surface concentration and average concentration in the tissue in the 5 plates membrane design during maturation. . . . .	48
3.24	The two complete designs for the 5 plates static simulations. . . . .	49
3.25	The complete designs for the 5 plates static simulations with the small membrane and the average concentration of the tissue in such model. . . . .	50
4.1	Depiction of the flow direction in the bottom plate. . . . .	51
4.2	Average concentration in the organoid in the 1 plate holes design with flow rate = $3.5 \times 10^{-11} \text{m}^3/\text{s} = 2.1 \mu\text{L}/\text{min}$ . . . . .	53
4.3	Average concentration in the organoid in the 1 plate holes design with flow rate = $3.5 \times 10^{-11} \text{m}^3/\text{s} = 2.1 \mu\text{L}/\text{min}$ during maturation. . . . .	53

4.4	Average concentration in the tissue and cutplane of surface concentration after 8 days in the 1 plate membrane design with flow rate = $7 \times 10^{-11} \text{m}^3/\text{s} = 4.2 \mu\text{L}/\text{min}$ . . . . .	54
4.5	Average concentration in the tissue and cutplane of surface concentration after 8 days in the 1 plate membrane design with flow rate = $7 \times 10^{-11} \text{m}^3/\text{s} = 4.2 \mu\text{L}/\text{min}$ during maturation. . . . .	55
4.6	Depiction of the flow direction in the side walls. . . . .	55
4.7	Average concentration in the organoid in the 5 plates holes design with flow rate = $4.5 \times 10^{-10} \text{m}^3/\text{s} = 27.0 \mu\text{L}/\text{min}$ . . . . .	56
4.8	Average concentration in the organoid in the 5 plates holes design with flow rate = $4.5 \times 10^{-10} \text{m}^3/\text{s} = 27.0 \mu\text{L}/\text{min}$ during maturation. . . . .	57
4.9	Average concentration in the tissue and cutplane of surface concentration after 8 days in the 5 plates membrane design with flow rate = $5 \times 10^{-9} \text{m}^3/\text{s} = 300.0 \mu\text{L}/\text{min}$ . . . . .	57
4.10	Average concentration in the tissue and cutplane of surface concentration after 8 days in the 5 plates membrane design with flow rate = $5 \times 10^{-9} \text{m}^3/\text{s} = 300.0 \mu\text{L}/\text{min}$ during maturation. . . . .	58
4.11	Average concentration in the organoid in the 1 plate membrane design with flow rate = $2.1 \times 10^{-10} \text{m}^3/\text{s} = 2.1 \mu\text{L}/\text{min}$ in growth and maturation phase with porosity 47.8%. . . . .	59
4.12	Average concentration in the organoid in the 5 plates membrane design with flow rate = $4.5 \times 10^{-10} \text{m}^3/\text{s} = 27.0 \mu\text{L}/\text{min}$ with two values of porosity. . . . .	60
4.13	Average concentration in the organoid in the 5 plates membrane design with flow rate = $4.5 \times 10^{-10} \text{m}^3/\text{s} = 27.0 \mu\text{L}/\text{min}$ with porosity 70% during maturation. . . . .	60
4.14	Average concentration in the organoid in the 1 plate membrane design as a function of inlet flow rate after 7 days. . . . .	61
4.15	Average concentration in the organoid in the 1 plate membrane design as a function of inlet flow rate after 7 days during maturation. . . . .	62
4.16	Average concentration in the organoid in the 5 plates membrane design as a function of inlets flow rate after 7 days. . . . .	62
4.17	Average concentration in the organoid in the 5 plates membrane design as a function of inlets flow rate after 7 days during maturation. . . . .	63
4.18	Plot of the chosen xz-cutplane at $y = 0$ . . . . .	64
4.19	Average concentration in the tissue and cutplane after 8 days in the lateral perfusion design with plate flow rate = $3.5 \times 10^{-11} \text{m}^3/\text{s} = 2.1 \mu\text{L}/\text{min}$ and needle flow rate = $1 \times 10^{-6} \text{m}^3/\text{s} = 60000 \mu\text{L}/\text{min}$ . . . . .	64
4.20	Cutplane concentration after 8 days with plate flow rate = $3.5 \times 10^{-11} \text{m}^3/\text{s} = 2.1 \mu\text{L}/\text{min}$ and no needle flow rate during maturation. . . . .	65

4.21	Average concentration in the tissue and cutplane after 8 days in the top needle design with plate flow rate = $3.5 \times 10^{-11} \text{m}^3/\text{s} = 2.1 \mu\text{L}/\text{min}$ and needle flow rate = $1 \times 10^{-6} \text{m}^3/\text{s} = 60000 \mu\text{L}/\text{min}$ injected at $z = 1.41$ . . . . .	66
4.22	Average concentration in the tissue and cutplane after 8 days in the top needle design with plate flow rate = $3.5 \times 10^{-11} \text{m}^3/\text{s} = 2.1 \mu\text{L}/\text{min}$ and needle flow rate = $1 \times 10^{-6} \text{m}^3/\text{s} = 60000 \mu\text{L}/\text{min}$ injected at $z = 1.41$ . Needle inflow concentration = 40 millimolar. . . . .	67
4.23	Average concentration in the tissue and cutplane after 8 days in the top needle design with plate flow rate = $3.5 \times 10^{-11} \text{m}^3/\text{s} = 2.1 \mu\text{L}/\text{min}$ and needle flow rate = $1 \times 10^{-6} \text{m}^3/\text{s} = 60000 \mu\text{L}/\text{min}$ injected at $z = 2.1$ . . . . .	68
4.24	Average concentration in the tissue and cutplane after 8 days in the top needle design with plate flow rate = $3.5 \times 10^{-11} \text{m}^3/\text{s} = 2.1 \mu\text{L}/\text{min}$ and needle flow rate = $1 \times 10^{-6} \text{m}^3/\text{s} = 60000 \mu\text{L}/\text{min}$ injected at $z = 2.1$ . Needle inflow concentration = 40 millimolar. . . . .	68
4.25	Average concentration in the tissue and cutplane after 8 days in the lateral perfusion and top inserted needle design with plate flow rate = $3.5 \times 10^{-11} \text{m}^3/\text{s} = 2.1 \mu\text{L}/\text{min}$ and needle flow rate = $1 \times 10^{-6} \text{m}^3/\text{s} = 60000 \mu\text{L}/\text{min}$ injected at $z = 2.1$ . . . . .	69
4.26	Average concentration in the tissue and cutplane after 8 days in the lateral perfusion and top inserted needle design with plate flow rate = $3.5 \times 10^{-11} \text{m}^3/\text{s} = 2.1 \mu\text{L}/\text{min}$ and needle flow rate = $1 \times 10^{-6} \text{m}^3/\text{s} = 60000 \mu\text{L}/\text{min}$ at $z = 1.41$ . . . . .	70
4.27	Velocity streamlines in the bottom plate channel in a 2D simulation with shallow channel approximation. . . . .	70
4.28	Lateral view of the bottom plate channel in a 3D simulation which shows the three layers: channel, membrane and tissue. . . . .	71
4.29	Geometry and surface concentration of the first tissue configuration with 4 slices. . . . .	72
4.30	Average concentration in each of the 4 slices in the first configuration. . . . .	72
4.31	Geometry and surface concentration of the second tissue configuration with 4 slices. . . . .	73
4.32	Average concentration in each of the 4 slices in the second configuration. . . . .	73
4.33	Geometry and surface concentration of the third tissue configuration with 9 slices. . . . .	74
4.34	Average concentration and zoom of the plot in each of the 9 slices in the third configuration. . . . .	74
4.35	Geometry and surface concentration of the fourth tissue configuration with 9 slices. . . . .	75
4.36	Average concentration and zoom of the plot in each of the 9 slices in the fourth configuration. . . . .	75
5.1	AEON MIRA5 CO <sub>2</sub> Desktop Laser Cutting Machine. . . . .	79

5.2	Bottom channel model recreated in RDWorks V8 to carve with the laser cutter on the PMMA. . . . .	80
5.3	Image of the PMMA piece over which we conducted some characterisation tests with the laser cutter. . . . .	80
5.4	Dektak 150 stylus profilometer. . . . .	82
5.5	Geometry of the stylus tip and how this geometry affects the measurement accuracy depending on the shape of the structure we are studying. . . . .	82
5.6	Image of the surface of the PMMA piece in section 2. The dark and pointy tip of the Dektak stylus can be seen on the left, the untouched surface is the yellow/brown part and on the right there is the beginning of the 5 millimeters lines cut respectively one and six times. . . . .	83
5.7	Image of the surface of the PMMA piece in section 1. The dark and pointy tip of the Dektak stylus can be seen on the left, the untouched surface is the yellow/brown part and on the right there is the beginning of the 5 millimeters lines cut respectively one and six times. . . . .	84
5.8	Image of the surface of the PMMA piece in section 5 and 3 respectively. The dark and pointy tip of the Dektak stylus can be seen on the left, the untouched surface is the yellow/brown part and on the right there is the beginning of the 5 millimeters lines cut six times. . . . .	84
5.9	"T" structures geometry and scan directions: on the left we have what we will call the "A" direction and on the right the "B" direction, both from beginning to end of the channel. . . . .	85
5.10	Cross section of the channel measured along direction A in the "T" structure in section 1, depth = $668.0\mu\text{m}$ . . . . .	85
5.11	Cross section of the channel measured along direction B in the "T" structure in section 1, depth = $532.8\mu\text{m}$ . . . . .	86
5.12	Cross section of the channel measured along direction A in the first "T" structure in section 2, depth = $417.1\mu\text{m}$ . . . . .	87
5.13	First edge of the channel measured along direction A in the second "T" structure in section 2, depth = $747.6\mu\text{m}$ . . . . .	87
5.14	Angle of two "T" structures cut with 10% power and writing speeds 30mm/s and 50mm/s respectively. . . . .	88
5.15	Square structure geometry and scan directions: A, B and C. For the edge measurements each arrow was followed, for the roughness measurement only the middle two. . . . .	88
5.16	Measurement in the square structure in section 2 scanned along direction B: edge depth = $424.4\mu\text{m}$ . . . . .	89
5.17	Measurement in the center of direction B, without the edge, of the square structure in section 2: random peak height = $30.2\mu\text{m}$ . . . . .	89

5.18	Bottom channel designed engraved in a piece of PMMA. . . . .	91
5.19	Bottom channel designed engraved in a piece of PMMA with design rotated by 90° in RDWorks. . . . .	92
6.1	Creality Ender-3 V2 filament 3D printer. . . . .	93
6.2	Creation of a model for a PLA 3D printer for a wall design with lateral perfusion. . . . .	94
6.3	Model and final piece for a practice chamber wall design, apt at testing the resolution of the printer. . . . .	95
6.4	3D printed piece from the side, where the tube with the hole is not resolved. The yellow arrows point to the outer diameter of the tube. . . . .	96
6.5	Final 3D printed piece for the first design of our needle wall chamber and resolution of the lateral tubing. . . . .	96
6.6	Model and final piece for the trivial wall design, 3D printed with biocompatible PLA. . . . .	97
6.7	Model and final piece for the complete lateral tube wall design, 3D printed with biocompatible PLA. . . . .	98
7.1	Cross section of the final chip with design descriptions to indicate the bonding steps. . . . .	99
7.2	View on the bottom channel with the first piece of tape. . . . .	100
7.3	View on the bottom channel with a piece of filter paper in the middle. . . . .	101
7.4	Both wall designs bonded to the bottom channel seen from below to observe alignment. . . . .	101
7.5	Full view of the final chip in the needle wall design for example. . . . .	102
7.6	White residue scattered in the bottom channel after isopropanol and super glue reacted. . . . .	103
7.7	Complete chips in both designs. . . . .	104
7.8	Four way flow splitter with attached pipette heads. . . . .	104
7.9	Sealing test to close the organoid chamber. . . . .	105
7.10	Flow test set up and results of three devices with the four-way flow splitter and dyed Milli-Q water. . . . .	106
8.1	Loading the organoids in the chips through pipettes. . . . .	111
8.2	Organoid inside of the central chamber of the chip. The pink colour is due to the medium colour. . . . .	112
8.3	Set up inside and outside of the incubator, connected through a tube going from the syringes to the flow splitters. The pump used is a Harvard Apparatus syringe pump PHD 2000. . . . .	112
8.4	Average concentration in the tissue and cutplane after 14 days in the lateral perfusion design with plate flow rate = $3.5 \times 10^{-11} \text{m}^3/\text{s} = 2.1 \mu\text{L}/\text{min}$ and needle flow rate = $3.5 \times 10^{-11} \text{m}^3/\text{s} = 2.1 \mu\text{L}/\text{min}$ . . . . .	113
8.5	Failed experiment with leakages and no waste collected in the output bottle after 2 days and a half of operation. . . . .	114

9.1	New design for the bottom channel and zoom in after the complete fabrication steps for the bottom half of the device. . . . .	118
9.2	Approximation of the hydraulic resistances in the tube-pipette head system with quoted lengths and radii: the green cylinder is the tube, the blue cylinder is the first part of the pipette head, the red cylinder is the end of the pipette head. . . . .	119
9.3	New sealing technique: we place a piece of parafilm slightly bigger than hole on top of it, we stick some tape over it and then seal it with silicone on the edges. . . . .	120
9.4	The 3D printed piece absorbs any liquid going through the device, either through the inlet and outlet holes or the chamber. . . . .	121
9.5	Example of laser damage caused by too many cuts at a too high laser power on the bottom of a piece of PMMA, especially close to the central square. . . . .	122
9.6	Final successful test with the device fully made of PMMA, on top is the normal design and below is the one with the pillar in the main chamber. We can see the inlet tubes coming directly from the two syringes, one per device, and the outlet tubes ending up in a collection bottle. . . . .	123
9.7	Details of the final test: bottom channel distribution of the water and main chamber filling seen from the side. . . . .	124

**Part I**

**Introduction**



# Chapter 1

## Brain organoids

The brain has always been one of the most intriguing topics of human research, was it from a sociological, ethical or physiological point of view. A great interest has been shown in what distinguishes a human from a machine: this is encapsulated in 86 billion neuronal cells temporally and spatially coordinated with 85 billion glial cells, and specialised vascular cells[1]. The result is a neuronal system consisting of circa 7000 synapses behaving similarly to a circuit that is still nowadays poorly understood in its entirety. Models may come close to an approximation, good enough for an initial research, but never quite get the full picture. Since there is no way to investigate a live brain tissue, technology has turned its attention to *in vitro* brain models, or brain organoids. The main culturing method for such organoids that we will be investigating are organ-on-a-chip systems, which in the last years have become fertile ground for great discoveries and future biomedical applications. Their peculiarity and appeal comes from the fact that they would open the door to new explorations on human brain development and disorders' pathogenesis, especially for illnesses with complex genetic origins that end up being very challenging to model. They would help study drug screening for individual patients, tailoring their specific needs to specific prescriptions and treatments. Moreover an advantage that is no less relevant is the reduction of animal testing that is prevalent in the medical field and is morally questionable. This thesis will explain how such systems are designed and developed in order to grow brain organoids and make them thrive in the long term.

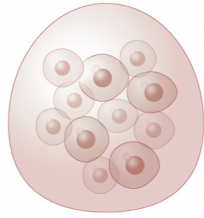
### 1.1 Classification and applications

When other attempts at growing brain-like architectures had just started, the reaserch was mainly dealing with traditional 2D cell culture, which however had encountered several limitations[2]:

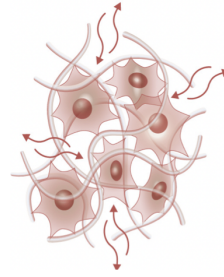
1. A lack of hierarchical structure;

2. No dimensionality;
3. No cellular diversity;
4. A failure of the cell-cell or cell-matrix interaction modeling;
5. Rare presence of the characteristic patient customization option;
6. An extremely challenging long-time *in vitro* maintenance.

This is why 3D cerebral organoids became a necessity to further explore these topics. Starting from human pluripotent stem cells (hPSCs) a self-assembling process begins to finally create an organised architecture. During the process we require a progenitor (maybe from a patient's biopsy), neuronal and glial cell types and a Matrigel suspension, or any type of supporting element that provides an apt environment for adhesion and growth. For a complete description, glial cells provide structure and supply nutrients to the neurons, and some also give the immunity response in case of external lesions. Through these elements we are able to form an organoid with similar phenotypes to a real fetal human brain, so that it can mimic its developmental stages and tissue structure allowing for a lot of new research trajectories. There are generally two approaches for brain organoid growth: unguided and guided. The former creates various cells stochastically, with no proportional differentiation of the cell types and dimensions, which may be problematic in the case of a quantitative analysis that requires a specific environment. Whereas the latter provides particular tissues and cells given by small molecules and growth factors instructing the hPSCs conscieously, resulting in consistent results. This can improve cell adhesion and cell to cell signalling, however one downside to this last method is that the external meddling has to be carefully controlled, otherwise it could affect the structures and cytoarchitectures. The technique used in the organoids we are going to work with was a guided process using Biosilk™ scaffolding that behaves as a porous network differently from the aqueous environment of an hydrogel (like the previously mentioned Matrigel) as can be seen in Figure 1.1. This helped reduce cell stress and hypoxia in long term cultures, thus making it possible to grow rather large organoids (in the millimeter scale), promoted the formation of the neuroectoderm and enhanced the homogeneity of cellular organization between individual organoids. The neuroectoderm is an ensemble of cells derived from the ectoderm and its formation is the first step in the development of the nervous system.



(a) Hydrogel matrix depiction.



(b) Biosilk scaffolding depiction.

Figure 1.1: Two possible techniques to aid the development and the growth of the cytoarchitectures. [4]

## 1.2 Microfluidic approaches and challenges

Fabricating chambers that are able to handle such delicate systems and making them thrive is the main objective of this thesis and of a lot of current research. In this section we are going to illustrate techniques that have already been tested and the challenges that have already been faced, taking inspiration for our future work. Microfluidic chambers rely on a precise control of the microenvironment while allowing good mass transportation through a fluid flow. However the main concern with any technique is providing vascularization and oxygenation, since failing to dispense nutrients and oxygen to every cell in the organoid can lead to hypoxia and apoptosis, limiting the size of the organoid, which in turn limits the accuracy of the model. We are dealing with laminar flow physics where the Reynolds numbers of these channels is well below 2000, and mostly even lower than 1. The different fabrication techniques are generally based on either passive or active flow. The former utilises osmosis, surface tension and hydrostatic pressure, while the latter engages mechanical pumps and mixers giving a more stable and precise result. Vascularization can be helped by microfluidic devices by combining a perfusion flow with shear stress induced by the transmural flow and the interstitial flow from the chip. Up until now we have seen three main types of microfluidics devices: with 3D-culture areas and channels, with micro-pillar arrays and with air-liquid interface as we can see in Figure 1.2.

In the case of the devices with 3D-culture chambers there are many different types, which include different perfusion techniques. Through these we found that usually bi-directional flow are more realistic in modelling the complex flows in the brain and that highly confining environments help accelerate maturation. In the article "*Microfluidic device with brain extracellular matrix promotes structural and functional maturation of human brain organoids*" [6], we have found an extremely interesting example which can be seen in Figure 1.3.

Here organoids were embedded in hydrogels and the lack of pumps and tubing led

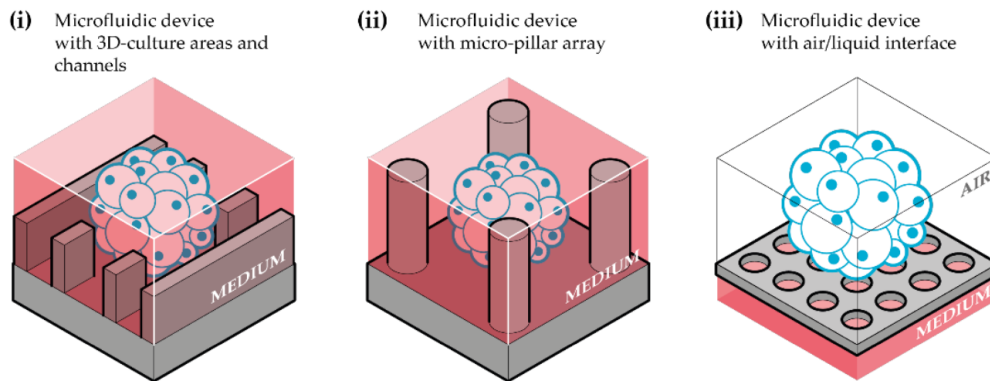


Figure 1.2: Schematic representation of the three main types of microfluidic devices used for brain organoid-on-chip systems. (i) Microfluidic device with 3D-culture areas and channels; (ii) Microfluidic device with micropillar array; (iii) microfluidic device with air-liquid interface.[5]

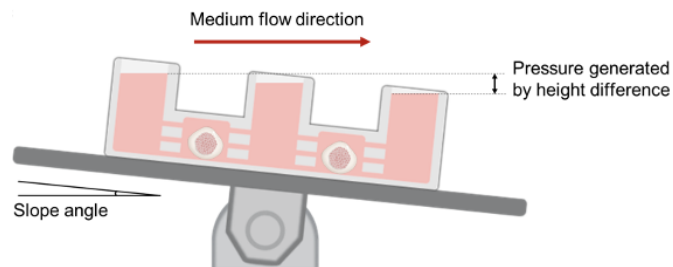


Figure 1.3: Design of a pump-free microfluidic device with a rocker system-driven medium flow in the chamber.[6]

to a larger scale culture. They observed that the level of glucose in the organoid equilibrated quite quickly with that in the medium, however in static conditions the concentration of glucose inside the organoid was quite low. As a solution they created a rocker system that would move the medium and help diffusion inside of the tissue, improving the neuronal maturation. A fascinating analysis that they made was observing how the number of connecting channels between the organoid chamber and the reservoir impacted on the diffusion of glucose to the core. Through a simplified COMSOL Multiphysics® simulation they found that horizontally parallel channels helped more than vertically parallel channels, while a combination of both was the best solution, their results are shown in Figure 1.4.

The micropillar arrays devices are of less interest to us, so we are going to discuss the air-liquid interface devices more in depth. Again our investigation led to another intriguing article, "*One-Stop Microfluidic Assembly of Human Brain Organoids To Model Prenatal Cannabis Exposure*"[7], on neurodevelopmental toxicity. In it a very

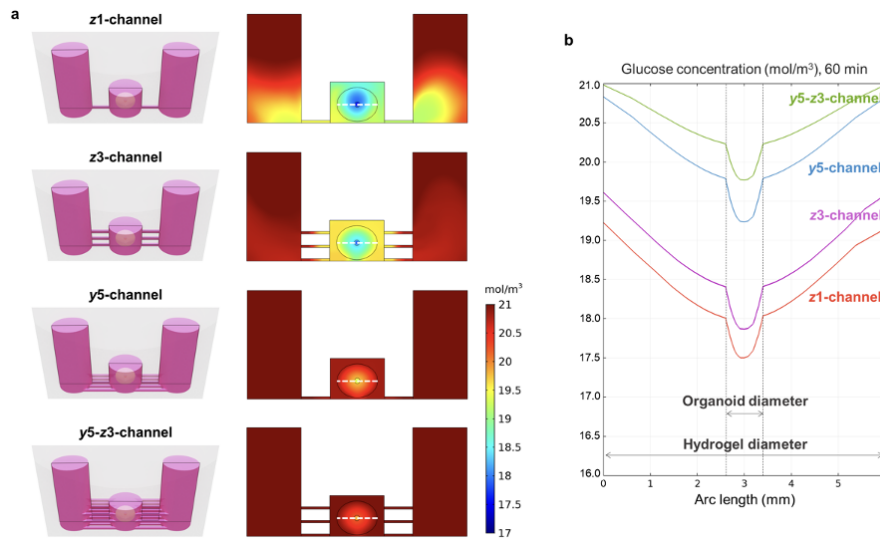


Figure 1.4: Simulation of glucose diffusion in a simplified version of microfluidic devices having different numbers of channels using COMSOL Multiphysics® .[6]

interesting design was created to study how prenatal cannabis exposure influences human brain development. They fabricated a one-stop microfluidic platform to assemble and culture human cerebral organoids from human embryonic stem cells (hESC). Designing a perfusable culture chambers which incorporates an air-liquid interface during maturation and a one-stop protocol, they were able to simplify the fabrication procedure and produce a large number of organoids with limited size variation and hypoxia. In their design each well with an organoid included a bottom chamber loaded with embryonic body formation medium, which was connected to the top chamber through a series of perfusable holes. This top chamber, according to the growth stage of the organoid was either loaded with the same medium, or it just had a thin layer of medium. The medium was then changed periodically to refurbish the chamber with nutrients and remove the organoid's waste. As we can see in Figure 1.5 their design has two main stages which interest us: EB formation, that resembles the environment of organoids in the devices with 3D-culture chambers, and organoid maturation, where we can note the air-liquid interface. These devices work well enough for now, but vascularization and long term growth are still big concerns for the organoids, for this reason we will try to find new solutions and hopefully advance this field of research.

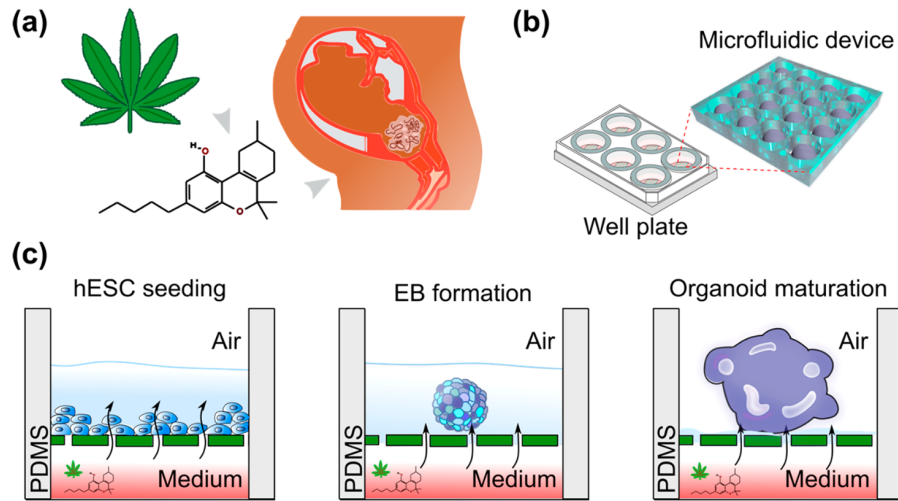


Figure 1.5: (a) Prenatal cannabis (e.g., cannabinoids such as THC) exposure may impact fetal brain development. (b) Schematics of a microfluidic brain organoid assembly device that compacts with well plates. (c) Schematics of brain organoid fabrication and cannabis exposure within the microfluidic device.[7]

### 1.3 Thesis aim and structure

The aim of this thesis is to design and fabricate a device for brain organoid culture, taking inspiration from and improving on the designs shown in section 1.2 in order to aid the problem of vascularisation. The objectives of the thesis are:

1. Use COMSOL simulations to design a device delivering a stable concentration of nutrients to an organoid;
2. Investigate fabrication methods for the designed device;
3. Fabricate and test the device using live brain organoids at KU.

Part II of this thesis deals with the simulations done on COMSOL Multiphysics® to find the right parameters for our devices studying the average concentration in the organoid. It is divided in two chapters concerning static and dynamic simulations, where the difference is in the fact that the latter have a flow going through the channels and not only static fluids. Each chapter deals with a 1 plate design and a 5 plate design, described later, where the 1 plate design is similar to those found in literature and the 5 plate one is our own idea. Since our main goal for the project was implementing this flow in designs that up until now have only had static media or a rocker systems, in the dynamic simulations chapter we studied the problem more thoroughly with a membrane porosity analysis and a concentration analysis. Moreover we included two new types of design with needles and tubes and a final

simulation of our bottom channel design for the bottom plate. Our main objective is proving that this continuous flow will cause the average concentration in the tissue to stabilise on a constant value by perpetually feeding more nutrients on its own, with no human intervention.

Part III will show the fabrication tests we conducted, where we divided our device in two parts: the bottom one done in PMMA with laser ablation and the top one built with a filament 3D printer, each with their chapter. Due to time constraints and fabrication limits we focused on creating two of the 1 plate designs previously studied, where the medium will only be present in the bottom plate. We will discuss how we characterised the CO<sub>2</sub> laser for depth and roughness for our final design and how we adapted our 3D design to the printer and our needs. In the last chapter we will describe the assembly process of the whole device step by step, including bonding, securing the tubes and the flow splitters and sealing the chamber. Finally we will show our preliminary tests done in our lab and the sterilisation process necessary for the application.

Part IV describes the actual experiment at KU with live organoids, the problems we encountered and the consequent troubleshooting in two different chapters. There will be a description of the experimental set up and the final results we observed, and later we delved into possible solutions to the flaws encountered until we found the successful one. Finally we included the conclusions to the whole project and described the future prospects of this thesis.



# Chapter 2

## Materials and methods

In this chapter we will discuss our choices of softwares, materials and machines crucial for our project and we will analyse each one for an introductory description.

### 2.1 COMSOL Multiphysics ®

For this project we used the Microfluidics Module from COMSOL, since in our case we need to analyse a single-phase flow with laminar flow and a transport of diluted species in both 2D and 3D spaces. These processes are simulated by COMSOL with the homonymous studies and, by computing them, it is actually solving them and the related equations iteratively, discretising them on each mesh element of our geometry and following the boundary conditions: the smaller the elements of the mesh the more precise the solution, but the longer it takes for the simulation to finish. When we will deal with static simulations where there will be no liquid flow, we only introduce the time-dependent "Transport of Diluted Species" study which simulates the nutrients' diffusion through the liquid and the tissue in a static fluid, but it will also be crucial in the dynamic simulations since the flow will be steady. When there are diluted particles in the fluid COMSOL has to do a study on their concentration variation over time and the analysis is based on the diffusion equation:

$$\delta_t c = -\mathbf{v} \cdot \nabla c + D \nabla^2 c \quad (2.1)$$

This time variation of the dilute species concentration is given as the difference between the convection term and the diffusion one (with  $D$  the diffusivity of the particle in the liquid), where the former is not considered in the static simulations. However when we move on to the dynamic ones, we have to integrate the "Laminar Flow" study and couple the fluid convection to the velocity field and specify that our fluid is incompressible to simplify the simulation. The incompressible Navier-Stokes equation is defined as:

$$\rho_f (\partial_t \mathbf{v} + (\mathbf{v} \cdot \nabla) \mathbf{v}) = -\nabla P + \eta \nabla^2 \mathbf{v} + \mathbf{f}_{ext} \quad (2.2)$$

where  $\rho_f$  is the fluid density,  $\mathbf{v}$  is the fluid velocity that causes acceleration and advection (first and second term in the equation respectively),  $\nabla P$  is the pressure gradient,  $\eta\nabla^2\mathbf{v}$  are the viscous forces of the fluid in the Newtonian picture (with  $\eta$  the dynamic viscosity) and  $\mathbf{f}_{ext}$  are the external forces that may affect the system. Since the fluid is incompressible its density is considered constant in time, so from the mass conservation law we get the continuity equation:

$$\delta_t\rho = -\nabla(\rho \cdot \mathbf{v}) = 0 \Rightarrow \nabla \cdot \mathbf{v} = 0 \quad (2.3)$$

and from this we can conclude that the change of flow velocity in all directions has to amount to zero. We can further simplify equation 2.2 considering the following: we are working with a system with Reynolds number well below 1; the flow is approximated as fully developed at every inlet, so constant in time; we are not considering any external force. As a consequence we get:

$$\nabla P = \eta\nabla^2\mathbf{v} \quad (2.4)$$

also known as the Stokes equation, which is what COMSOL's solver will use. As one may have already guessed, using COMSOL is fundamental for solving these equations for quite complicated geometrical models as our own, but most of all its advantage comes from the results visualisation. With COMSOL we are able to create multiple types of graphs, streamlines and much more to easily picture the simulation results in a clear and organised manner. In a case like ours where we would like to send multiple simulations with different parameters to scope out the best ones, we will need fast simulations so we will have to take some factors into consideration when setting them up, as well as choosing the correct boundary conditions. The details of the simulations will be seen in the appropriate chapter.

## 2.2 Desktop laser cutter

To fabricate the bottom piece of our device we decided to use laser ablation on a piece of PMMA. This acrylic material (formally polymethyl methacrylate) is transparent and rigid, but easy to cut and cost-effective, which opens the possibility of doing multiple tests without wasting resources. The thickness of the piece has to be taken into consideration when looking to put bigger organoids inside, but if sterilised it is biocompatible and it is tough enough to withstand scratches. However PMMA's biggest obstacle is its limited chemical resistance towards organic solvents and our choices for the sterilisation are between ethanol and isopropanol, the former is more polar than the latter which may be a greater danger to the polymer chains of PMMA leading to cracking and swelling. Our solution was then to use isopropanol really quickly and drying it immediately to reduce the risk it still posed to the acrylic.

We will use a desktop laser cutter with a CO<sub>2</sub> laser (main information taken from the

website here cited [8]) since it does not require contact with the material, reducing damage on both the PMMA and the machine, and gives an extremely precise replica of the model fed through the computer program. The working principle is based on the generation of an electric current through a tube filled with a mixture of carbon dioxide, nitrogen, hydrogen, and helium that ionises the gas molecules causing them to emit light. A couple of mirrors (one highly reflective and one partially reflective) at both ends of the tube collect the light and collimate it on the surface of the PMMA once it has an extremely high intensity. CO<sub>2</sub> lasers usually work in the mid-infrared range with a wavelength from 9300 to 10600 nm and, even if the energies are not some of the highest ones, the extremely high heat produced on the surface vaporises the material leaving little to no residues. According to the needed feature we have to find the best parameters to get the required result by testing different values of cutting speed, power and number of passes with either a raster scan or just an outline cut. Laser cutters risk swelling the lines due to the material melting and could leave a rough surface especially when doing small feature like ours, so we will keep an eye out for that by characterising a test piece with a stylus profilometer to find the best settings for our application. Some roughness would not be too much of a problem for us since the bottom piece channel will not be directly in contact with the organoid, but it is an interesting information to have to get the full picture of our fabrication.

## 2.3 Filament 3D printer

For what concerns the top piece of our device we will use a filament 3D printer in an additive manufacturing process that first requires a digital model (done in our case with Fusion 360) later converted to an STL file and fed to a slicer. This software will divide our model in slices, as the name suggests, that the printer will process one at a time, building the object layer by layer from the bottom up. The settings for the print are decided here, for example infill density, printing temperature and speed and most importantly the supports settings, and the program will give an approximation of how long the print will take. Supports are sacrificial structures needed by the printer to build free-standing parts of the model where the filament could not hold on its own before cooling down. They are therefore mandatory the bigger the unconnected structures are, but there are ways to avoid them where they would pose a problem for removal in small features, like tilting the model or rotating it. The result is a physical replica of the model that follows all of our instructions, with a resolution dependent on the type of printer and on the required quality of the piece. In our case we chose 3D printing due to its ability of creating hollow structures with ease, without requiring the fabrication of multiple pieces to be bonded. The material used is a PLA (polylactic acid) filament, which is made from organic sources and is indeed biocompatible and sustainable; it provides quite a high printing speed compared to other materials and the resulting piece is tough

enough for us, since we do not require moving parts. In the nozzle of the printer the filament is preheated above melting temperature (170-180°C[9]) and, once it is ready, it is placed on the heated bed of the printer, where it builds up layer by layer as the printer nozzle moves upwards. Once the print is done the bed and, as a consequence, the bottom layer of the object have to cool down so that the latter does not warp during the removal.

The reasons why the PLA printer was chosen over a SLA (stereolithography) resin printer are multiple; starting from the practical side resin printers are more complex to use and require a post-processing cleaning and UV-curing step which would take too much time and the materials are too expensive for our fast prototyping needs. Most importantly it uses some solvents that are toxic and not at all biocompatible which is our main priority. Due to this, even if the SLA printer would give a much higher resolution and smoother surfaces, we agreed that this level of detail was not necessary in the face of the other drawbacks.

## 2.4 Bonding method

We will bond our two main pieces with double sided tape, which was chosen on the basis of simplicity and because it can be cut using the desktop laser cutter in a design specific to our needs. First of all we will have to find the right laser settings for this flimsy material, and we will have to be extremely careful when manually aligning it on our device. The main issues that could come from this simple technique is the risk of leakages if the adhesion is not optimal. For this reason we will have to carry on multiple tests to check if high flow rates, long terms usage or other factors could cause problems to the adherent characteristic of the tape.

**Part II**

**COMSOL Multiphysics®**  
**simulations**



Design	Holes	Membrane	Description
1 plate static	3.1.1	3.1.2	No flow, only bottom reservoir.
5 plates static	3.2.1	3.2.2	No flow, bottom reservoir and 4 on the walls.
1 plate dynamic	4.1.1	4.1.2	Holes flow rate: $2.1\mu\text{L}/\text{min}$ , membrane flow rate: $4.2\mu\text{L}/\text{min}$ . Only bottom reservoir.
5 plates dynamic	4.2.1	4.2.2	Holes flow rate: $27.0\mu\text{L}/\text{min}$ , membrane flow rate: $300.0\mu\text{L}/\text{min}$ . Bottom reservoir and 4 on the walls.
Porosity study	/	1 plate: 4.3.1; 5 plates: 4.3.2	Study on the porosity of the membrane to check if it influences the operation.
Concentration analysis	/	1 plate: 4.4.1; 5 plates: 4.4.2	Analysis on the minimum usable flow rate for good results.
Needle and tubing	/	4.5	Bottom plate and lateral/top tube flow rate: $2.1\mu\text{L}/\text{min}$ and $60000\mu\text{L}/\text{min}$ respectively. No wall reservoir.
Bottom plate	/	4.6	Study on the dynamics of the bottom plate and design optimisation.

Table 2.1: Summary of all the designs simulated in COMSOL with the section number where they are situated and a brief description.



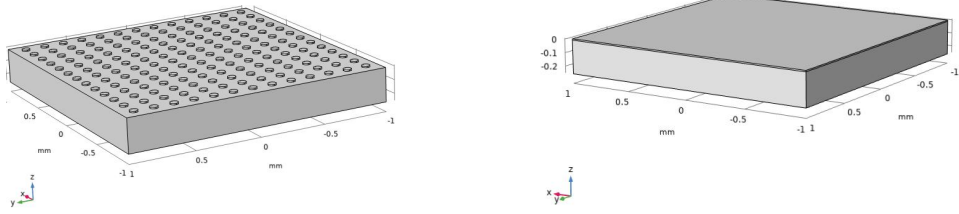
# Chapter 3

## Static simulations

As said in the COMSOL introduction, these simulations will only be solved through the diffusion equation 2.1, considering the diffusion term alone for now. As you will see we dealt with both a hole and a membrane design, the first one being closer to the original design from paper [7] and the second one being what we will use in practice. We did this because punching the holes through any material would have been a very complicated and cumbersome task, and also not extremely relevant to our work. Instead membranes have more of a mesh structure with a multitude of small holes and cavities that resemble paper more than straight holes and were readily available to us. However as you will see we made sure of simulating an equivalent design for the best comparison. In order to better approach this task, we have decided to start simulating the device in different configurations according to some values that were given to us by KU and some found in the literature. The main stages we will be dealing with are what in article [7] they called the embryonic body formation, which we will call “growth” and is similar to what they did in article [6], and the organoid maturation with the air-liquid interface, called simply "maturation". Also of course we would expect the organoid to grow, but in the simulation we kept it at constant dimension to simplify the simulation load. However it is important to highlight and keep in mind that the longer the organoid matures the more difficult it is to feed, especially towards the core, so parameters will need to be adjusted accordingly when considering the full picture.

### 3.1 1 plate design

The first step was setting up the geometry and for our intents we needed to engineer an equivalent "membrane" design to the "holes" design with a membrane of equivalent porosity to the original 13x13 array of holes of  $30\mu\text{m}$  of radius as we can see in Figure 3.1. The plate has dimensions  $2\text{mm}\times 2\text{mm}\times 0.25\text{mm}$  which gives a volume of  $1 \times 10^{-3}\text{mL}$ .



(a) 1 plate holes geometry.

(b) 1 plate membrane geometry.

Figure 3.1: Two designs for the 1 plate static simulations.

On top of this plate we added a block of medium 5mm high, defined as water since anyway it composes most nutrient solutions. If we consider an arbitrary starting concentration in the medium and the tissue of  $28 \text{ mol/m}^3$ , the diffusion time to travel a length  $L = 0.5\text{mm}$  (from the bottom of the plate to just above the holes) with the general diffusivity of sugar ( $D = 2.0 \times 10^{-10} \text{m}^2/\text{s}$ ) is 20.8 minutes, following the formula:

$$\tau_{diff} = \frac{L^2}{D} = 1250s \quad (3.1)$$

As we can see from the graphs in Figure 3.2 that time is not enough to reach complete 50/50 concentration distribution in the chamber and that is due to the porosity of the surface which elicits accounting for an effective diffusivity in the path due to a friction effect. This effective diffusion coefficient through the holes can be calculated by multiplying the diffusion coefficient by what we define as porosity. The porosity can be roughly calculated as being the ratio between the area of the holes and the total area of the plate. In the hole configuration that gives a porosity of 47.8% and an effective diffusivity of  $9.56 \times 10^{-11} \text{m}^2/\text{s}$ . This will be the value we are going to use when defining the diffusivity through the membrane to get a comparable result, considering a damping factor so high that there is no fluid convection but only diffusion through it. With the membrane design we have a slightly faster diffusion, but the end result is the same.

If we calculate the diffusion time with the effective diffusivity we get:

$$\tau_{diff} = \frac{L^2}{D_{eff}} = 2615s \quad (3.2)$$

which is approximately 43.6 minutes. If we go and use that in the simulation we can then see in Figure 3.3 that this time the 50/50 distribution in the system is reached as we would expect.

Now introducing a 2mm diameter tissue, simplified as a sphere pressed on the bottom we can start simulating the organoid consumption of nutrients and see how fast

### 3.1 – 1 plate design

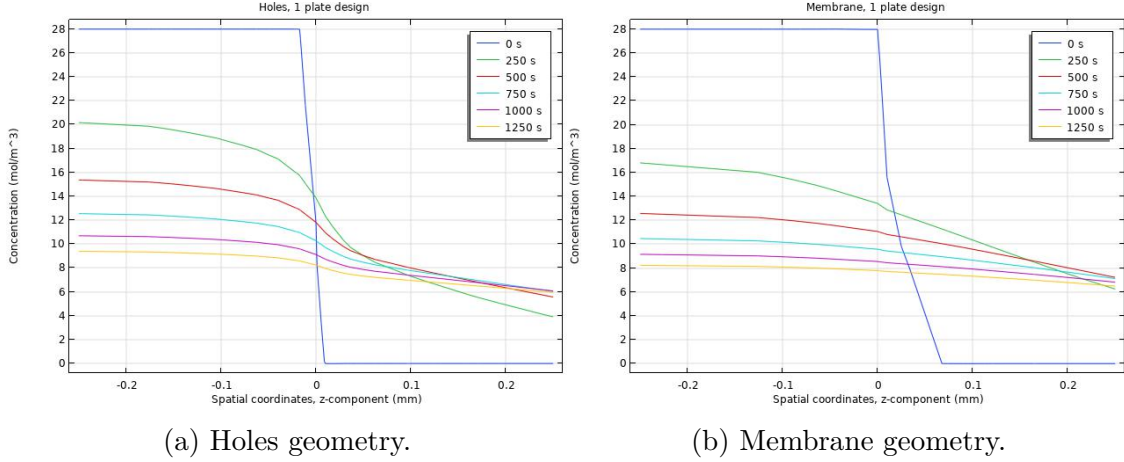


Figure 3.2: Sugar concentration diffusion in the system from the bottom of the plate to slightly above the holes/membrane layer in circa 20.8 minutes with diffusivity  $D = 2.0 \times 10^{-10} \text{m}^2/\text{s}$ .

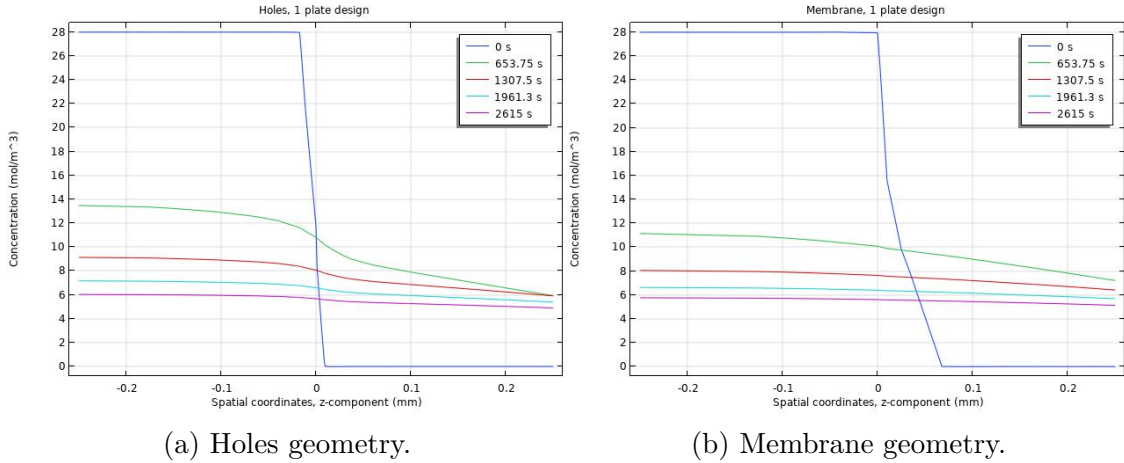
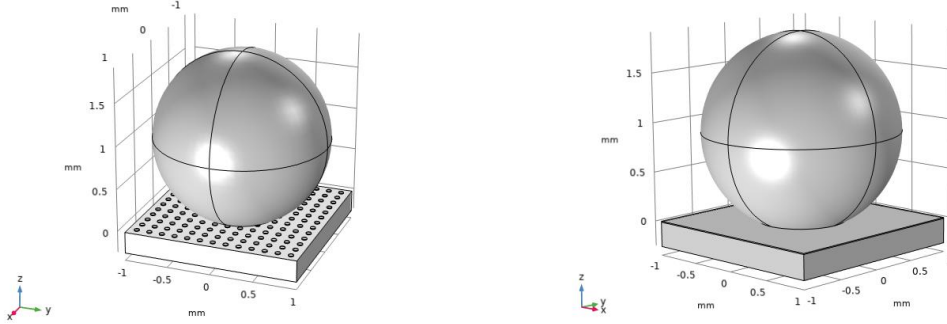


Figure 3.3: Sugar concentration diffusion in the system from the bottom of the plate to slightly above the holes/membrane layer in circa 43.6 minutes with diffusivity  $D = 9.56 \times 10^{-11} \text{m}^2/\text{s}$ .

it depletes in the course of a week. In the first step we are perfusing only through the bottom plate as in the original paper with a static medium inside of the plate. The nutrient transport is completely governed by diffusion and there is no convection, which is why we only use the time dependent Transport of Diluted Species study. During the growth stage the medium was changed each day, whereas during maturation it was changed every other day, so we will use this information to gather more or less the reaction rate for the consumption of the nutrients starting from 28

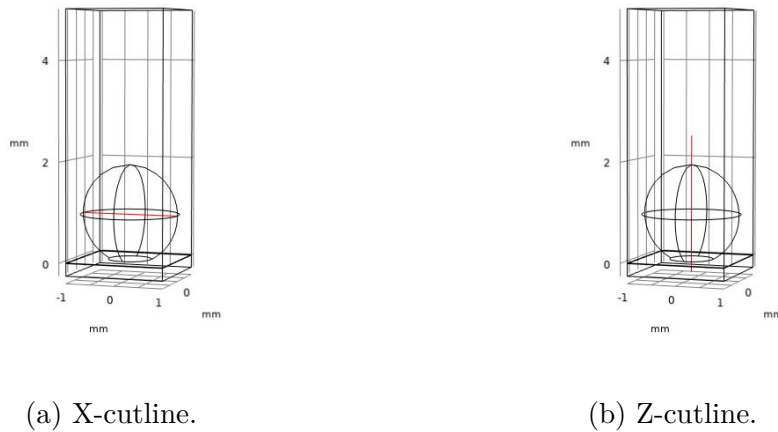
millimolar. In the growth stage it is found to be  $-3.2407^{-4}\text{mol}/(\text{m}^3 \cdot \text{s})$  whereas it is  $-1.6204 \times 10^{-4}\text{mol}/(\text{m}^3 \cdot \text{s})$  during the maturation phase. The geometry now can be observed in Figure 3.4. The porosity of the tissue is arbitrarily taken as 20% since we found that the interstitial space (ISS) component of brain extracellular space typically has this value[10]. Note that the brain extracellular space is the narrow microenvironment that surrounds every cell of the central nervous system.



(a) 1 plate holes geometry with tissue. (b) 1 plate membrane geometry with tissue.

Figure 3.4: Two designs for the 1 plate static simulations with the tissue on top.

We studied two different cutlines (along the x-axis and the z-axis) and the average concentration in the tissue through a probe domain. We can see the cutlines' plots in Figure 3.5.



(a) X-cutline.

(b) Z-cutline.

Figure 3.5: Plots of the two cutlines taken to analyse the concentration inside of the organoid.

### 3.1.1 Holes design

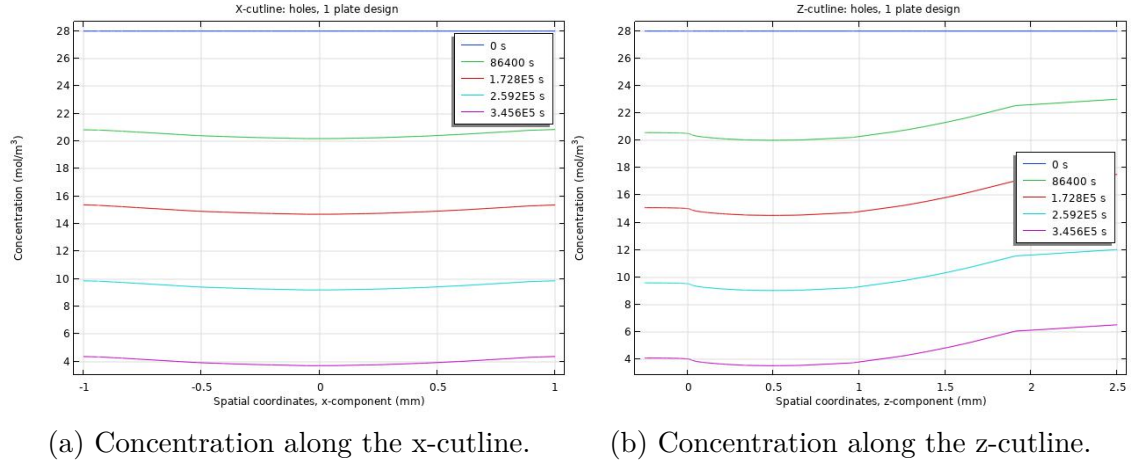


Figure 3.6: Concentration in the cutlines of the 1 plate holes design in the span of 4 days.

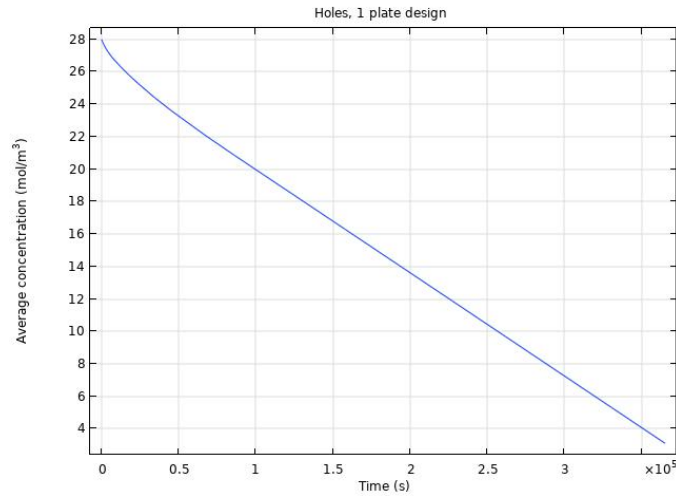


Figure 3.7: Average concentration in the organoid in the 1 plate holes design in 4 days.

During growth we can see that after a day the average concentration (Figure 3.7) decreases by almost 30%, which is why the medium was changed that frequently. The average concentration is found to be linear due to the fact that we are still doing a static analysis. We can see in the x-cutline (Figure 3.6a) that the center is slightly more depleted than the edges as we would expect, due to the low diffusivity through the tissue. This is the main problem that we are facing nowadays, even if

here it seems less relevant due to the concentration value still being quite constant throughout the tissue. We can see that after 2 days the core cells have halved their concentration. In the z-cutline in Figure 3.6b we can observe how different the value of concentration at the extremities is compared to the core, especially at the top of the tissue where we have close contact with the medium and so more nutrients can be fed more directly.

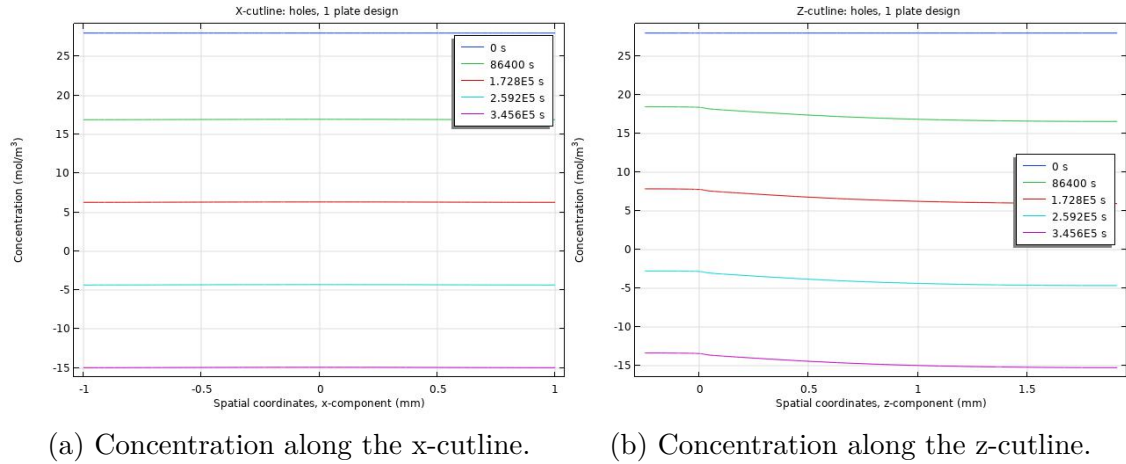


Figure 3.8: Concentration in the cutlines of the 1 plate holes design in the span of 4 days during maturation.

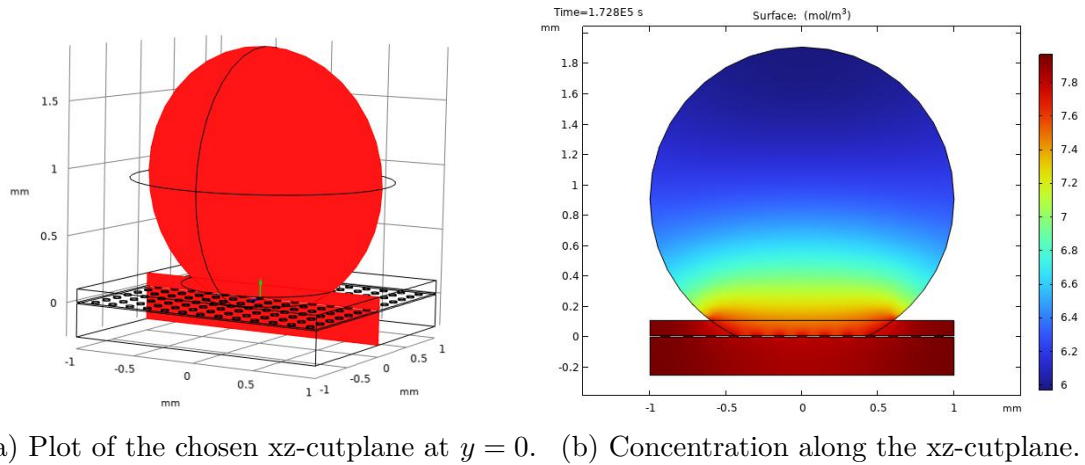


Figure 3.9: Chosen cutplane to measure the concentration in the cross section of the 1 plate holes design in the span of 2 days during maturation and result.

During maturation we see a big loss after the 2-day mark, which is why they changed it every other day. We can see in Figure 3.10 that after 2 days and a half

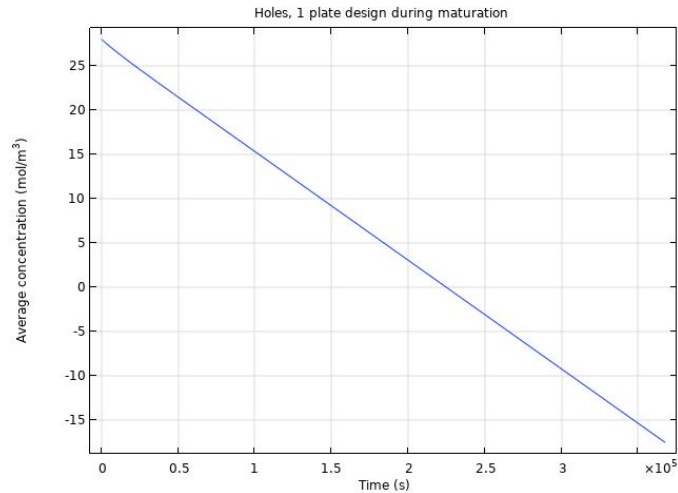


Figure 3.10: Average concentration in the organoid in the 1 plate holes design during maturation in 4 days.

the concentration would be negative, which physically speaking means that the tissue would be in a deficit. Here, adding to the cutlines in Figure 3.8, we decided to show a surface map of the cutplane at the center of the sphere of the system after 2 days. The cutplane plot can be seen in Figure 3.9a while the actual data plot is in Figure 3.9b. By doing so we can better visualise how the concentration is pretty homogeneously distributed in the tissue, with obviously a higher value the closer to the source of nutrients. This is because there are no lateral inputs of concentration that would come from the medium, so the core and the outer layers of the organoids are fed equally, with diffused nutrients exclusively from the bottom plate.

### 3.1.2 Membrane design

The same study was done with the aforementioned membrane, following the same process as before, and as a result we get the same behaviour and more or less equal values. In the results of the growth phase, seen in Figure 3.11, the core is slightly more depleted than the edges of the sphere and the encompassing medium feeds the top of the tissue better than the source since it is not hindered by the membrane. The average concentration in Figure 3.12 is also exactly the same.

For the maturation the outcome is equivalent to the previous one. Looking at Figures 3.13 and 3.14, the concentration is more or less homogeneously distributed in the tissue, but we can clearly see that the top is less nourished due to the slower diffusion through the tissue. Again after 2 days and a half the tissue no longer has any nutrients.

As we can see, our membrane design is good enough to simulate their holes design

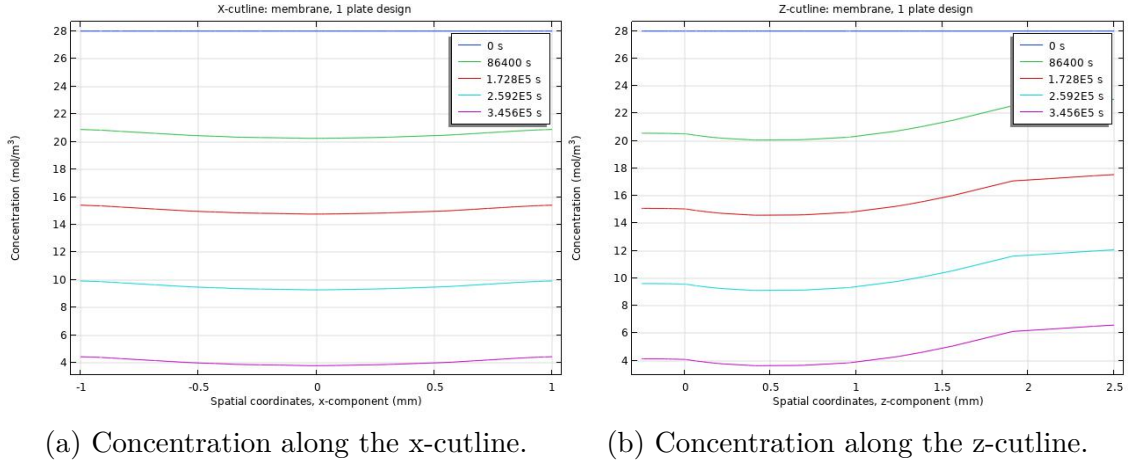


Figure 3.11: Concentration in the cutlines of the 1 plate membrane design in the span of 4 days.

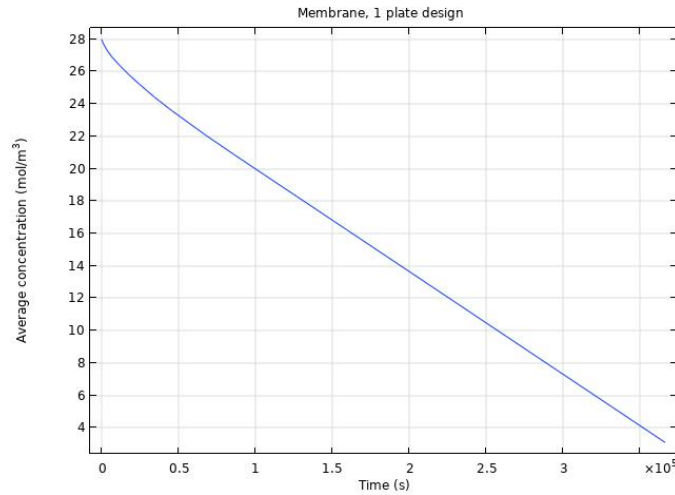


Figure 3.12: Average concentration in the organoid in the 1 plate membrane design in 4 days.

and is also a lot less computationally heavy. For such a small organoid these designs work well enough for keeping a good concentration level, but our first resolution was trying to design a chamber where the nutrients were not only coming from the bottom plate, but also 4 other surrounding plates that in the original design would just be normal walls. The inspiration came from paper [6], where we saw that many lateral channel could help the organoid’s nutrition level in Figure 1.4 in under 60 minutes. We decided to combine that idea with the original model from paper [7] and see if we would get some improvements, especially in the core concentration.

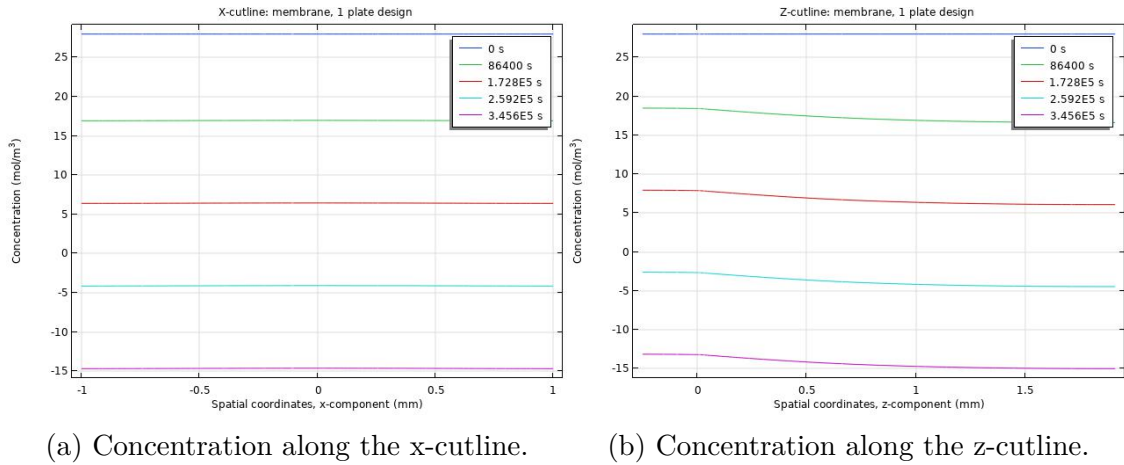


Figure 3.13: Concentration in the cutlines of the 1 plate membrane design in the span of 4 days during maturation.

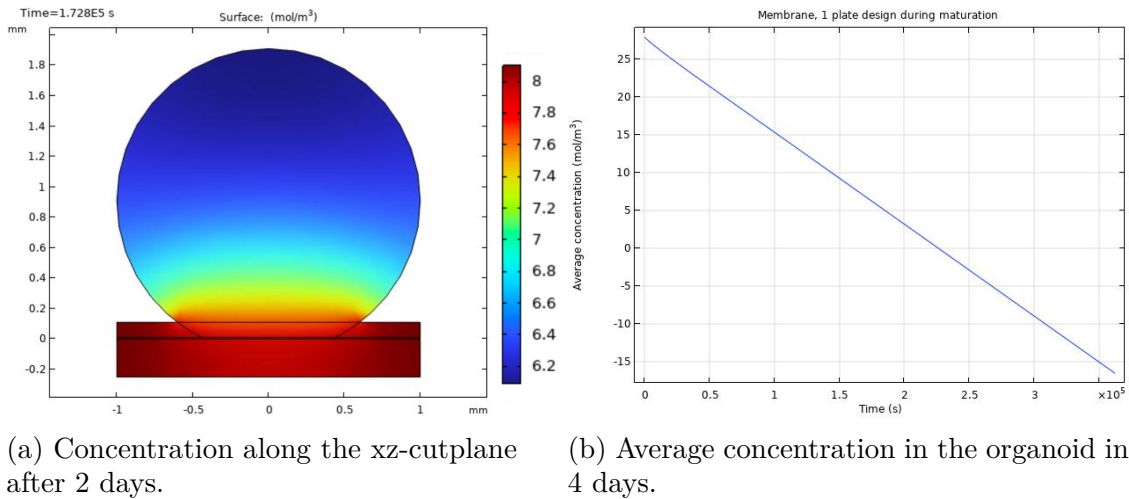
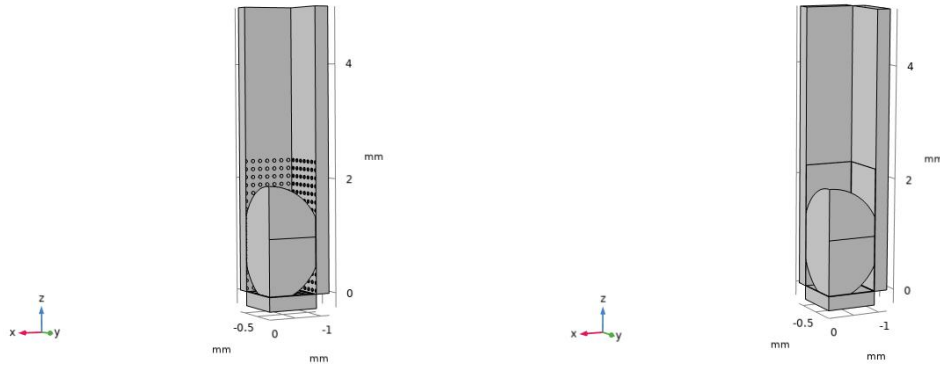


Figure 3.14: Cutplane surface concentration and average concentration in the tissue in the 1 plate membrane design during maturation.

## 3.2 5 plates design

The two designs for the holes and the membrane were originally created as a quarter of the geometry, since everything would then be symmetrical, to test the computational weight of the simulations and check the cross-sectional behaviour all in one. We have to keep the top open to allow for the necessary air-liquid interface, but the rest of the walls, although complicated to fabricate, could very well work as additional reservoirs. By doing so we are not only increasing the amount of nutrients

a chamber can hold and dispense, but also we are helping with the diffusion to the higher parts of the organoid that would be farther away the more it grows. The organoid has been simulated as moderately squeezed between the walls to adhere better to the sidewalls. This confinement technique has been proven to enhance the size homogenization of organoids and constrained environments accelerate maturation and the appearance of wrinkles and folding in the organoid (see paper [5], Table 1, 3rd row). Every other detail about the simulations was kept the same to better compare them to the 1 plate design's ones. The geometry of the designs can be seen in Figure 3.15.



(a) 5 plates holes geometry with tissue. (b) 5 plates membrane geometry with tissue.

Figure 3.15: Two quarters of the designs for the 5 plates static simulations with the tissue inside.

### 3.2.1 Holes design

If we go and compare the results in Figure 3.7 for the 1 plate design with the 5 plates design graph in Figure 3.17 we can observe that the latter, as expected, has higher average concentrations of nutrients in the tissue throughout the days and can potentially last longer. In fact, during growth, up to the fourth day it still has an acceptable value of nutrient concentration. As we can see in the x-cutline in Figure 3.16a we only have the result for half of the sphere, but the rest can be imagined to be mirrored for the other half of the tissue. Also the value of concentration in correspondence with the wall shows the influence of the new reservoir with a more definite uptick.

When we enter the maturation phase we can clearly see how the system can work for longer periods of time before changing medium: where before the tissue would finish the nutrients in the span of 2 days and a half, now it could go for even longer than four days (see Figures 3.14 and 3.19). This is a critical difference that is

### 3.2 – 5 plates design

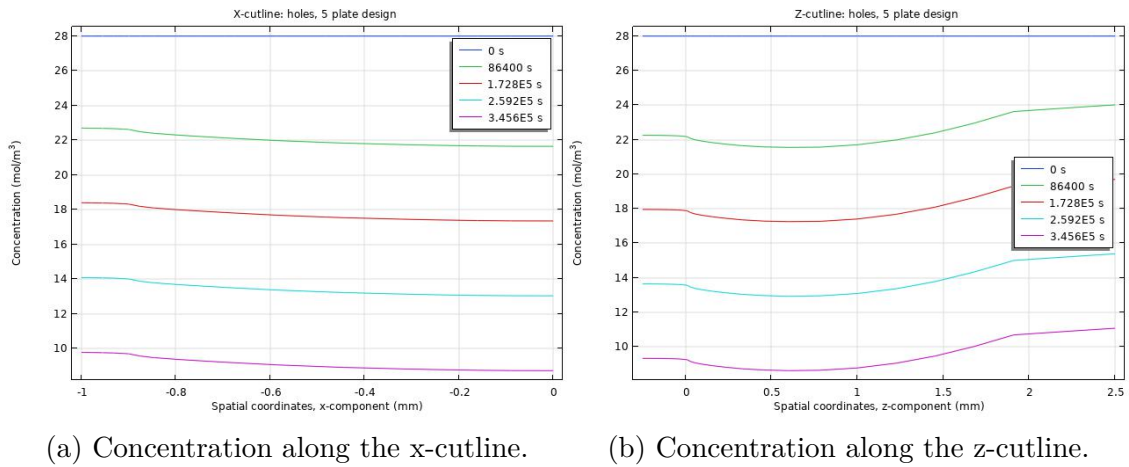


Figure 3.16: Concentration in the cutlines of the 5 plates holes design in the span of 4 days.

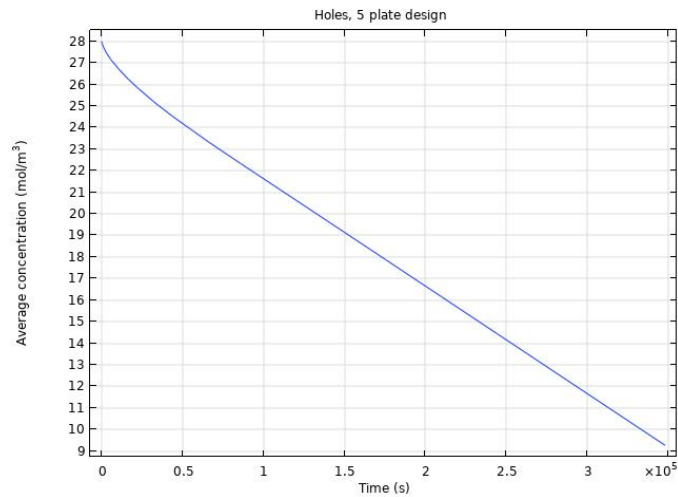


Figure 3.17: Average concentration in the organoid in the 5 plates holes design in 4 days.

extremely relevant to our cause: not only can it work for longer times, but this also means less human intervention in the process to manually change the fluid, which can lead to less contamination and mechanical disruption. It is also interesting to note how in the surface concentration distribution in Figure 3.19a we can clearly see the sides supplying some nutrients and as a result increasing the concentration at the top of the tissue and in the core and overall homogenizing it even more in the whole organoid.

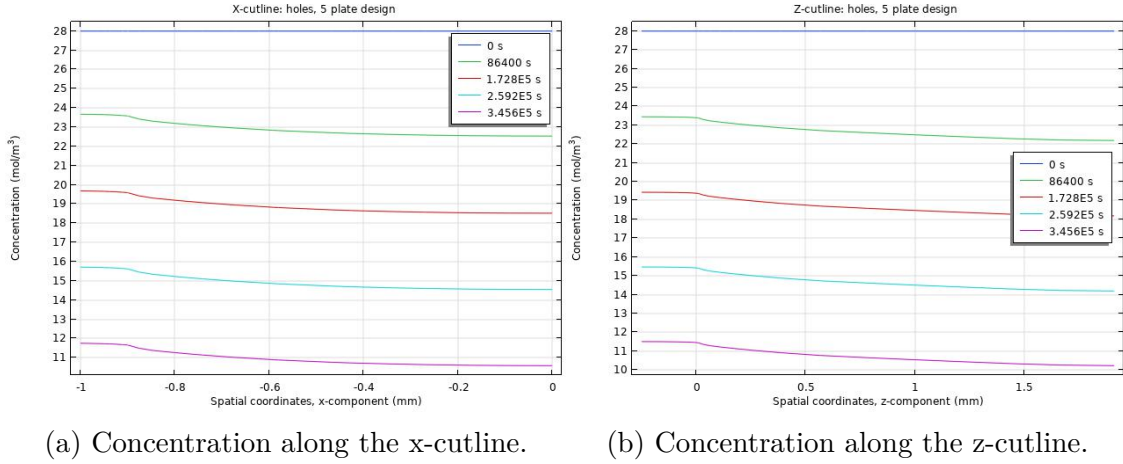
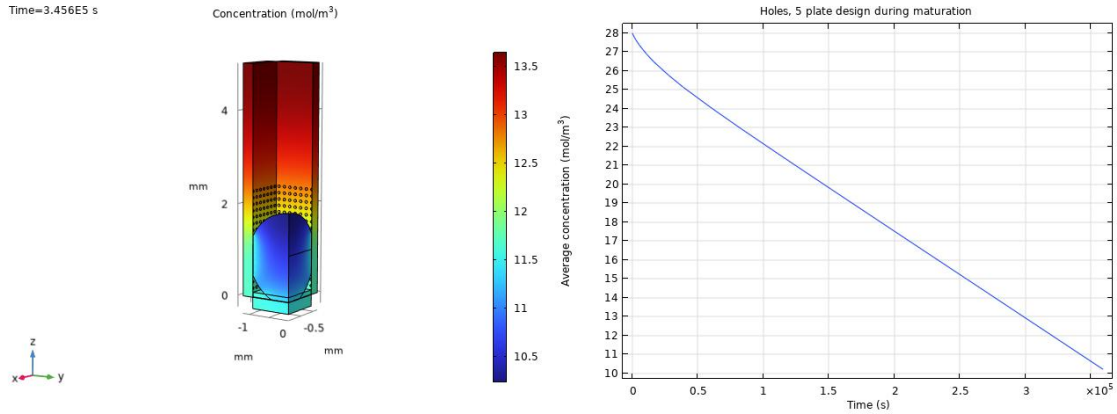


Figure 3.18: Concentration in the cutlines of the 5 plates holes design in the span of 4 days during maturation.



(a) Concentration along surface of the quarter of the design after 4 days. (b) Average concentration in the organoid in 4 days.

Figure 3.19: Surface concentration and average concentration in the tissue in the 5 plates holes design during maturation.

### 3.2.2 Membrane design

Again the results, and as a consequence the comments, with the membrane are closely related to the previous ones with the holes. The average concentration has increased in both growth and maturation stage (Figures 3.21 and 3.23b) and the latter works as well as the former. This opens new doors for less frequent medium change and overall waste, while introducing an air-liquid interface to combat hypoxia.

### 3.2 – 5 plates design

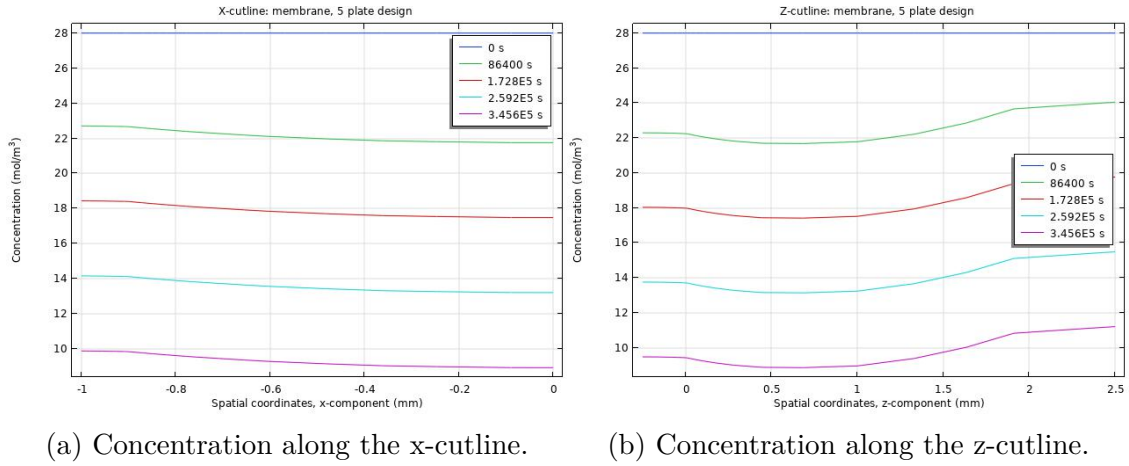


Figure 3.20: Concentration in the cutlines of the 5 plates membrane design in the span of 4 days.

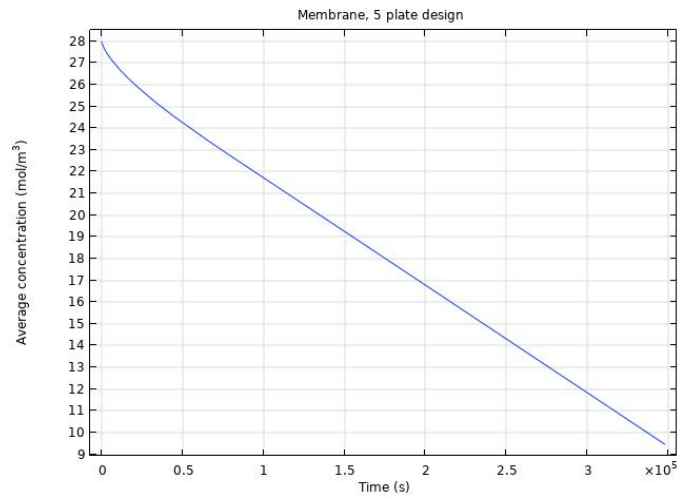


Figure 3.21: Average concentration in the organoid in the 5 plates membrane design in 4 days.

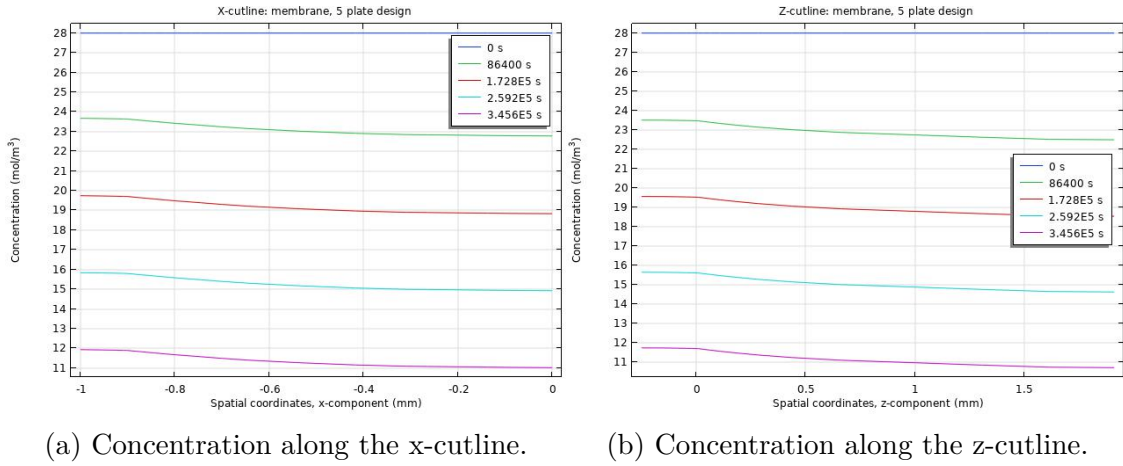
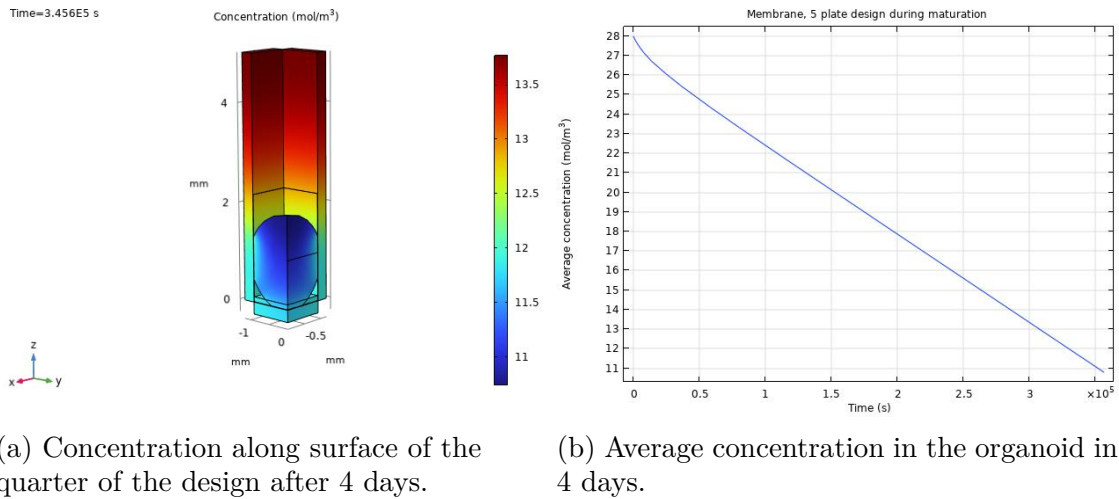


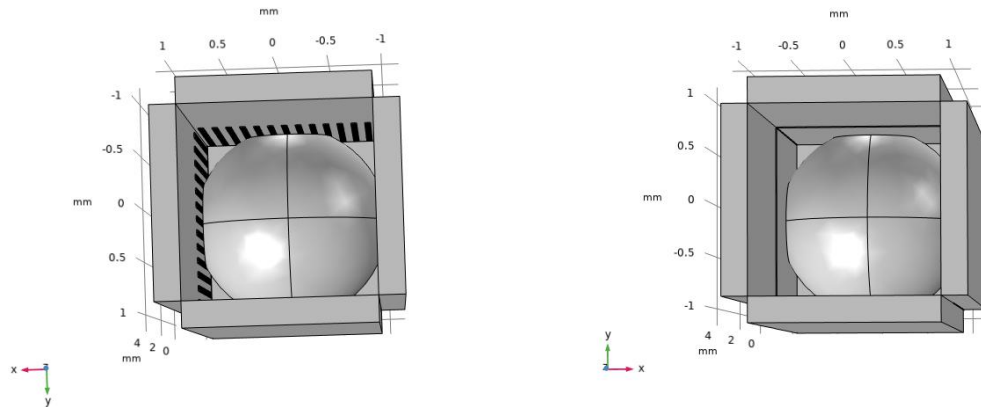
Figure 3.22: Concentration in the cutlines of the 5 plates membrane design in the span of 4 days during maturation.



(a) Concentration along surface of the quarter of the design after 4 days. (b) Average concentration in the organoid in 4 days.

Figure 3.23: Surface concentration and average concentration in the tissue in the 5 plates membrane design during maturation.

### 3.2.3 5 plates design with complete geometry

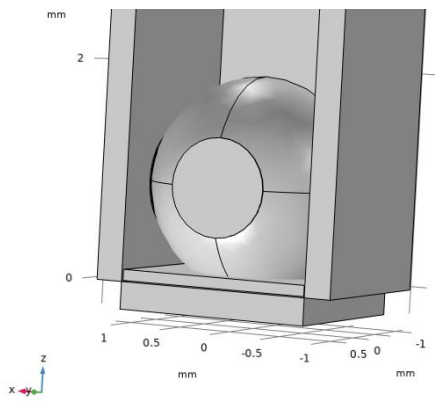


(a) 5 plates holes complete geometry. (b) 5 plates membrane complete geometry.

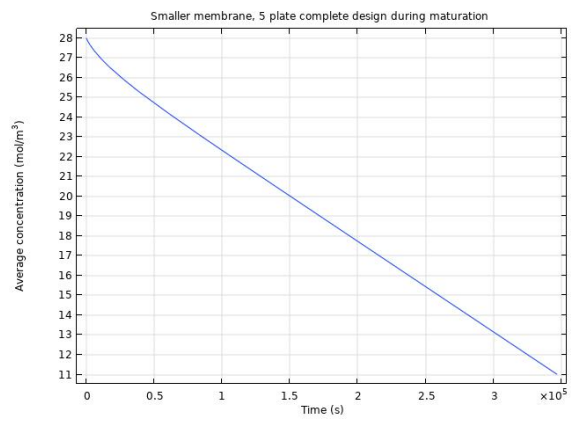
Figure 3.24: The two complete designs for the 5 plates static simulations.

To complete the picture we simulated the entire geometry, since it will also be needed in future analyses, only in the maturation phase, to check that the result were correct. In Figure 3.24 we can observe the two geometries seen from the top. We can note that there are no overlapping of walls which would cause fluid passing from one to the other, which would alter the results. Without reporting repetitive results, since the graphs are completely compatible with the previous ones, we can confirm that our design work as intended and that the computation was not even as long as expected. This is extremely promising for the rest of the work.

To further simplify our next 5-plates simulations, for the membrane design we decided to create a structure where the membrane only covered the contact area between the tissue and the wall (as can be seen in Figure 3.25a). By doing so the results are exactly comparable to the full design, were it not for an almost unnoticeable difference in the overall average concentration, comparing Figure 3.25b and 3.23b. This confirms to us that we can move on with this structure for future reference.



(a) 5 plates complete geometry with the small membrane.



(b) Average concentration in the organoid.

Figure 3.25: The complete designs for the 5 plates static simulations with the small membrane and the average concentration of the tissue in such model.

## Chapter 4

# Dynamic simulations

As a next step we decided to introduce a flow through the reservoirs, which would change the medium automatically, remove possible waste from the chamber and keep the nutrient's concentration as constant as possible if not completely stable in time. Doing so practically will be a challenge, but it is the natural progression of the original design because it lessens drastically the need for a human interference with the chip and automates the operation. We know that the velocity of interstitial flow is circa between  $0.1\text{--}1\mu\text{m/s}$ [11] =  $5\times 10^{-13}\text{m}^3/\text{s}$  (found by multiplying  $1\mu\text{m/s}$  for the cross-sectional area of the inlet  $A_i = 0.25\text{mm}\times 2\text{mm}$ ) so to have an efficient diffusion through the tissue the chosen flow rates will need to be a lot higher than this value. We introduce a Laminar Flow physics inside of each reservoir, parallel to the face where we have the holes/membrane as shown in Figure 4.1. By doing so COMSOL will solve the Stokes equation (2.4) coupled with both diffusion and convection from the diffusion equation (2.1).

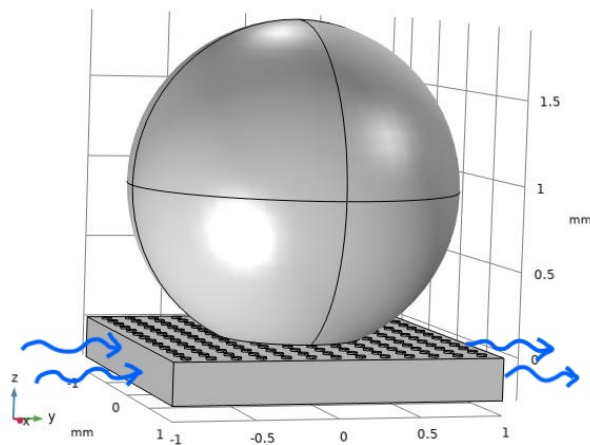


Figure 4.1: Depiction of the flow direction in the bottom plate.

We have a stationary study that resolves for the Laminar Flow physics and then a time-dependent Transport of Diluted Species study. The latter is now the one that includes convection, which takes its velocity field from the former study. As before we have kept into account that through the membrane there needs to be no convection, but only diffusion, same as for the tissue. Up to this point we had been using physics-controlled fine mesh, but from now on we had to use a user-controlled mesh to account for some artifacts and to help the simulation converge and solve in less time. For the time-dependent analysis we have extended the time frame to 8 days to better observe the stabilization of the average concentration in the tissue after the one-week mark. Whether we have 1 or 5 plates, each inlet was simulated to have the same flow rate and our goal was to find the correct one that utilised the convection to its advantage. After some tentative values we have found the following ones to be the most effective and we will now display them for each design.

## 4.1 1 plate design

The designs used are the same as in Figure 3.4. From this section on we decided to leave the cutlines plots behind, since for our purpose they became less relevant. We will now be observing mainly average concentration in the tissue and cutplanes plot of the surface concentration. Also you will see that our interest will shift more towards the membrane design since we have been proving that it is mostly equivalent to the holes one and it is what we will be working with in practice, so it is more important to get more specific and quantitative results.

### 4.1.1 Holes design

Here the mesh was set as normal everywhere, but fine in the holes to have a better result. During growth the best value we found for the inlet flow rate into the bottom plate was  $2.1\mu\text{L}/\text{min}$  and, as we can see in Figure 4.2, with this flow rate the concentration inside of the tissue remains more or less the same throughout the days after a very quick fall within the first day. It is not a perfectly constant plateau, but it was our closest result.

During maturation we observed that keeping the same flow rate gives again a good constant behaviour towards the end of a week (Figure 4.3), but the initial slope is less steep and the final average concentration is slightly lower than during growth, as previously detected in the 1 plate design. It is to be expected that the slope is gentler because there is less medium to help with the homogenization of the concentration throughout the tissue. Increasing the inlet flow rate would just increase the average concentration at constant value by a very small amount and not help with the overall operation, so saving some medium seems like the best option.

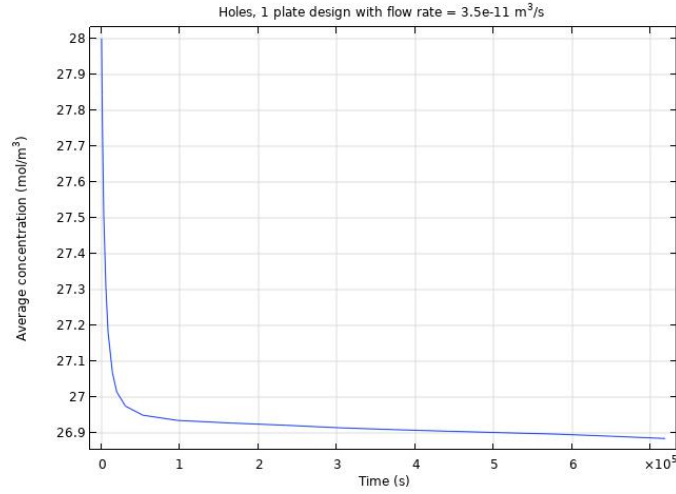


Figure 4.2: Average concentration in the organoid in the 1 plate holes design with flow rate =  $3.5 \times 10^{-11} \text{ m}^3/\text{s} = 2.1 \mu\text{L}/\text{min}$ .

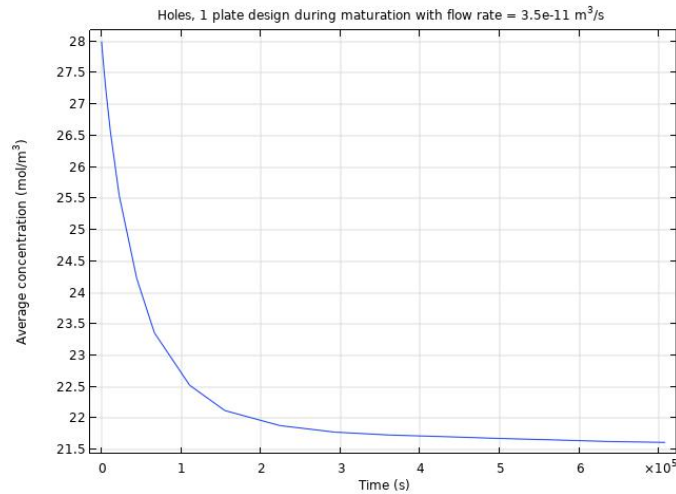


Figure 4.3: Average concentration in the organoid in the 1 plate holes design with flow rate =  $3.5 \times 10^{-11} \text{ m}^3/\text{s} = 2.1 \mu\text{L}/\text{min}$  during maturation.

## 4.1.2 Membrane design

This design was subject to a lot of mesh artifacts so the mesh was changed to fine in the membrane, normal in the tissue and coarse in the rest of the structure. Moreover we took more points for the time-dependent analysis in the initial part of the simulation because the deep slope in the average concentration was more difficult to detect properly. During growth the design requires twice the flow rate,  $4.2 \mu\text{L}/\text{min}$ , than before. However the resulting concentration at the end is quite

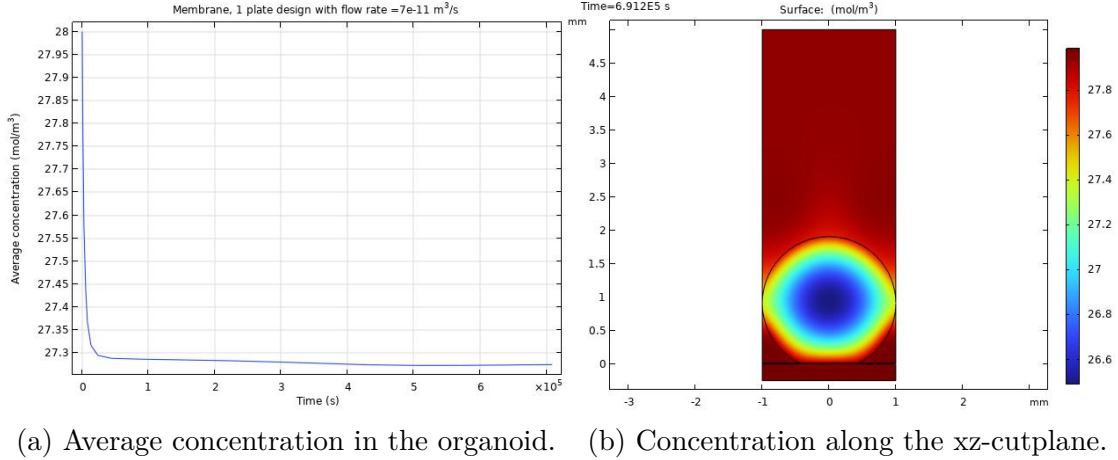
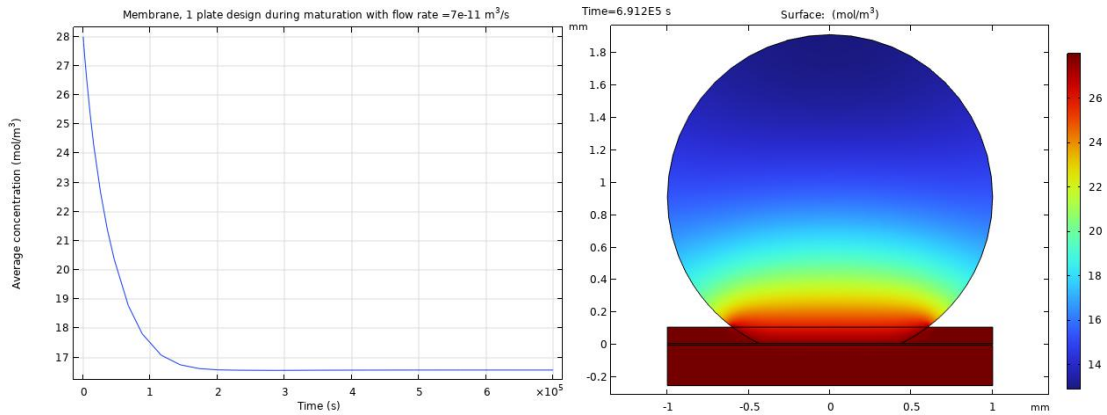


Figure 4.4: Average concentration in the tissue and cutplane of surface concentration after 8 days in the 1 plate membrane design with flow rate =  $7 \times 10^{-11} \text{ m}^3/\text{s} = 4.2 \mu\text{L}/\text{min}$ .

high (Figure 4.4a), which gives hope for this design. If we take a cut-plane in the middle of the tissue as we already did in Figure 3.9a we can observe, after more than a week, how the center of the organoid appears less nourished (Figure 4.4b). In the simulation we just assumed the tissue to be close to the walls, which gives a slightly lower concentration in the fluid at the top, but even if there was more space at the edges for the medium to refurbish everywhere, the situation would be pretty similar. A more realistic approach will be taken further down in the analysis, while this still stands as a valuable result on its own. Obviously we can see here how a bigger tissue could impact significantly the concentration gradient all over, however some suggestions to combat this will be shown later.

During maturation the same flow rate was used, as it proved itself to be good enough and the results in Figure 4.5a were really nice, even though there is a slower plateau and an overall lower average concentration value as expected. Differently from the growth phase, during maturation the membrane design has a lower average concentration than the holes design. It may be that having a higher flow rate in the plate, the membrane is able to let through less nutrients, which are more easily transported away by the flow. So, whereas with the medium all around the nutrients are more likely to feed the tissue, when it is just a thin layer it is not the same. The cutplane in Figure 4.5b now shows another problem of the maturation phase: not only is the core less fed, but also the top of the tissue shows a particularly lower value of concentration than the rest. The gradient here is far more clear and justifies the inferior value of average concentration.



(a) Average concentration in the organoid. (b) Concentration along the xz-cutplane.

Figure 4.5: Average concentration in the tissue and cutplane of surface concentration after 8 days in the 1 plate membrane design with flow rate =  $7 \times 10^{-11} \text{ m}^3/\text{s} = 4.2 \mu\text{L}/\text{min}$  during maturation.

## 4.2 5 plates design

These simulation were quite complex and elicited the need for a mesh adjustment: defining a user-controlled mesh with coarser medium and holes/membrane, extra coarse tissue and the rest extremely coarse allowed the simulations to run for a shorter time.

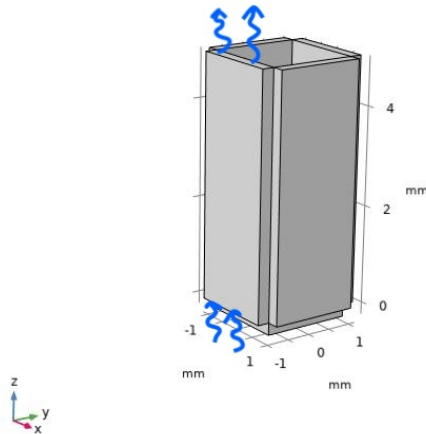


Figure 4.6: Depiction of the flow direction in the side walls.

In these structures each of the side walls has an inlet on the bottom and an outlet at the top, as seen in Figure 4.6, which makes it a very complicated design to reproduce

practically. However we were particularly interested in seeing how it would work and decided to go on with simulating it anyway. Obviously we still have the same flow in the bottom plate as it was in Figure 4.1. Each inlet will have the same flow rate for simplicity’s sake and as we will see the flow rates have increased an order of magnitude because now there is a more complex diffusion-convection coupling

### 4.2.1 Holes design

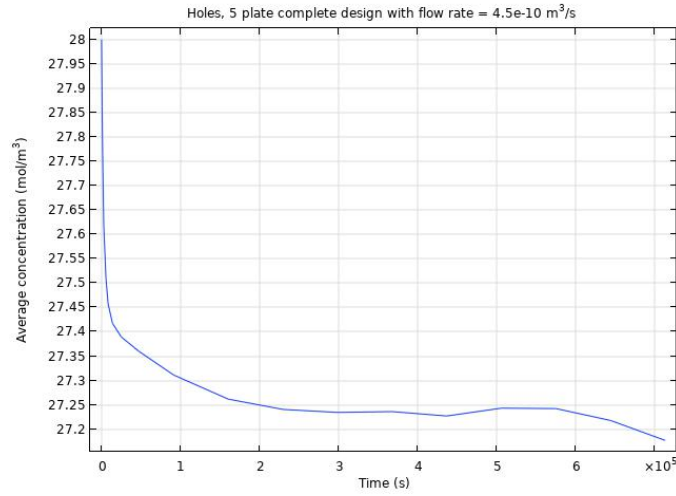


Figure 4.7: Average concentration in the organoid in the 5 plates holes design with flow rate =  $4.5 \times 10^{-10} \text{ m}^3/\text{s} = 27.0 \mu\text{L}/\text{min}$ .

It was extremely difficult to get a constant behaviour of average concentration going through the days, but for the growth stage the value of flow rate we ended up choosing was  $27.0 \mu\text{L}/\text{min}$ . Looking at the average concentration in Figure 4.7 we can notice that, even if it is not as stable as we would like, the variation in value is extremely small. Because of this we can accept this result as it was found to not be a mesh artifact. To be thorough we decided to investigate how the trend was after 2 months and the result is a quite unstable behaviour but overall the values of concentration is kept high enough for the tissue to survive that long.

The same can be said for the maturation phase: with the aforementioned flow rate the average concentration in Figure 4.8 does not reach a steady state in time, but the values remain in an acceptable interval and it seems better than the growth stage in terms of linearity.

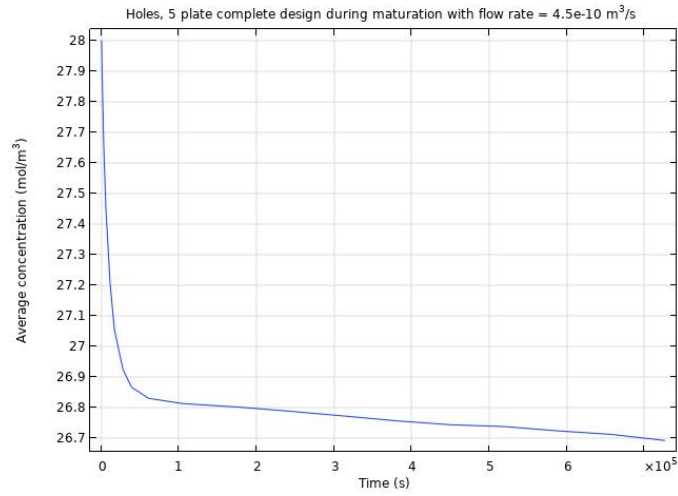
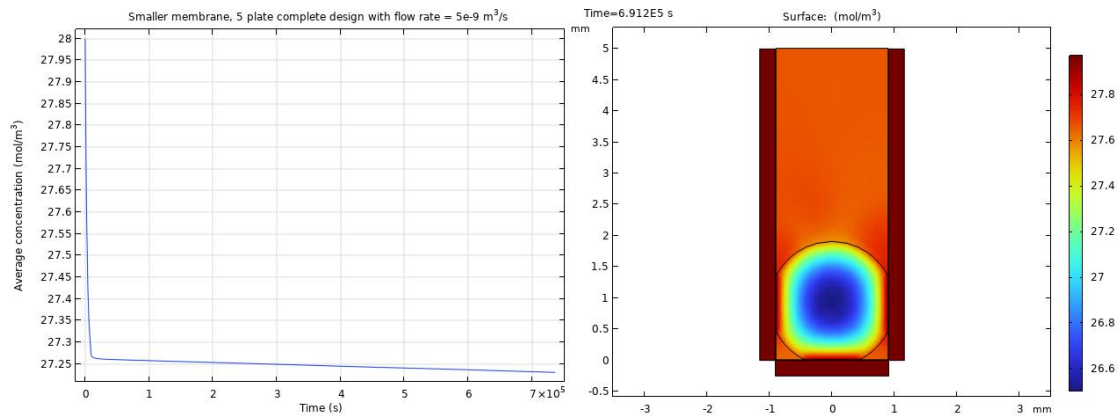


Figure 4.8: Average concentration in the organoid in the 5 plates holes design with flow rate =  $4.5 \times 10^{-10} \text{ m}^3/\text{s} = 27.0 \mu\text{L}/\text{min}$  during maturation.

### 4.2.2 Membrane design

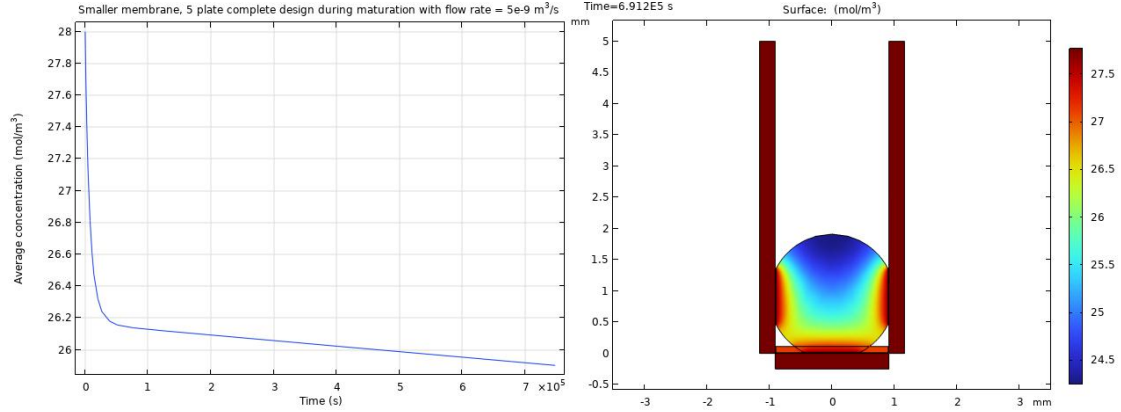


(a) Average concentration in the organoid. (b) Concentration along the xz-cutplane.

Figure 4.9: Average concentration in the tissue and cutplane of surface concentration after 8 days in the 5 plates membrane design with flow rate =  $5 \times 10^{-9} \text{ m}^3/\text{s} = 300.0 \mu\text{L}/\text{min}$ .

This design works a lot better than the holes design, but as for the 1 plate ones it requires a higher inlet flow rate. This has to be taken into account when considering the medium usage per minute and its cost, since the flow rate found for both growth and maturation is  $300.0 \mu\text{L}/\text{min}$ . During growth we get a good result in Figure 4.9a since the behaviour, even if slightly decreasing, is still varying between very close

number and especially with this design it is no longer unstable. Also looking at the cut plane in Figure 4.9b we get a sense of the concentration gradient in the tissue, which, differently from the 1 plate design in Figure 4.4b, has higher core concentration: this is mainly due to the support from the side walls which supply more nutrients. However the average concentration is more or less the same.



(a) Average concentration in the organoid. (b) Concentration along the xz-cutplane.

Figure 4.10: Average concentration in the tissue and cutplane of surface concentration after 8 days in the 5 plates membrane design with flow rate =  $5 \times 10^{-9} \text{m}^3/\text{s} = 300.0 \mu\text{L}/\text{min}$  during maturation.

During maturation the curve in Figure 4.10a falls faster however that was the best we could get since it will still work well for a long time. From the cross section in Figure 4.10b we can see that the core has a slightly lower concentration, but the side walls help greatly with keeping it higher than what we previously observed in this phase (see Figure 4.5b) and this also stands for the concentration at the top of the tissue. So the main advantages of this complicated design come during the maturation stage, rather than in growth, where the medium can very well supply the tissue on his own.

### 4.3 Study on the porosity of the membrane

Our goal in this section was to see if playing with the porosity of the membrane we were able to use this design with the same flow rates as for the holes design. The purpose of this was to see if we managed to save medium since the membrane design requires more fluid and could possibly be more expensive in the long term. The results were not as promising as we expected, because there is more to consider.

### 4.3.1 1 plate design

We aim at finding the porosity to obtain constant average concentration with a flow rate of  $2.1\mu\text{L}/\text{min}$  at the inlet. Despite our best effort we were not able to find a suitable value for the growth phase and whatever we chose the curve did not change much with respect to this with the original 47.8% (seen in Figure 4.11a). This is probably because the bottom plate has to replenish both the tissue and the whole column of medium, which makes this flow rate is too low.

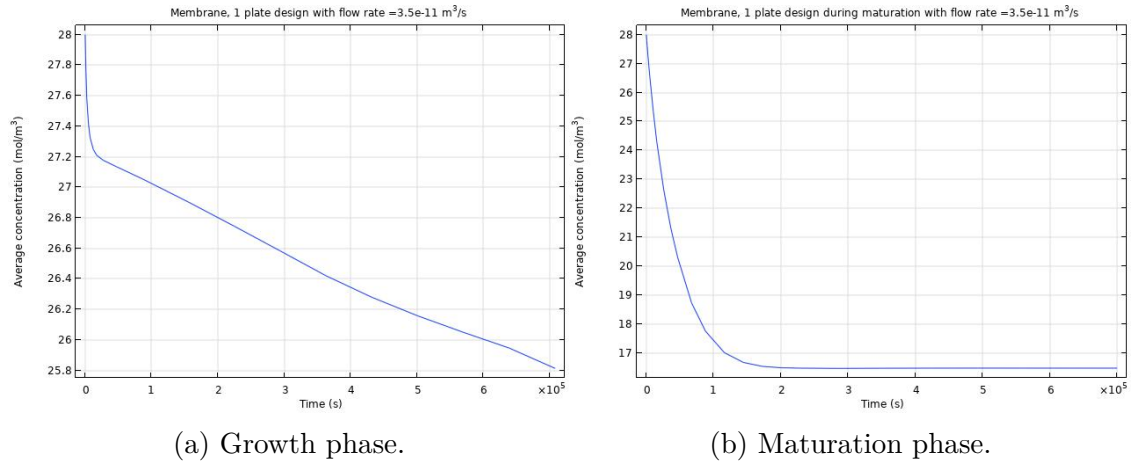


Figure 4.11: Average concentration in the organoid in the 1 plate membrane design with flow rate =  $2.1 \times 10^{-10} \text{m}^3/\text{s} = 2.1\mu\text{L}/\text{min}$  in growth and maturation phase with porosity 47.8%.

During maturation instead we found that this flow rate was good enough even with the original porosity value, as we can see from the nice plateau in Figure 4.11b. In this case the reservoir only has to refurbish with nutrients the tissue and a thin layer of medium, which is why this flow rate is enough.

### 4.3.2 5 plates design

The objective here is finding the best porosity to get a constant average concentration with the inlets' flow rate equal to  $27.0\mu\text{L}/\text{min}$ . If we look at the average concentration during growth with the usual porosity (Figure 4.12a) it has a clear downwards slope that we want to prevent. Increasing the porosity more only improves the concentration value overall it but it does not change the slope. With 70% porosity (Figure 4.12b) it seems good enough to withstand for longer periods of time, especially since even in Figure 4.9a it was not perfectly constant. This works better probably because we have more walls to help replenish both the tissue and the whole medium volume.

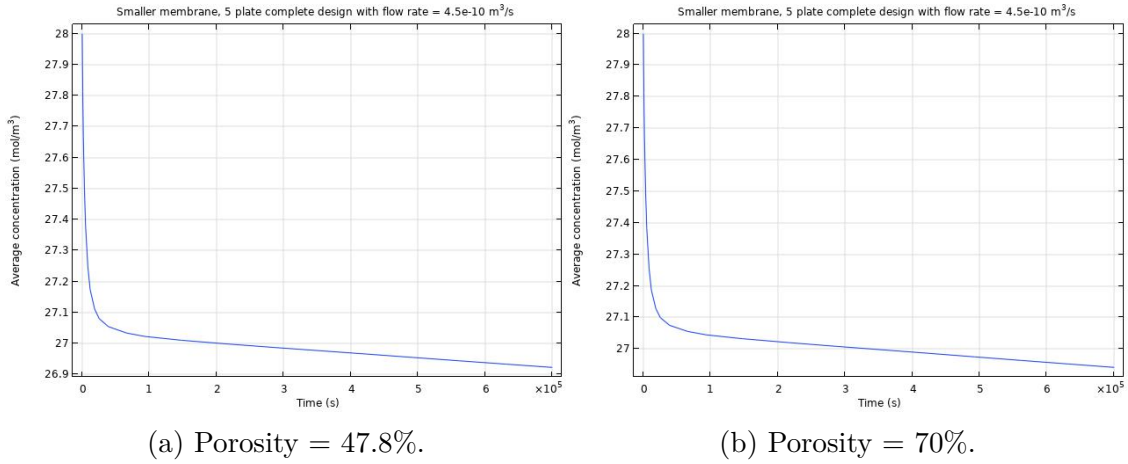


Figure 4.12: Average concentration in the organoid in the 5 plates membrane design with flow rate =  $4.5 \times 10^{-10} \text{ m}^3/\text{s} = 27.0 \mu\text{L}/\text{min}$  with two values of porosity.

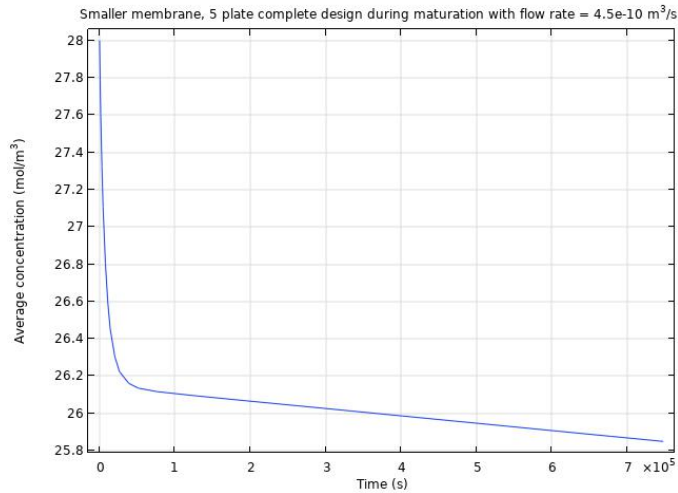


Figure 4.13: Average concentration in the organoid in the 5 plates membrane design with flow rate =  $4.5 \times 10^{-10} \text{ m}^3/\text{s} = 27.0 \mu\text{L}/\text{min}$  with porosity 70% during maturation.

And as expected also during maturation these values work well enough for us (Figure 4.13) as they did in the 1 plate design and for the same reasons. As a conclusion, this analysis was done mainly to see which parameter we were able to tweak and what would the results be, especially since practically it was still not clear what membrane porosity we would be working with. This demonstrates that any choice can be tailored to the needs and the resources at ones disposal and that there is no one way to approach these designs.

## 4.4 Concentration analysis

Since our main objective will be fabricating membrane systems, we decided to better investigate the right value for the inlet flow rate in this setup. This was found analyzing the average concentration of the tissue after each day in a week to observe when it would plateau. By doing so we would be seeing what is the lowest possible flow rate with which we can get a high enough value of average concentration that would be more or less constant from then on. This means that using any flow rate value over this hypothetical one is wasteful because the concentration value will not change significantly. We have observed that the faster in the week that we want to reach this ideal concentration value, the higher is the flow rate needed. Here we will now show the results of these concentration analyses only considering the seventh day, which as we saw in previous sections is a good time frame to get a constant behaviour. Because we expect to use the device for long periods of time, waiting for a week for the concentration to stabilise is good enough with the prospect of saving medium.

### 4.4.1 1 plate design

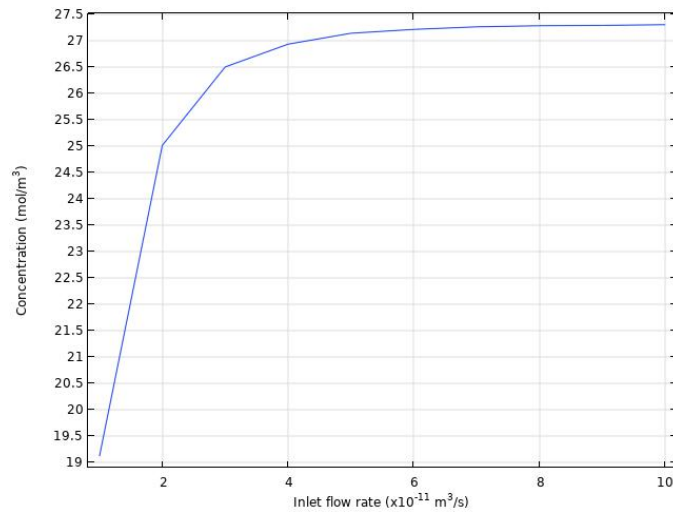


Figure 4.14: Average concentration in the organoid in the 1 plate membrane design as a function of inlet flow rate after 7 days.

We can note in Figure 4.14 that during growth in the course of a week a good plateau is reached starting from  $3 \times 10^{-11} \text{ m}^3/\text{s}$  or  $1.8 \mu\text{L}/\text{min}$ , so our previous find of  $4.2 \mu\text{L}/\text{min}$  was obviously good, but not as optimised from a waste point of view. During maturation the constant behaviour is not easily observed in Figure 4.15, but it is important to note that the values of concentration are so close here that

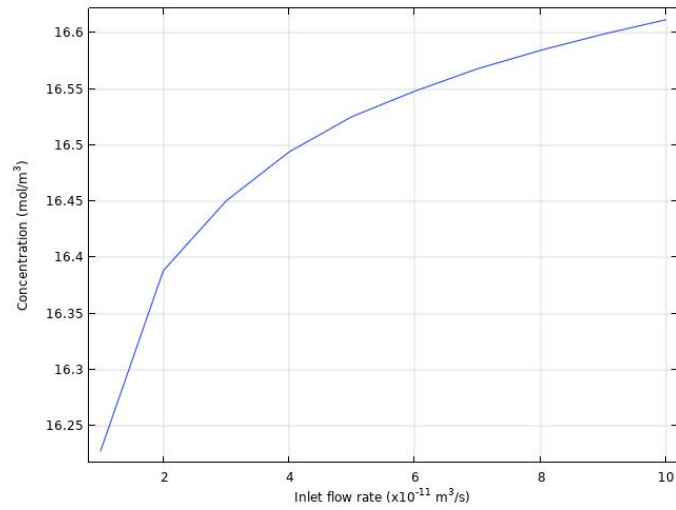


Figure 4.15: Average concentration in the organoid in the 1 plate membrane design as a function of inlet flow rate after 7 days during maturation.

we can determine that since  $3 \times 10^{-11} \text{ m}^3/\text{s}$  or  $1.8 \mu\text{L}/\text{min}$  any value is good enough, as in fact we saw previously.

#### 4.4.2 5 plates design

Let us remind you that now we are using a 70% membrane porosity to better compare our results and honour our previous analysis.

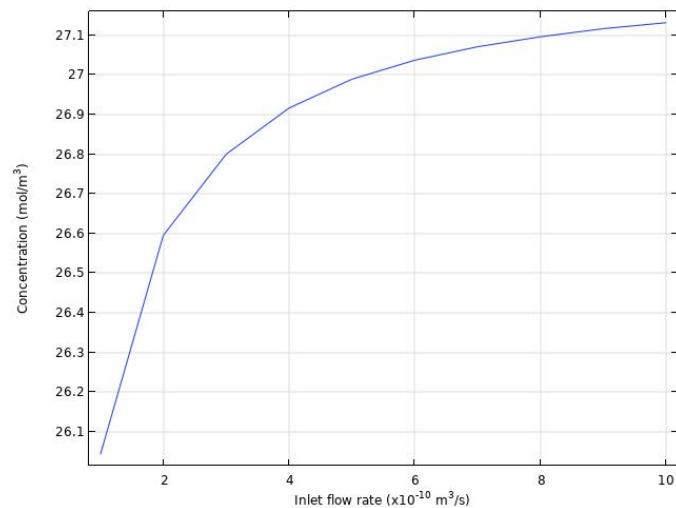


Figure 4.16: Average concentration in the organoid in the 5 plates membrane design as a function of inlets flow rate after 7 days.

During growth, as expected, it is not as constant as we would like it to be. However the variation has become quite small as we can see in Figure 4.16, especially after  $4 \times 10^{-10} \text{m}^3/\text{s}$  or  $24.0 \mu\text{L}/\text{min}$  which means that anything above that would be superfluous.

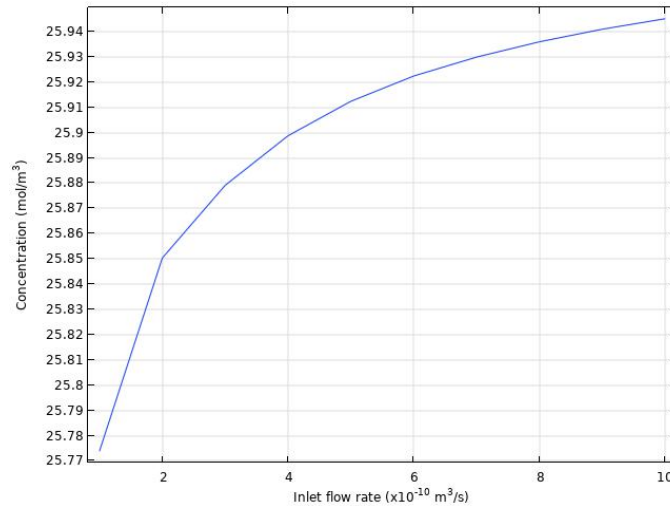


Figure 4.17: Average concentration in the organoid in the 5 plates membrane design as a function of inlets flow rate after 7 days during maturation.

During maturation the variations in concentration value are truly minimal (see Figure 4.17), so we could basically accept any value. Anyway for precision's sake we can say that above  $3\text{-}4 \times 10^{-10} \text{m}^3/\text{s}$  or  $18.0\text{-}24.0 \mu\text{L}/\text{min}$  we are in the best cases.

## 4.5 Needle and tubing simulations

Lastly we wanted to go back to a more realistic approach and explore ways to improve the 1 plate systems without introducing new reservoirs. Our tissue will be in a chamber apt for its growth, first we study it in growth phase and then maturation phase and look for ways to support it with nutrients up to its core. The tissue was now enlarged to a 3mm diameter sphere in order to challenge our model and see how such a small difference can impact the results that were previously very promising. The mesh is normal on the membrane, coarse in the tissue and coarser in the rest of the design.

We still have flow in the bottom plate, but we will be now introducing a tubing or needle system that will inject more diluted particles either in the medium environment or directly inside of the organoid. The size of these inputs has been simulated as that of a normal 30 gauge insulin needle, which means a diameter of 0.3mm, since it was the best choice for our small organoids. This model is equivalent to a tubing system where the liquid is pushed inside the same as a needle, so we

will use the two terms, "tubing" and "needle", interchangeably to describe the design. The membrane porosity was brought back to our original value of 47.8% and initially the concentration in the needle was set as the usual 28 millimolars for uniformity. For the needle simulation a realistic input flow rate is around 0.1mL/s[12] or  $1 \times 10^{-6} \text{m}^3/\text{s}$  for COMSOL or 60000 $\mu\text{L}/\text{min}$ .

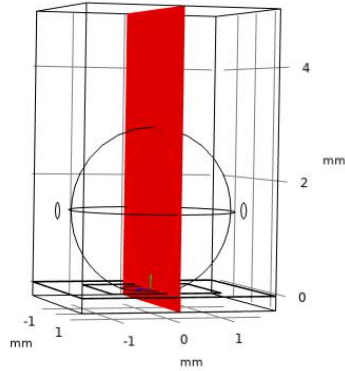
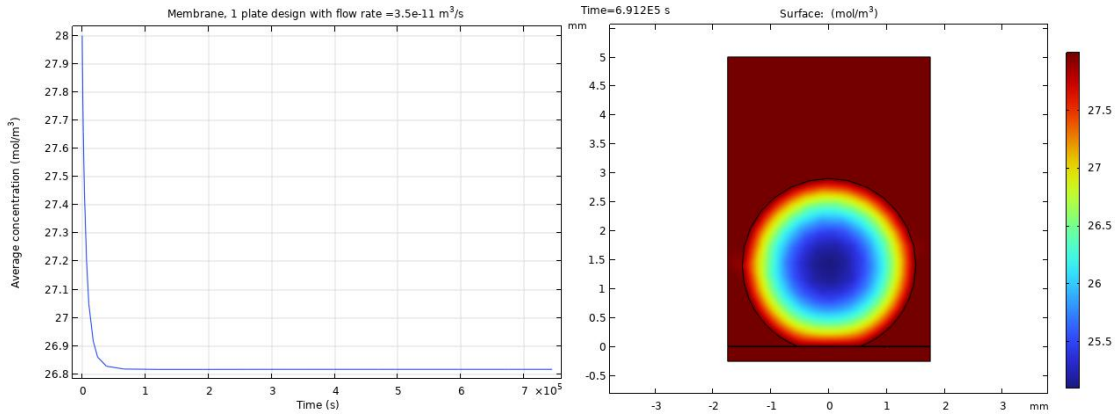


Figure 4.18: Plot of the chosen xz-cutplane at  $y = 0$ .



(a) Average concentration in the organoid. (b) Concentration along the xz-cutplane.

Figure 4.19: Average concentration in the tissue and cutplane after 8 days in the lateral perfusion design with plate flow rate =  $3.5 \times 10^{-11} \text{m}^3/\text{s} = 2.1 \mu\text{L}/\text{min}$  and needle flow rate =  $1 \times 10^{-6} \text{m}^3/\text{s} = 60000 \mu\text{L}/\text{min}$ .

For the growth stage we will be employing the previous parameters and the bottom plate flow rate will be taken from the minimum value found before:  $2.1 \mu\text{L}/\text{min}$ . Taking the cutplane in Figure 4.18, we can note that the tubing was put at half

the height of the tissue for the time being, but it was not that relevant. Also a zero pressure outlet was designed on the other side to have an exit for the medium without having to go through the membrane, keeping it at zero convection. As a result we get a high and perfectly constant average concentration as well as a very high core concentration as we can see in Figure 4.19. If we compare it with the cut plane of the previous, and smaller, tissue without tubing in Figure 4.4b, we can observe how the tubing greatly helps the design: in fact the core concentration is quite high even if the organoid is bigger, which is exactly our goal. However differently from what we observed in paper [6], we found that more input channels were not helping the diffusion to the core, probably because in the paper they did not have the help from the lower plate which is much more impressive. For this reason we limited ourselves to only one inlet, which was actually even easier to fabricate.

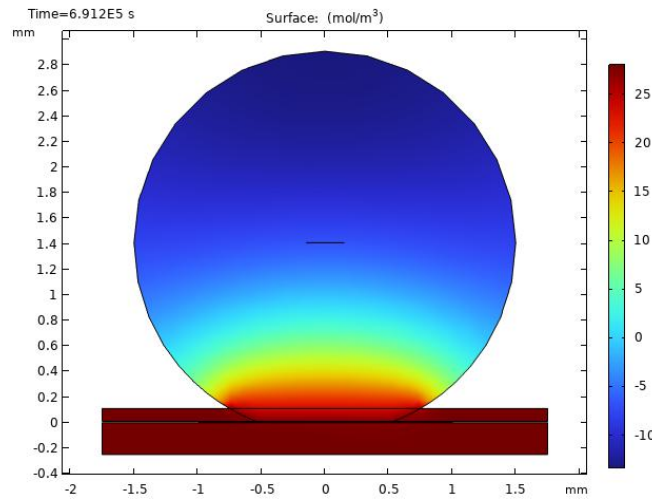
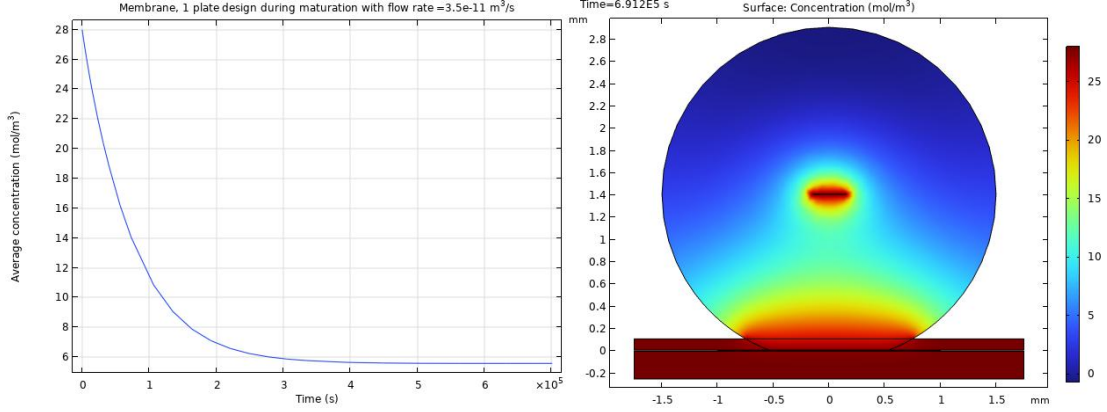


Figure 4.20: Cutplane concentration after 8 days with plate flow rate =  $3.5 \times 10^{-11} \text{ m}^3/\text{s} = 2.1 \mu\text{L}/\text{min}$  and no needle flow rate during maturation.

However in the maturation phase, instead of pushing nutrients in the environment, since the medium is not enough, we will be puncturing the tissue with a needle and directly feeding it from the inside. The simulation does not take into consideration the space taken by the needle, but models it as a simple input with a diluted species inflow and a liquid medium inlet. The only outlet here is the one in the bottom plate, which is extremely relevant. A crucial parameter is the height at which we will insert the needle especially with this organoid size. As we can see from the cutplane in Figure 4.20, the top of the organoid would be completely devoid of nutrients if we cannot manage to help with the injection. The negative concentration is of course non-physical, but purely mathematical: this means the organoid would die way before the eighth day due to lack of nutrients. Here the stark difference between

a 2 and 3 millimeters tissue is clear and it is why investigating a bigger one was necessary to actually tackle the problem.



(a) Average concentration in the organoid. (b) Concentration along the xz-cutplane.

Figure 4.21: Average concentration in the tissue and cutplane after 8 days in the top needle design with plate flow rate =  $3.5 \times 10^{-11} \text{ m}^3/\text{s} = 2.1 \mu\text{L}/\text{min}$  and needle flow rate =  $1 \times 10^{-6} \text{ m}^3/\text{s} = 60000 \mu\text{L}/\text{min}$  injected at  $z = 1.41$ .

When we actually push nutrients in from a needle inserted from the top, the liquid has no output, other than the one in the bottom plate. For this reason it will be forced to go through the membrane, having to solve the Navier-Stokes equation considering also convection in it. When dealing with convection in a porous medium, we have to take into account the Darcy number which helps including a damping factor in the flow velocity. So in the simulation we had to add the membrane domain to the Laminar Flow solution and couple it with the Transport of Diluted Species through the convection velocity solved in the former study. By doing so we will introduce a volume force in the membrane domain described as  $\mathbf{F} = -\alpha \cdot \mathbf{u}$ . The parameter  $\alpha$  can be found through the Darcy number, which represents the relation between the permeability of the medium and its cross-sectional area. This Darcy number can be defined as

$$Da = \frac{\eta}{\alpha \cdot L^2} \quad (4.1)$$

where  $\eta$  is the dynamic viscosity of the fluid and  $L$  is the characteristic length of the system. In our design we use the viscosity of water,  $1 \text{ mPa}\cdot\text{s}$ , and the characteristic length is the thickness of the membrane,  $10 \mu\text{m}$ . The Darcy number can be assumed to be  $10^{-4}$ [13] and as a result the factor  $\alpha$  is found to be  $10^{11} \text{ kg}/\text{m}^3\cdot\text{s}$  and introduced in the simulation. After we had introduced this element to the simulation we did not observe visible changes, however at the time we failed to notice it and we forgot to include this volume force inside of the tissue as well. We later found that the

permeability ( $\chi$ ) of brain tissue is on the scale of  $10^{-16}\text{m}^2$ [14], which with a tissue of 3mm of diameter gives a Darcy number of

$$Da = \frac{\chi}{d^2} \approx 10^{-11} \quad (4.2)$$

which characterises a semi-pervious material. In the future it would be necessary to include this analysis and it could also improve the results since a convection in the tissue should move the nutrients faster than simple diffusion, so for now keep this in the back of your mind. The mesh here was pushed to coarse everywhere, but normal in the tissue and fine in the membrane to help compute the volume force. If we insert the needle in the middle, as shown in Figure 4.21b, we would not be helping with the top concentration as much as we would need and therefore the overall average concentration (Figure 4.21a) is quite low.

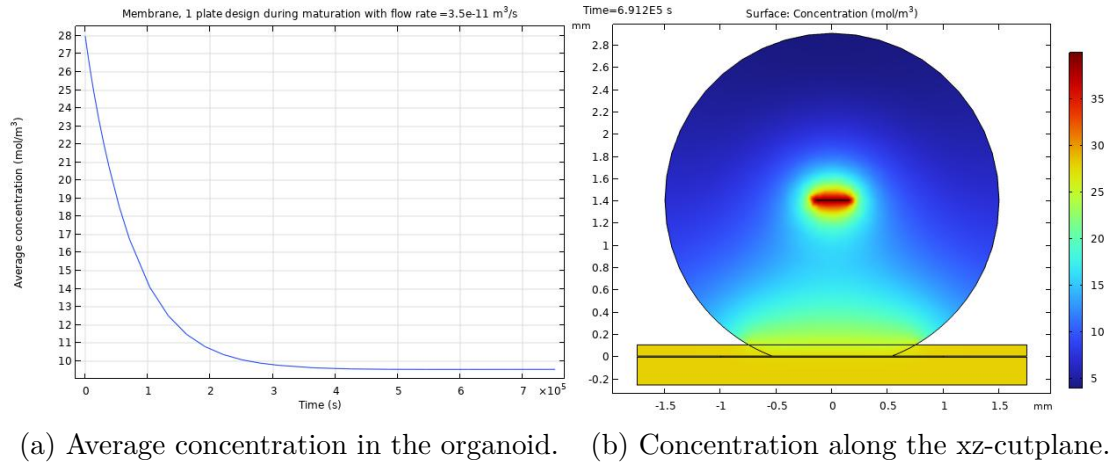
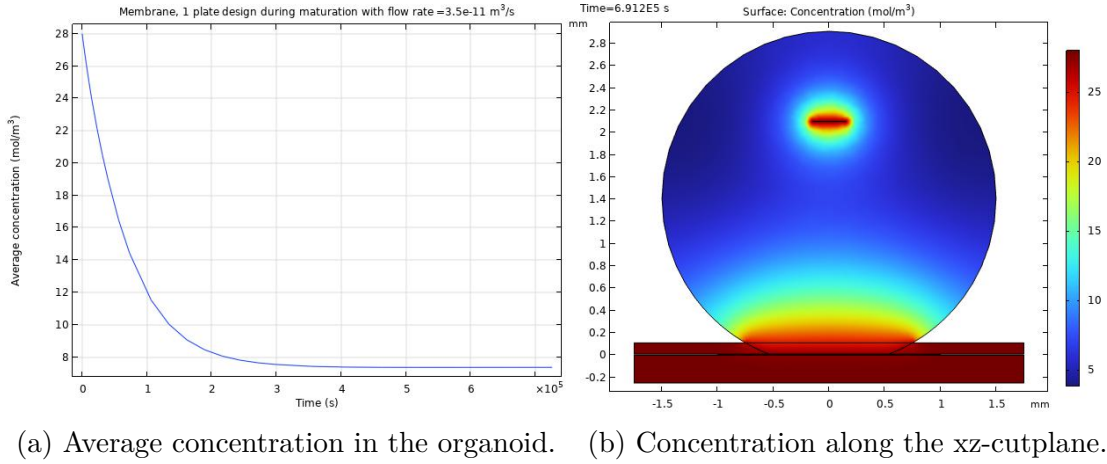


Figure 4.22: Average concentration in the tissue and cutplane after 8 days in the top needle design with plate flow rate =  $3.5 \times 10^{-11}\text{m}^3/\text{s} = 2.1\mu\text{L}/\text{min}$  and needle flow rate =  $1 \times 10^{-6}\text{m}^3/\text{s} = 60000\mu\text{L}/\text{min}$  injected at  $z = 1.41$ . Needle inflow concentration = 40 millimolar.

If we increase the needle flow rate nothing changes, but if we arbitrarily increase the concentration of dilute species in the needle from 28 to 40 millimolar we get some better results. By looking at Figure 4.22, the average concentration has slightly increased to a better value as expected, however the problem of the concentration on the upper part of the tissue remains.

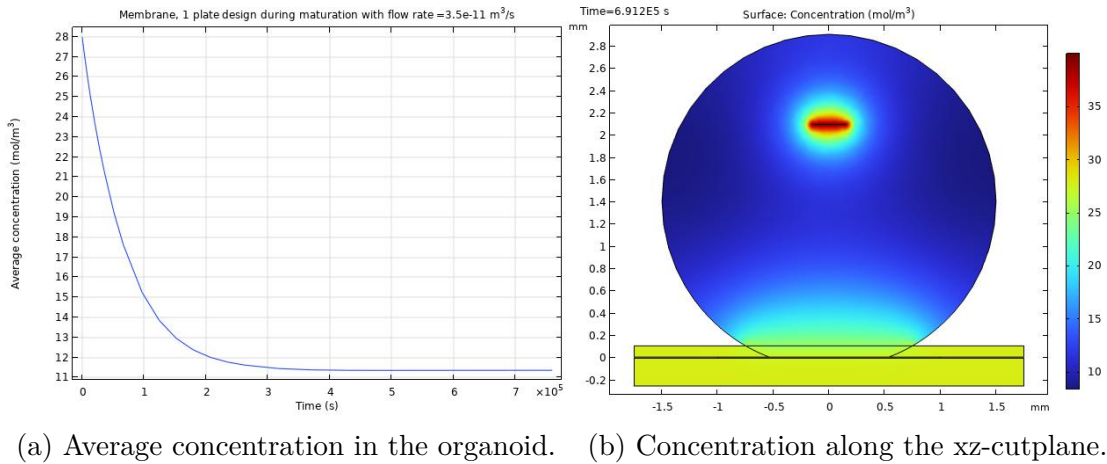
To solve it we can try inserting the needle more towards the top of the organoid and let the diffusion do the rest. The coordinate  $z = 2.1$  was found to be the best height because it left some space around the needle to let diffusion help with homogenizing the concentration. Here the concentration was put back to 28 millimolar and comparing it with the previous one (Figure 4.21) we can see the slight improvement in both average concentration and concentration distribution in Figure 4.23. With



(a) Average concentration in the organoid. (b) Concentration along the xz-cutplane.

Figure 4.23: Average concentration in the tissue and cutplane after 8 days in the top needle design with plate flow rate =  $3.5 \times 10^{-11} \text{ m}^3/\text{s} = 2.1 \mu\text{L}/\text{min}$  and needle flow rate =  $1 \times 10^{-6} \text{ m}^3/\text{s} = 60000 \mu\text{L}/\text{min}$  injected at  $z = 2.1$ .

this configuration the core will have lower concentration of nutrients, but overall the tissue will be more likely to survive.

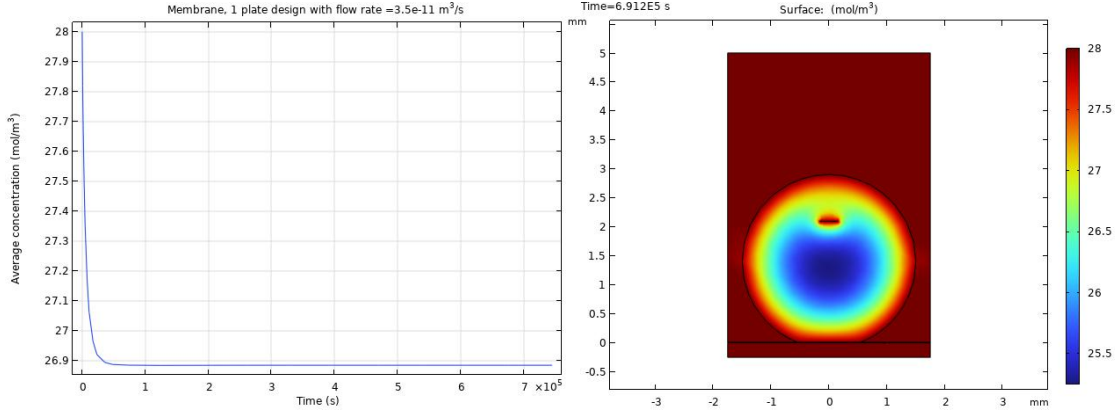


(a) Average concentration in the organoid. (b) Concentration along the xz-cutplane.

Figure 4.24: Average concentration in the tissue and cutplane after 8 days in the top needle design with plate flow rate =  $3.5 \times 10^{-11} \text{ m}^3/\text{s} = 2.1 \mu\text{L}/\text{min}$  and needle flow rate =  $1 \times 10^{-6} \text{ m}^3/\text{s} = 60000 \mu\text{L}/\text{min}$  injected at  $z = 2.1$ . Needle inflow concentration = 40 millimolar.

If we increase again the needle nutrients' inflow to 40 millimolar obviously the situation improves even more (Figure 4.24). Consequently it depends on what the research requires, either high average concentration or core concentration. Also since we are dealing with millimeters dimensions it is relevant to note that the

precision needed for a manual insertion of the needle is quite high, so we will never be sure how far we are inserting the needle unless we take the necessary precautions. As a last experiment on the matter we decided to see what would happen in the growth phase if we combined tubing and the needle insertion and if we could help the inner concentration even more. The needle inflow rate is still  $60000\mu\text{L}/\text{min}$  and the diluted species' concentration is 28 millimolar in both the lateral and the top needle.



(a) Average concentration in the organoid. (b) Concentration along the  $xz$ -cutplane.

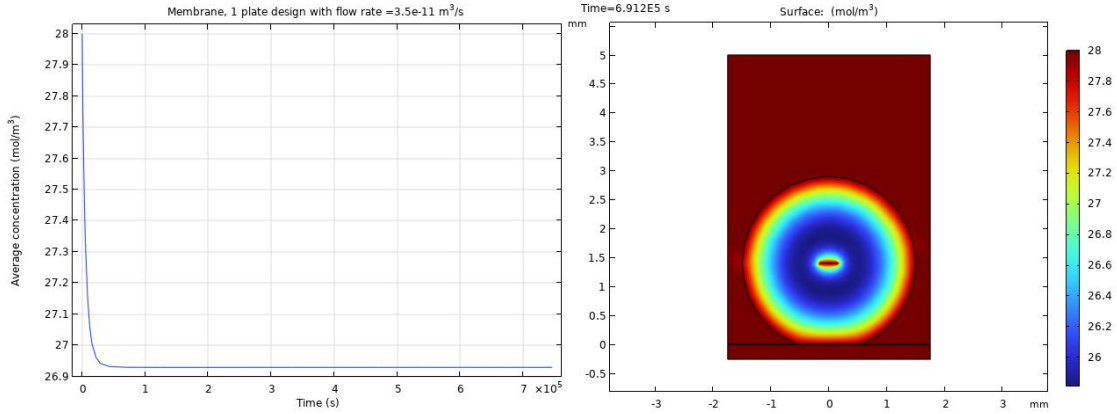
Figure 4.25: Average concentration in the tissue and cutplane after 8 days in the lateral perfusion and top inserted needle design with plate flow rate =  $3.5 \times 10^{-11}\text{m}^3/\text{s} = 2.1\mu\text{L}/\text{min}$  and needle flow rate =  $1 \times 10^{-6}\text{m}^3/\text{s} = 60000\mu\text{L}/\text{min}$  injected at  $z = 2.1$ .

If we leave the needle input at the height of  $z = 2.1$  we observe how the average concentration has trivially improved, benefiting from the new nutrients input, but the core still has the same concentration (Figure 4.26). This is because due to the presence of the medium all over the organoid the sides are well fed and the only issue is the middle. For this reason in this case a better design would have the needle more towards the center of the tissue at  $z = 1.41$ .

In fact if we do so we can observe how both the average concentration and the core concentration improve (see Figure 4.26), compared to the previous design without the needle in Figure 4.19b. Again a case can be made for increasing the nutrients concentration in the needle, but as for the previous analysis, by doing so the overall concentration would increase but there would be nothing more to note.

## 4.6 Bottom plate channel

As a final simulation we decided to investigate a possible design for the bottom plate flow, more specifically in the case where in the future we would be growing more



(a) Average concentration in the organoid. (b) Concentration along the xz-cutplane.

Figure 4.26: Average concentration in the tissue and cutplane after 8 days in the lateral perfusion and top inserted needle design with plate flow rate =  $3.5 \times 10^{-11} \text{ m}^3/\text{s}$  =  $2.1 \mu\text{L}/\text{min}$  and needle flow rate =  $1 \times 10^{-6} \text{ m}^3/\text{s}$  =  $60000 \mu\text{L}/\text{min}$  at  $z = 1.41$ .

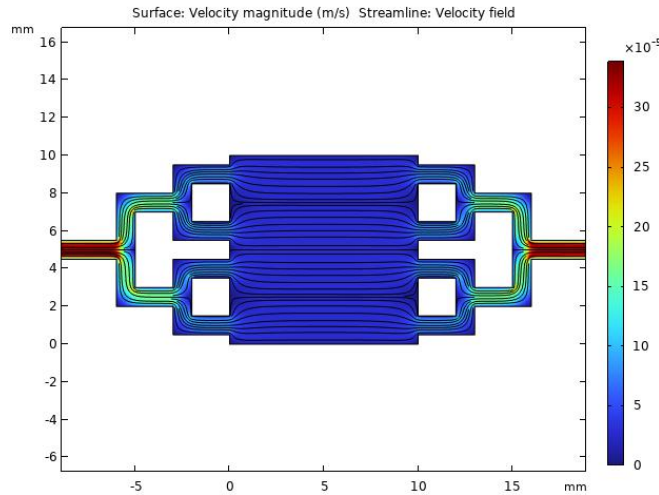


Figure 4.27: Velocity streamlines in the bottom plate channel in a 2D simulation with shallow channel approximation.

than one sample at a time. This was initially done as a 2D simulation with shallow channel approximation to test the equipartition of the flow in the big chamber, as we show in Figure 4.27. Aiming for uniformity and no vortices we finally chose this design with a fully developed flow at the inlet with flow rate  $4.2 \mu\text{L}/\text{min}$ . As we can see from the streamlines and the colour map the inlet flow rate is firstly halved and secondly halved once more. By doing so at each channel separation both parts would be fed an equal and well distributed amount of flow, and as a result so would

be the main chamber.

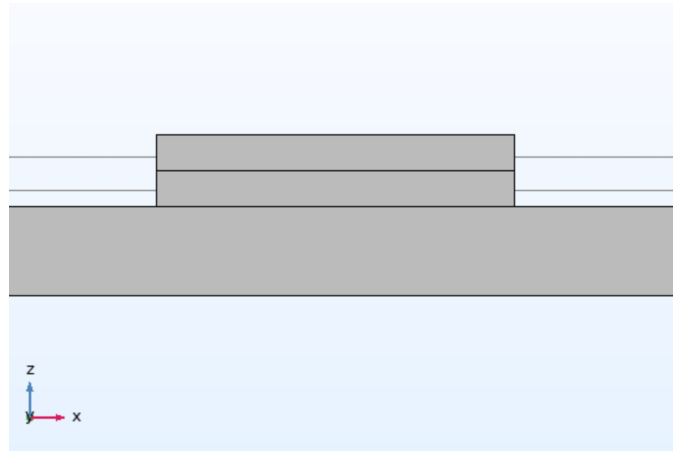
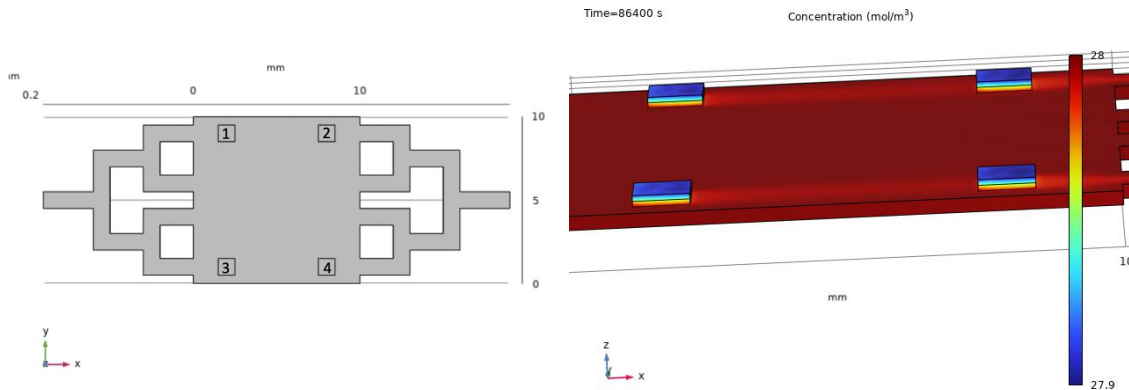


Figure 4.28: Lateral view of the bottom plate channel in a 3D simulation which shows the three layers: channel, membrane and tissue.

Now moving the design to a 3D simulation we will be studying how multiple tissues will behave in this same chamber, while sharing the nutrients source, and the best way to allocate them. The parameters that have been used are the same: initial 28 millimolar of nutrients all over; 47.8% of porosity in the membrane and 20% in the organoid; inlet flow rate is  $4.2\mu\text{L}/\text{min}$ ; for the reaction rate of the nutrients' consumption we used the growth one which is  $-3.2407 \times 10^{-4} \text{mol}/(\text{m}^3 \cdot \text{s})$ . The simulation was done for the duration of 1 day. The system has been simplified to act as an initial analysis in order to understand the basic concepts of this design and to investigate its simplest form. As we can see in Figure 4.28 the bottom part is the channel, the second layer is the membrane and the third one is a slice of tissue. We will now show some of the configurations we have simulated and the conclusions we drew from them.

### 4.6.1 First configuration

In our first design we chose a simple case of four organoids that need to be positioned in the chamber. The first configuration we chose was the obvious one in Figure 4.29a. As we can see from the simulation in Figure 4.29b the biggest problem we are going to face is what we will call a “shadowing effect”, where slices directly behind others in the nutrients' flow will receive less due to the first ones consuming them beforehand. From the probe plot in Figure 4.30 we can clearly see how tissues 2 and 4 lack some nutrients, even if for a small amount. Another nice result is that we can observe how after not even a day the concentration settles on a constant value, like we have previously found in the other membrane simulations.



(a) First tissue configuration geometry in the bottom channel.

(b) Concentration along the model's surface.

Figure 4.29: Geometry and surface concentration of the first tissue configuration with 4 slices.

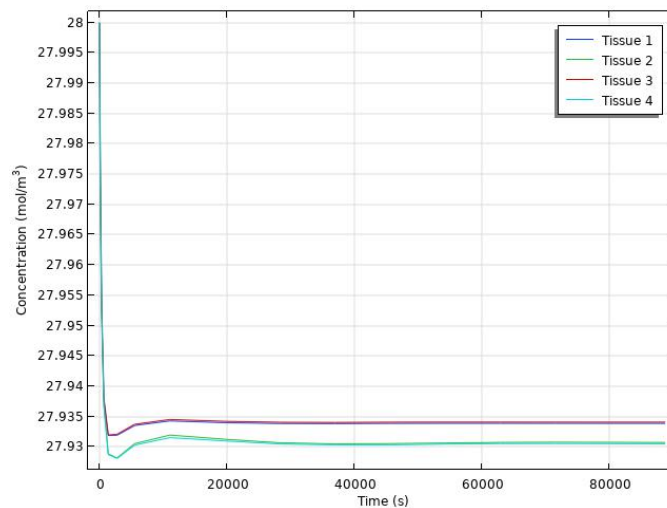
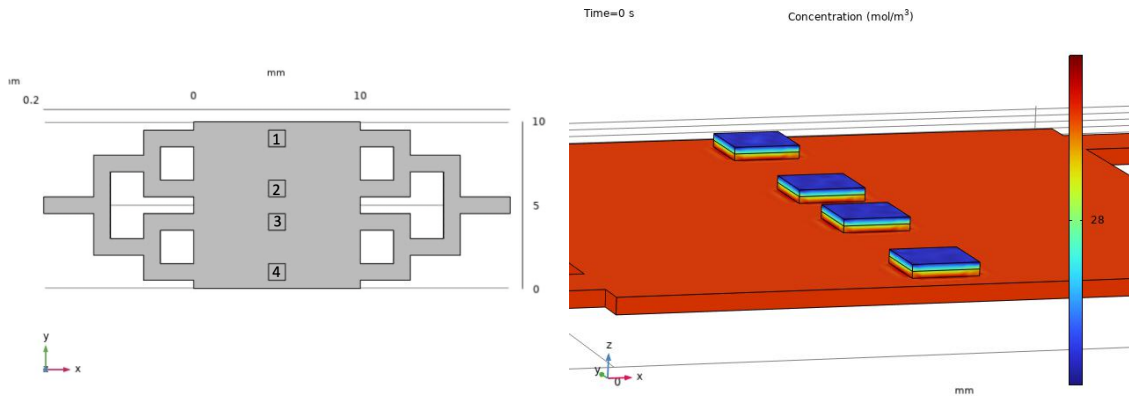


Figure 4.30: Average concentration in each of the 4 slices in the first configuration.

#### 4.6.2 Second configuration

To solve this problem we have to look for a tissue display that prevents the shadowing effect and with four slices it is quite easy. Our solution was to dispose them on a line as shown in Figure 4.31a so that no organoid was behind another and we can see that they all get the same average concentration in Figure 4.32. This solution is trivial and more difficult to achieve when the organoids become too big or we want to study more at once. This is why we decided to investigate also a more challenging situation with 9 tissue slices, where allocating them on a line was not possible.



(a) Second tissue configuration geometry in the bottom channel.

(b) Concentration along the model's surface.

Figure 4.31: Geometry and surface concentration of the second tissue configuration with 4 slices.

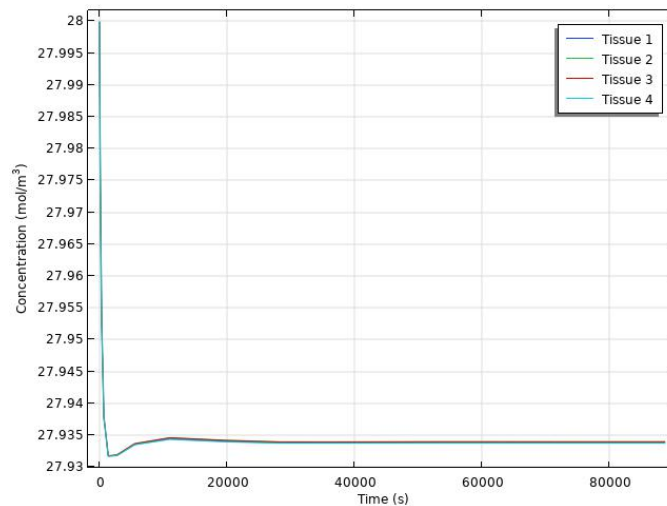
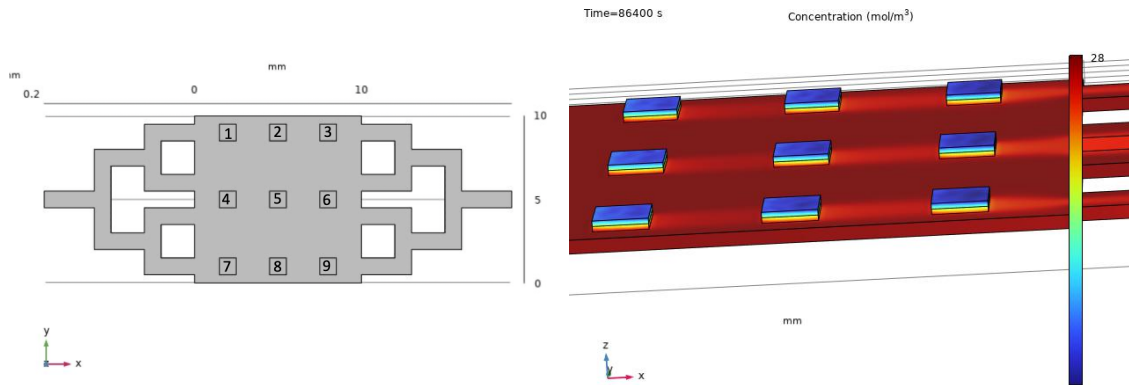


Figure 4.32: Average concentration in each of the 4 slices in the second configuration.

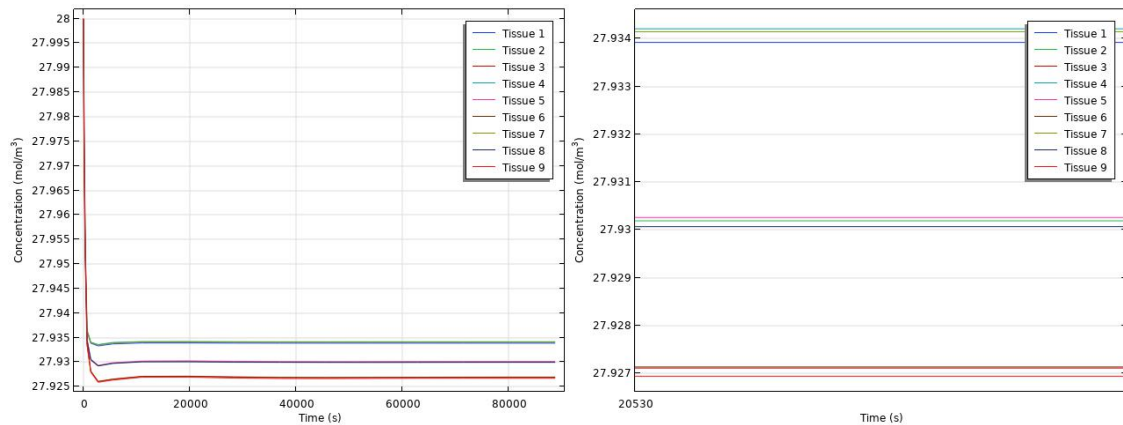
### 4.6.3 Third configuration

If we display the organoids as shown in Figure 4.33a the shadowing effect is easier to see and more prominent for the last column of organoids with respect to the second one (see Figure 4.34b). The difference is still small, but we can certainly improve the result still.



(a) Third tissue configuration geometry in the bottom channel. (b) Concentration along the model's surface.

Figure 4.33: Geometry and surface concentration of the third tissue configuration with 9 slices.

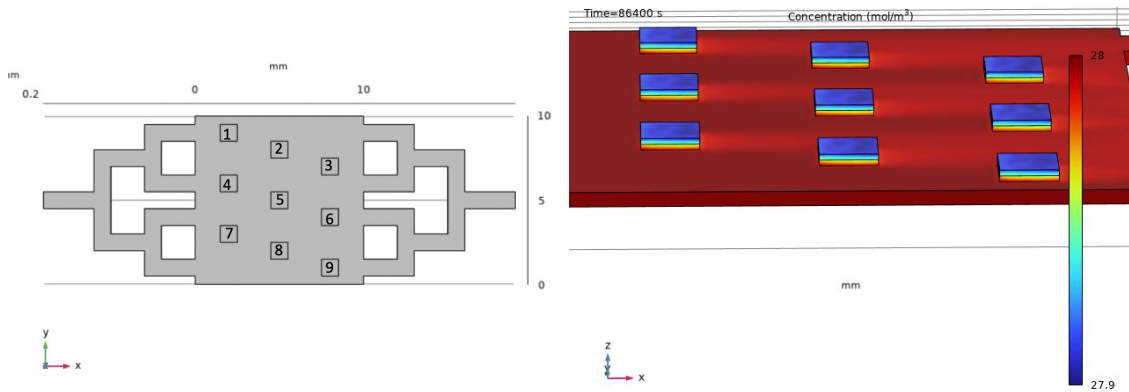


(a) Average concentration in each slice. (b) Zoom on the average concentration.

Figure 4.34: Average concentration and zoom of the plot in each of the 9 slices in the third configuration.

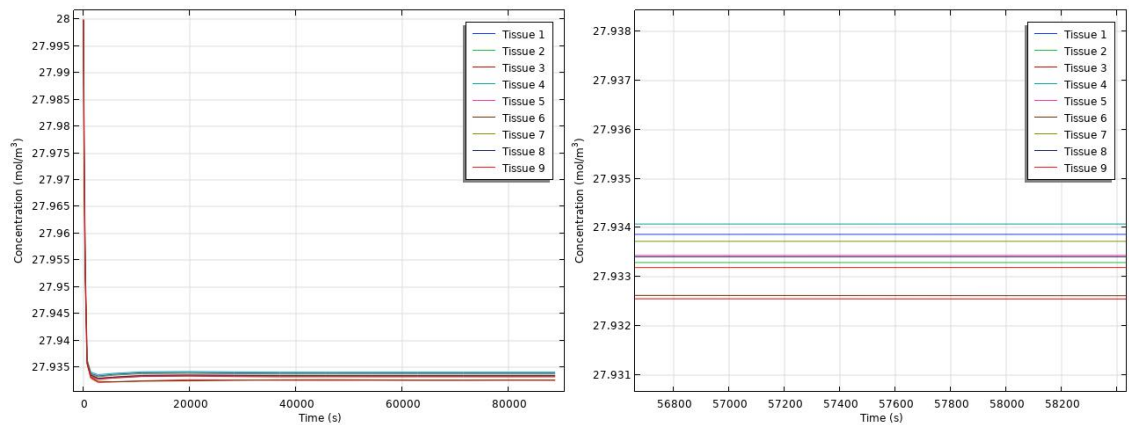
#### 4.6.4 Fourth configuration

Here in Figure 4.35a a solution was proposed that would minimise the shadowing effect, while still leaving enough space for each slice. We can analyse the system from the probe plot and, more specifically, the zoom in on such plot (Figure 4.36b). Tissues directly in front of the inlet, like 1 and 4, have the highest concentration and generally the closer to the center of the channel you are, like organoids in the second row (4, 5 and 6), the higher the concentration is with respect to the other rows. In fact putting both these observations together we can see that tissue 4 is the one with highest average concentration. Overall this design is good enough for



(a) Fourth tissue configuration geometry in the bottom channel. (b) Concentration along the model's surface.

Figure 4.35: Geometry and surface concentration of the fourth tissue configuration with 9 slices.



(a) Average concentration in each slice. (b) Zoom on the average concentration.

Figure 4.36: Average concentration and zoom of the plot in each of the 9 slices in the fourth configuration.

a generally well working chip, we would just have to make sure that the organoids do not overlap as much as possible in the flow stream to get the best out of the nutrients delivery.

## 4.7 Simulations summary

This concludes our simulation chapter, where we have discovered that we are able to replicate the original paper's design with a membrane that will deliver nutrients to the tissue through diffusion. Any design with flow in the plates will be more effective

than a static one in the long term, because it will require less manual medium change since the average concentration becomes more or less constant, leading to less possible damage the chip and the organoid itself. A 5-plates design would be great for the organoid since it would provide more nutrients and reach more areas of the tissue, battling the problem of core necrosis. However to be more realistic for the time we have for this thesis, we have found that using needles and lateral tubing is also a good solution, while being less heavy from the fabrication point of view as well. The design for the bottom plate will be used for our models since it works well enough as it is, but as we showed it could be taken into consideration even for future, more complex, developments.

**Part III**

**Fabrication tests**



## Chapter 5

# Laser ablation

In this part we will be discussing our steps to creating the designs that have been simulated up to now. At first in this chapter we will show how we fabricated the bottom plate channel with a CO<sub>2</sub> Desktop Laser Cutter, which will then be closed with the membrane and double sided tape. We will then describe how we modelled and built the top chamber with a filament 3D printer. The assembly will be better discussed later, but we have to make sure to align the two systems at the inlet, at the outlet and at the window for the chamber.



Figure 5.1: AEON MIRA5 CO<sub>2</sub> Desktop Laser Cutting Machine.

To start we designed an initial model for the bottom channel on Fusion 360 to get an idea of the dimensions and then recreated it in RDWorks V8 as shown in Figure 5.2. The software is connected to an AEON MIRA5 CO<sub>2</sub> Desktop Laser Cutting Machine, shown in Figure 5.1, that follows the exact design using the settings we define. Before delving into the final bottom plate design and fabrication we conducted a test to define which parameters suited our goals best. Keep in mind

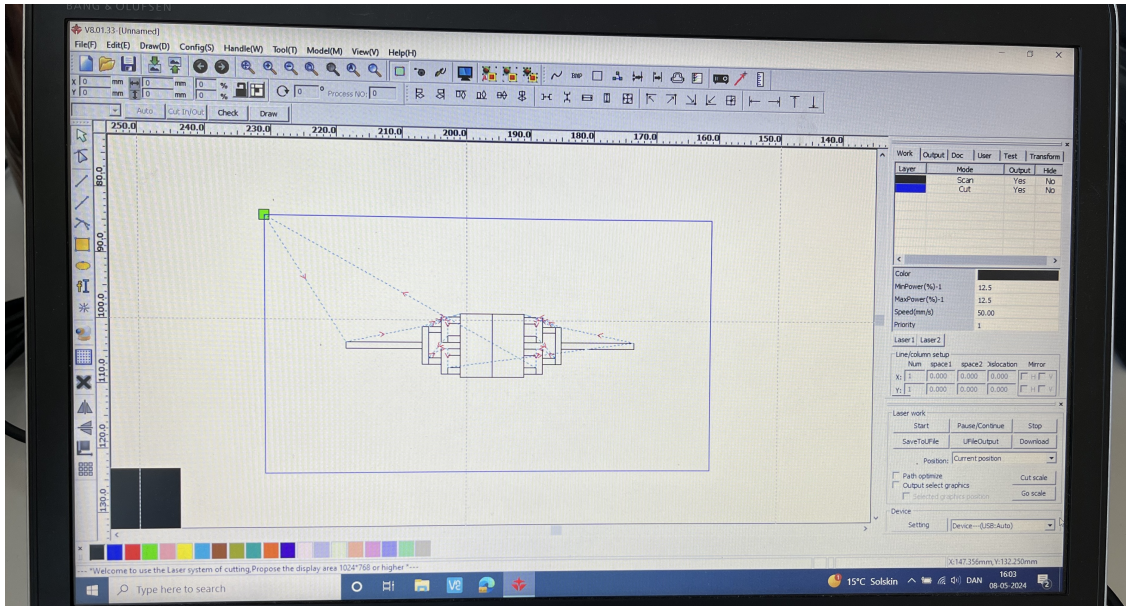
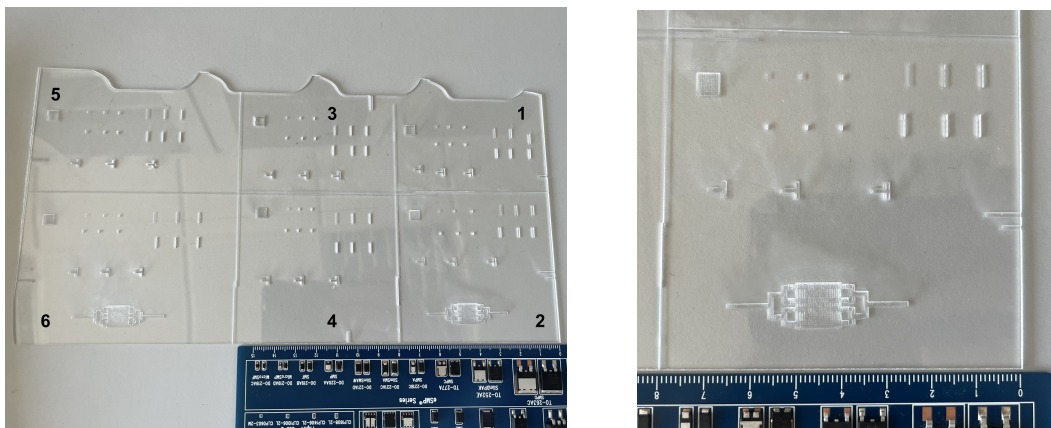


Figure 5.2: Bottom channel model recreated in RDWorks V8 to carve with the laser cutter on the PMMA.

that we want a channel that is approximately 0.5mm deep, so that it is closer to our simulations value, while still being relatively easy to fabricate. The main parameters we played with were laser power, cutting speed and how many times we went over the same spots.



(a) Laser cutter tests on PMMA divided in six sectors.

(b) Zoom on the laser cutter tests on the second sector.

Figure 5.3: Image of the PMMA piece over which we conducted some characterisation tests with the laser cutter.

In Figure 5.3a we can see 6 numbered sections that have been separated to better keep track of the settings changes. Each column has a different power setting, while the two rows have a different speed and it is summarised in the following table for an easier understanding.

	Power: 10%	Power: 12.5%	Power: 15%
Speed: 30 mm/s	Section 1	Section 5	Section 3
Speed: 50 mm/s	Section 2	Section 6	Section 4

Table 5.1: Laser power and speed settings for each section of the test PMMA piece.

Each section has been cut with the same designs for better comparison, aside for some small additions like the full channels done in sections 6 and 2. Looking at Figure 5.3b we can see on the top left a 5mm×5mm square done by raster scanning; next to it are six 1mm long lines where progressively we cut one more time with the laser up to six times; next to them we repeated the process with 5mm long lines; below the square we have 3 rotated "T" structures scanned increasingly 1, 2 and 3 times; finally on the edge we scanned a 10mm line to observe the cross section to get an initial idea of which setting was closer to giving us the needed depth. After doing so we used a Dektak 150 profilometer to characterise the cuts and choose which settings were more useful for our design.

## 5.1 Stylus profilometer characterisation

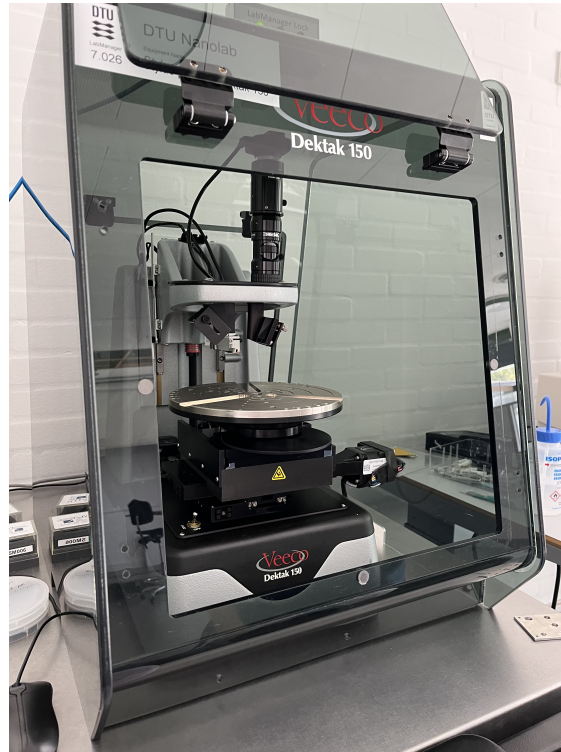


Figure 5.4: Dektak 150 stylus profilometer.

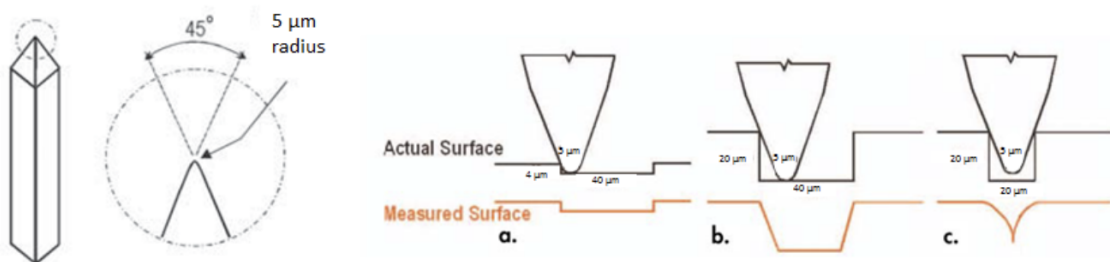
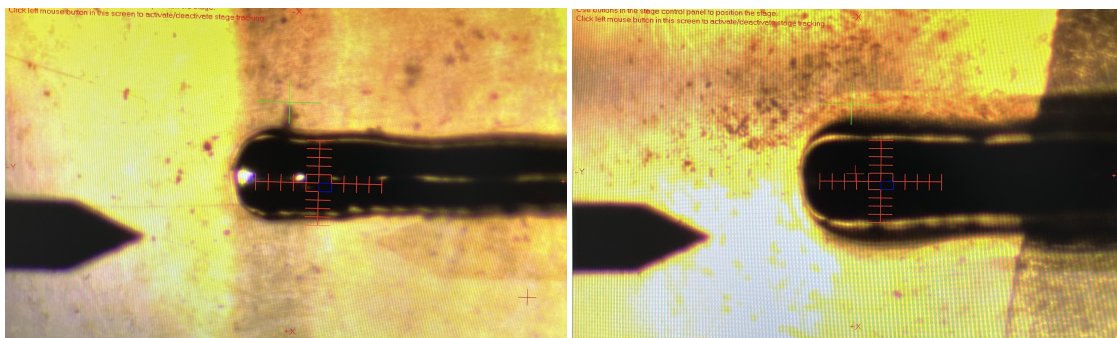


Figure 5.5: Geometry of the stylus tip and how this geometry affects the measurement accuracy depending on the shape of the structure we are studying.

In Figure 5.4 we can observe the machine we used to study our test pieces, with the center stage and the stylus tower. The stylus itself can be seen in Figure 5.5, which comes from the Dektak 150 manual provided by DTU. It has a radius of  $5\mu\text{m}$  and a standard force of  $3.00\text{ mg}$ , which was good enough for us not to scratch the PMMA. We made standard scans with the maximum vertical range of  $1000\mu\text{m}$ , which gives

a vertical resolution of ideally  $160 \text{ \AA}$ , however due to the vibrational noise of the stylus it is definitely worse. The machine was then calibrated and we began our analysis which will be summarised in the following sections. Keep in mind that we were not able to study the cross section of the 1mm lines in the different sectors because the aspect ratio between depth and width is greater than 1. So when we scanned perpendicularly to the line the geometry of the stylus did not fit correctly, due to the incompatibility of the structures that can be seen in Figure 5.5 image c, and the measurement was then inconsequential.

### 5.1.1 5 millimeters long lines



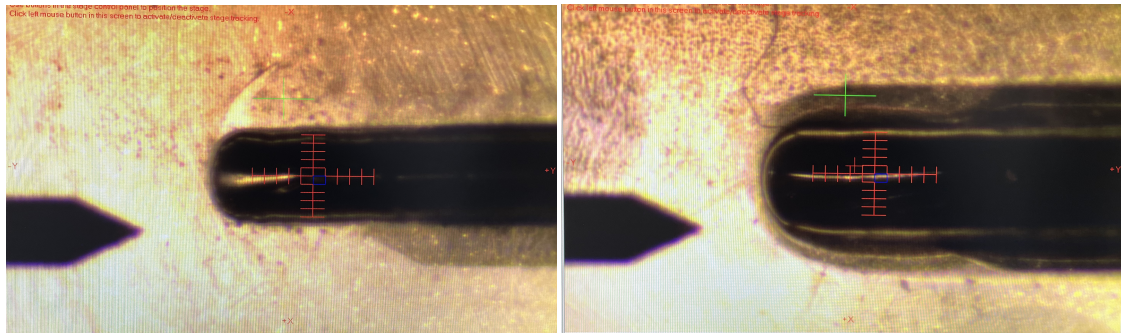
(a) Cut one time.

(b) Cut six times.

Figure 5.6: Image of the surface of the PMMA piece in section 2. The dark and pointy tip of the Dektak stylus can be seen on the left, the untouched surface is the yellow/brown part and on the right there is the beginning of the 5 millimeters lines cut respectively one and six times.

The 5mm long lines were studied to observe how much a line would blow out each time we passed on it. This analysis is completely qualitative, due to the stylus not fitting transversally in the line as previously stated, so we can only compare the camera images and use the red marker as a reference. First we can observe the results of the least damaging settings of section 2 (10% power and 50mm/s writing speed) in Figure 5.6, which is a view of the PMMA surface from the top: the dark pointy object on the left is the Dektak stylus, the black line on the right is the beginning of our 5mm line and the yellow and brown background is the untouched surface of the acrylic. We can see that the red cursor has 10 lines, so we can say that the line that has been cut 1 time is approximately 10% smaller than the one cut six times.

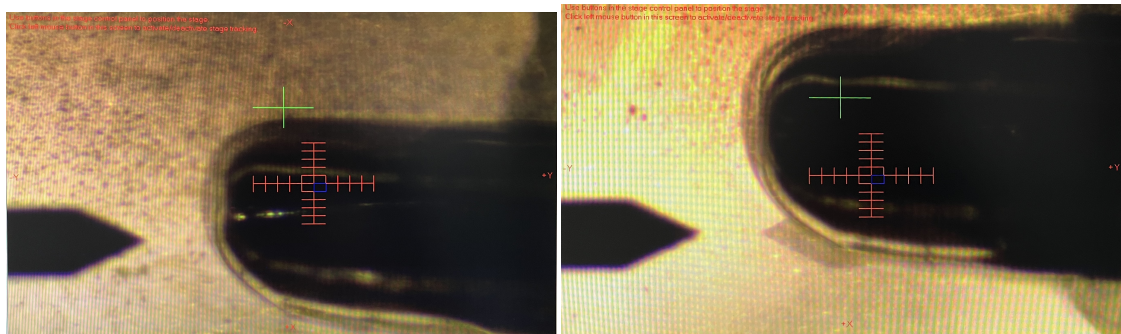
Secondly in Figure 5.7 we can see the lines of section one (10% power and 30mm/s writing speed) and since it is slower the blowout is bigger. In this case the line cut six times is more or less 20% bigger than the line cut only once, and also it has a bigger affected area around it that caused tapering.



(a) Cut one time.

(b) Cut six times.

Figure 5.7: Image of the surface of the PMMA piece in section 1. The dark and pointy tip of the Dektak stylus can be seen on the left, the untouched surface is the yellow/brown part and on the right there is the beginning of the 5 millimeters lines cut respectively one and six times.



(a) 12.5% power.

(b) 15% power.

Figure 5.8: Image of the surface of the PMMA piece in section 5 and 3 respectively. The dark and pointy tip of the Dektak stylus can be seen on the left, the untouched surface is the yellow/brown part and on the right there is the beginning of the 5 millimeters lines cut six times.

Finally to compare the worst case scenarios we can observe in Figure 5.8 the 5mm lines cut six times in sectors 5 and 3 (12.5% and 15% power respectively and 30mm/s writing speed). As expected the situation gets worse with the power increasing and still having the slowest writing speed, as the lines no longer have a uniform and straight blow out. Approximately, compared to the line done with 12.5% power, the one done with 10% power in Figure 5.7b is 30% smaller; while compared to the one done with 15% power it is 40% smaller. This kind of precision is not our first priority, but it was relevant to see how power and speed affect the line profile.



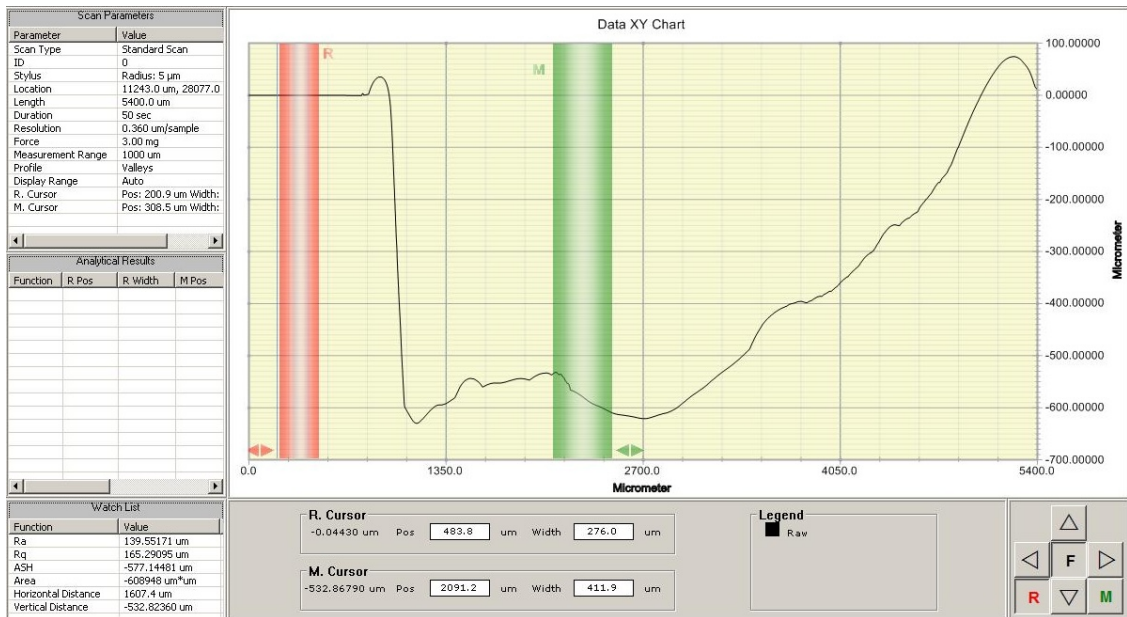
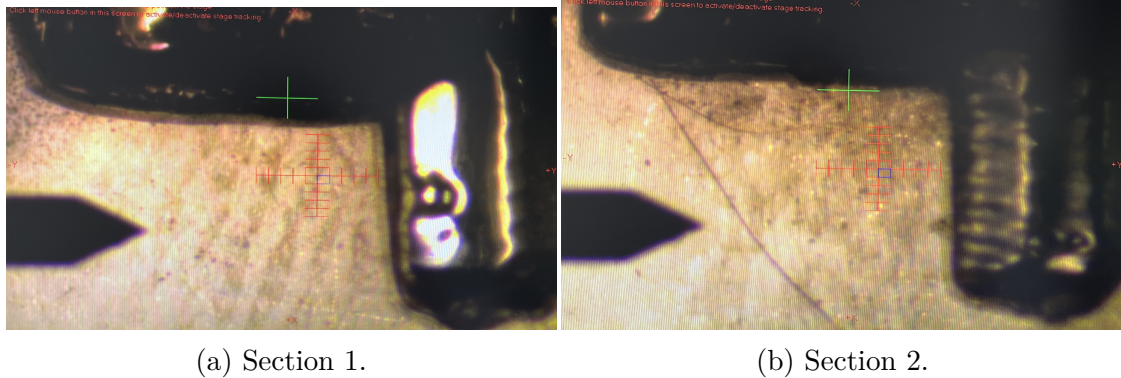


Figure 5.11: Cross section of the channel measured along direction B in the "T" structure in section 1, depth =  $532.8\mu\text{m}$ .

We tried measuring the cross section of the channels in the A and B directions shown in Figure 5.9 and the outcome is shown in Figures 5.10 and 5.11 respectively. In both cases we can observe how the plastic piled up before the edge and is more carved right after the edge: this is due to the melting and consequent cooling of the PMMA close to the area impinged by the laser. Moreover it was impossible to get a good rendition of the second edge, because we get an unexplained artifact of the stylus dragging on the edge, which we are not sure is to blame entirely on the geometry incompatibility explained earlier for the 1mm and 5mm lines. As a result it is impossible for us to determine if the channels have the expected width and length. The depths appear to be different, but it might just be that in the second case we encounter more roughness that makes the analysis more complicated. From Figures 5.12 and 5.13, studying the A scanning direction of the first and the second "T" structures in sector 2 respectively, we can see how cutting twice makes the channel too deep for our needs, so we will not be considering this avenue anymore when cutting the final channel. For this reason the third "T" structure that had been cut was not even measured because it is out of our needs and sometimes cut through the PMMA piece, making it unsafe to measure it with the Dektak. Another interesting analysis comes from qualitatively observing how the intersection is cut and how well it is represented using different writing speeds. As expected when we write slower (Figure 5.14a) the acrylic melts more and we can observe bubbles and rounder lines, compared to when we cut faster with the same power (Figure 5.14b). This is in accordance with the 5 millimeters lines we studied previously.





(a) Section 1.

(b) Section 2.

Figure 5.14: Angle of two "T" structures cut with 10% power and writing speeds 30mm/s and 50mm/s respectively.

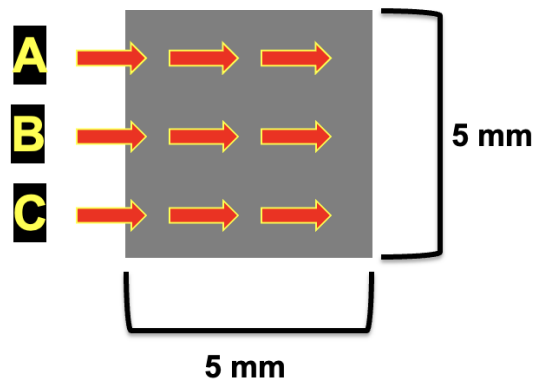


Figure 5.15: Square structure geometry and scan directions: A, B and C. For the edge measurements each arrow was followed, for the roughness measurement only the middle two.

### 5.1.3 5mm×5mm squares

One of the most relevant structures in our tests are the squares we scanned in each section, which were used for depth and roughness analyses. The Dektak scans were done along each of the directions shown in Figure 5.15 and the results for both depth and roughness were averaged out to have a general sense of the structures' properties. The second edge was left out of the scans because as shown previously it holds no significant meaning. To quantify roughness we took some peaks on the surfaces and averaged out their heights to get their overall value. The square depth analysis was done close to the edge, whereas the roughness was analysed along 3mm inside the structure and two examples are shown in Figures 5.16 and 5.17. In Table 5.2 we will summarise our findings, where the error on the measurements was calculated with the standard deviation. Note that section 3 is not included

## 5.1 – Stylus profilometer characterisation

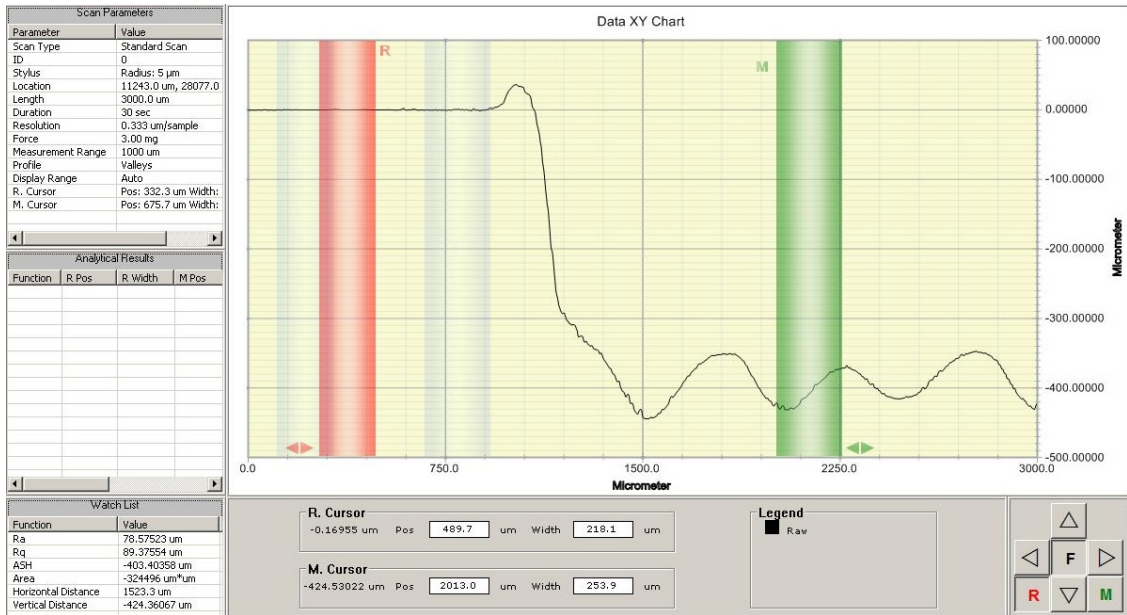


Figure 5.16: Measurement in the square structure in section 2 scanned along direction B: edge depth =  $424.4\mu\text{m}$ .



Figure 5.17: Measurement in the center of direction B, without the edge, of the square structure in section 2: random peak height =  $30.2\mu\text{m}$ .

because the combination of high power (15%) and slow writing speed (30mm/s) cut through the PMMA, making it impossible to study it and also outside of our

region of interest.

Section	Depth, $\mu\text{m}$	Roughness, $\mu\text{m}$	Relative roughness = (Roughness/Depth)*100
1	$678.2 \pm 19.9$	$29.5 \pm 8.4$	4.3%
2	$376.8 \pm 41.2$	$50.8 \pm 20.2$	13.5%
4	$786.4 \pm 42.3$	$178.5 \pm 68.0$	22.7%
5	$818.8 \pm 24.8$	$39.4 \pm 12.8$	4.8%
6	$475.9 \pm 9.2$	$113.1 \pm 31.1$	23.8%

Table 5.2: Measurement values of average depth, average roughness height and relative roughness in the square structures in each section.

Looking at these results, the ones closer to our desired depth are the squares in section 2 and 6, which in both cases write with the faster speed of 50mm/s, but use 10% and 12.5% power respectively. The square in section 6 comes closer to the required depth of 0.5mm and has a much lower deviation, but looks a lot rougher relatively to the square in section 2. The fact that it is also rougher than the square in section 4, which has 15% power and the same writing speed, is not easily understandable without section 3 to compare. As expected the sections with slower speeds (1 and 5) also have lower relative roughness than the ones where the writing was fast and less precise. However now we need one last test to definitely choose our settings between section 2 and 6.

### 5.1.4 Bottom channels

A bottom channel design had been recreated on both sections 2 and 6 and from it came some important considerations for the design overall. The model on RDWorks has to be carefully done to have each connecting channel close enough in order to not leave some uncut barriers, while also not overlapping them which would give the same result. Both mistakes had been done in these two designs, but they were noticed and rectified for the actual final model. Here we will show the depth and roughness measurements and finally decide our definite settings. The data were taken in the middle square chamber just as for the square structure in Figure 5.15, then the values for depth and roughness peaks were averaged and collected in Table 5.3, with the respective standard deviations.

We can see that with the settings from section 6 (12.5% power and 50mm/s writing speed) not only we get a closer value to the expected 0.5mm depth, but also the relative roughness is a lot better. The roughness value for the channel in this section is significantly lower than the square structure’s roughness in the same section from Table 5.2, which probably comes from the way the channel is cut. In the Dektak camera, but also by eye, it was easy to see that the squares are scanned in lines,

Section	Depth, $\mu\text{m}$	Roughness, $\mu\text{m}$	Relative roughness = (Roughness/Depth)*100
2	$340.1 \pm 65.1$	$39.1 \pm 27.1$	11.5%
6	$465.8 \pm 14.9$	$33.9 \pm 14.5$	7.3%

Table 5.3: Measurement values of average depth, average roughness height and relative roughness in the channel structures in sections 2 and 6.

whereas the channel is scanned in a grid motion. The reason is not clear, but the overall effect is that some of the lines are evened out and the roughness is much better.

## 5.2 Bottom channel fabrication

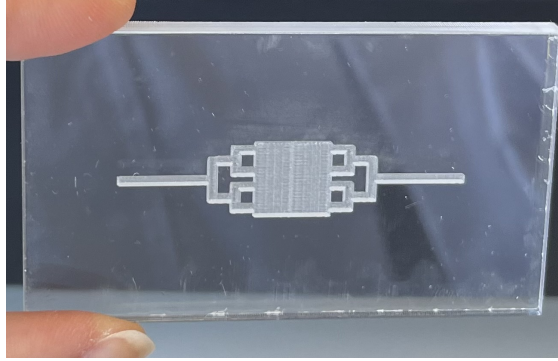


Figure 5.18: Bottom channel designed engraved in a piece of PMMA.

Finally after all of these analyses we can actually draw and cut the bottom channel on a piece of PMMA following the design in Figure 5.2, based on our previous simulations (Figure 4.27). By setting the previously mentioned power and writing speed (12.5% and 50mm/s) for the channel and defining a much higher power to cut through the PMMA, we end up with a 4cm×7cm chip shown in Figure 5.18. Both by eye and profilometer we observed that in the small channels the roughness lines were mostly perpendicular to the flow direction, which could interfere with its simulated homogeneity. We assumed that at least by turning the design by 90° in RDWorks these lines would be parallel to the flow and aid the device’s working principle.

However when conducting this test, as seen in Figure 5.19, the resulting channel showed an increased roughness and especially the barriers between intersecting channels became more prominent. Especially the middle of the central chamber is strongly divided and this rough channel would be more problematic than what

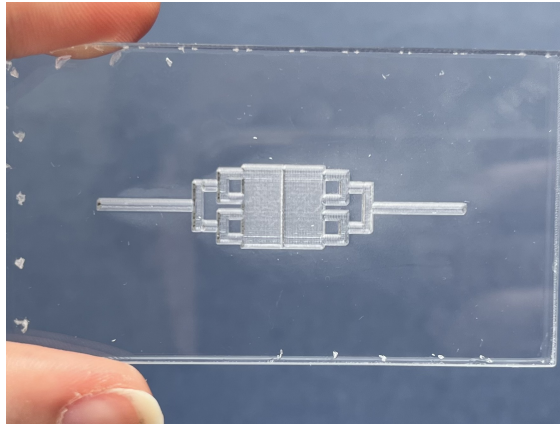


Figure 5.19: Bottom channel designed engraved in a piece of PMMA with design rotated by  $90^\circ$  in RDWorks.

previously observed in Figure 5.18, so this avenue was not explored further.

## Chapter 6

# 3D printer fabrication



Figure 6.1: Creality Ender-3 V2 filament 3D printer.

In this chapter we will be fabricating the wall system around the organoid that will be attached to the bottom plate. Since the dimensions we are working with are typically around the millimeter scale we will be able to achieve our goals with a filament 3D printer, and more specifically the model we used is a Creality Ender-3 V2 with a particularly flexible white PLA filament that is also biocompatible (see Figure 6.1). We chose not to use the laser cutter for this piece because the lateral perfusion design would have required us to carve half of the design and the channels on two pieces of PMMA and then bond them together with pressure. The procedure

would not have been too complicated, but this 3D printing technique seemed easier since it especially did not require any alignment for the top piece itself.

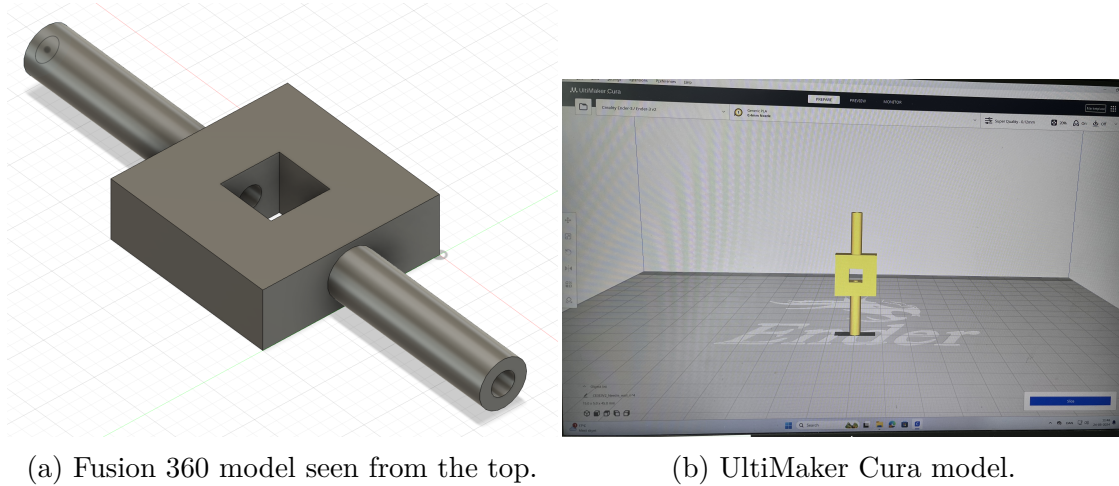


Figure 6.2: Creation of a model for a PLA 3D printer for a wall design with lateral perfusion.

The models were done with Fusion 360 and prepared and sliced for the printer on UltiMaker Cura 5.7.0, as we can see in Figure 6.2. We will now list the parameters used for every print, but note that the infill density and the supports' density was changed in accordance with the magnitude of the print, to have reasonable print duration and easy removal of the sacrificial material. The printing temperature was set to  $220^{\circ}$ , while the build plate was set to  $60^{\circ}$  to avoid breakage as the filament cools down. While doing so on the slicer we also pre-heated the printer's filament and plate with the same settings at the same time to reduce waiting time. The printing speed was usually kept at the default  $50\text{mm/s}$  as it appeared to be a good value. For the infill we usually employed a grid design to have a tough and durable structure. We used the "Super Quality" setting, which defines the height of each layer of filament to be  $0.12\text{mm}$ , combined with a heated nozzle of  $0.4\text{mm}$  of width. As we can see from Figure 6.2b the print had to be done with a rotated model to simplify the removal from the plate and for structures with tunnels to avoid having support inside of them, which would be difficult to remove. For this reason in our future designs we will have to remove supports from the central chamber and from around the bottom tunnel in the presence of such structure. The settings for these supports were a overhang angle of  $45^{\circ}$ , a density ranging from 6% to 10% and we remove the setting "connect support zigzag". Nonetheless this removal can sometimes leave damages to the structure that have to be taken into consideration when dealing with liquids and possible leakages. Finally after a print was done, it was important to let the build plate cool down to at least  $30^{\circ}/40^{\circ}$  not to ruin part of the design by scraping it when it was still warm and pliable. We will now show

some of the results we obtained and the problems we encountered on the road to our final models.

## 6.1 Initial experiments

As first tests we printed some preliminary designs to get an idea of the modelled dimensions and what structures would actually be viable for our printer. Even though we chose the best settings for the highest resolution in the slicer program, the machine still has some inherent limits, mainly posed by the nozzle dimension.

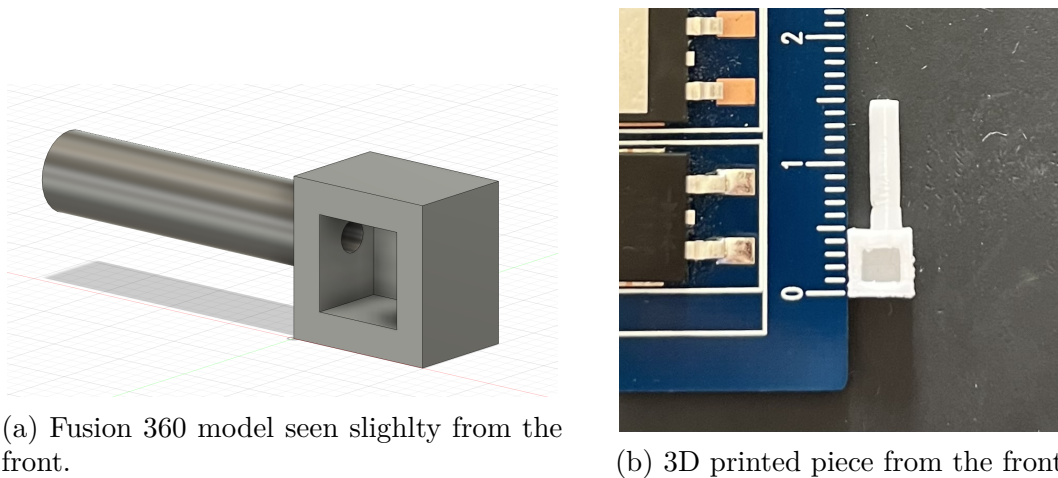


Figure 6.3: Model and final piece for a practice chamber wall design, apt at testing the resolution of the printer.

As we can see from Figure 6.3b the  $3\text{mm} \times 3\text{mm}$  hole in the wall is more or less resolved, but the supports inside create some roughness. The  $2.5\text{mm}$  outer diameter lateral tube as a kink near the chamber, but it is otherwise well printed. However the biggest problem can be seen in Figure 6.4: the  $1\text{mm}$  diameter tunnel inside of it is missing and is completely closed. We can assume this to be a limit for our future designs, so we will switch to more comfortable dimensions.

As a second step we referred ourselves to the model seen in Figure 6.2a, we printed it and the results can be seen in Figure 6.5. This is the original idea for the lateral perfusion design simulated in section 4.5 with results shown in Figure 4.19. We can observe the central  $5\text{mm} \times 5\text{mm}$  chamber that would host the organoid and the lateral hollow cylinders where we would introduce needles or tubes. The tunnels in this case have a  $2\text{mm}$  inner diameter and we can see that they are perfectly resolved all throughout the structure. However our plans for the bonding of the PMMA bottom channel and the 3D printed chamber involve using double-sided tape, which works better with larger contact area. Moreover we would not want to leave some sticky surface area in the open, for these reasons we have to remodel

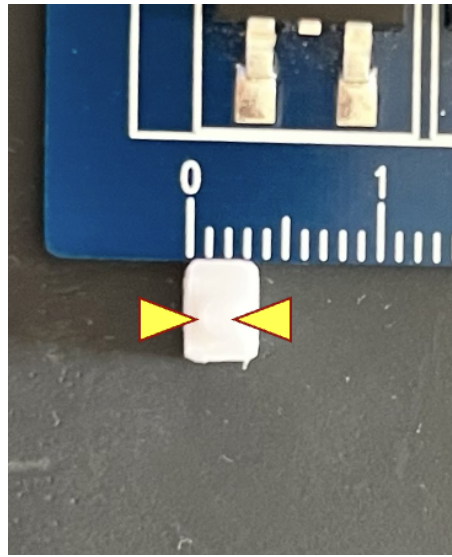
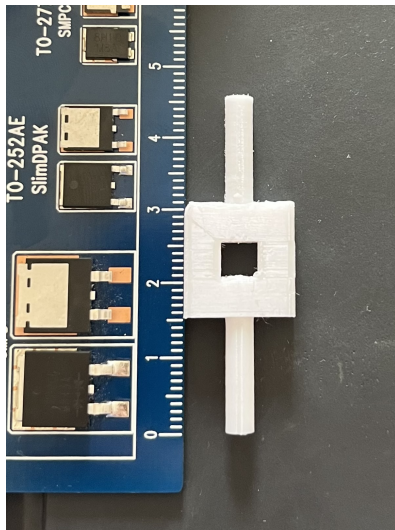
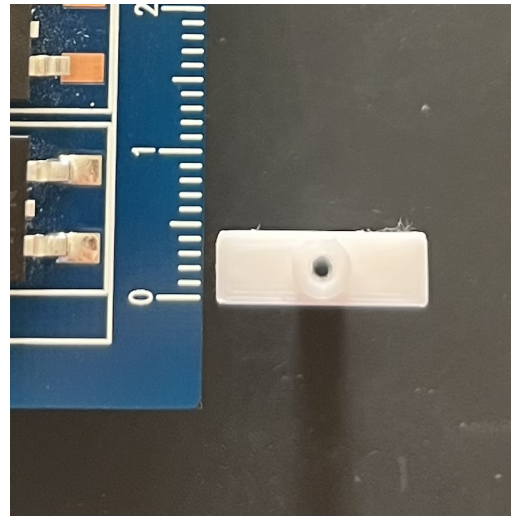


Figure 6.4: 3D printed piece from the side, where the tube with the hole is not resolved. The yellow arrows point to the outer diameter of the tube.



(a) 3D printed piece from the top.



(b) 3D printed lateral 2mm tunnel. Due to the perspective it looks smaller.

Figure 6.5: Final 3D printed piece for the first design of our needle wall chamber and resolution of the lateral tubing.

our design to account for this and for the insertion of inlet and outlet tubes for the bottom channel.

## 6.2 Dynamic 1 plate membrane design

As a first simple, but complete, design we decided to fabricate the device in which nutrients would only come from the bottom plate, having the aqueous medium go through it with the previously simulated flow rate of  $2.1\mu\text{L}/\text{min}$ . These nutrients would then move by diffusion to the organoid chamber which in this case is just four normal walls. This is based on the simulations that we can see in section 4.1.2 and in Figures 4.4 and 4.5. As previously explained the printed piece should have holes to host the inlet and outlet tubes for the bottom channel and only the middle square hole for the tissue.

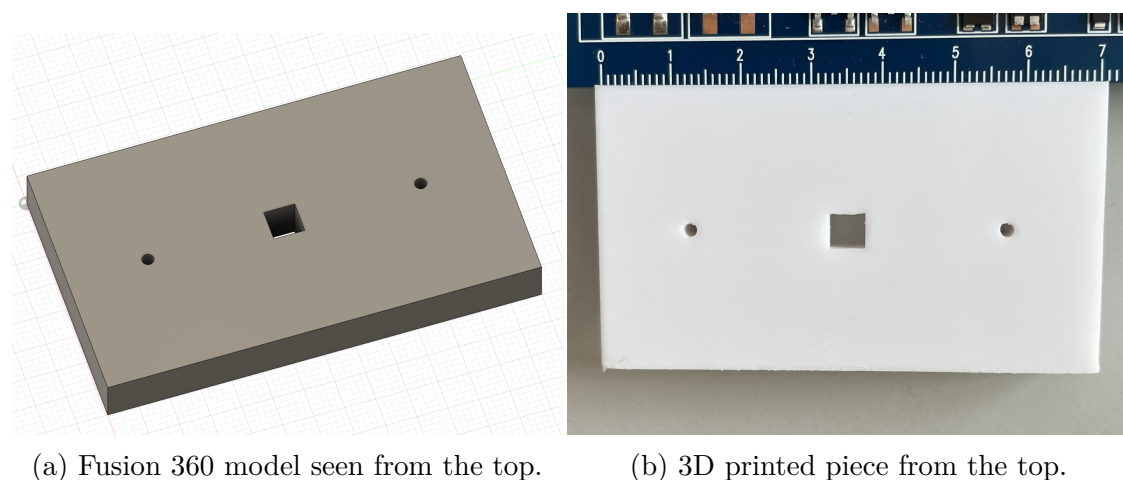
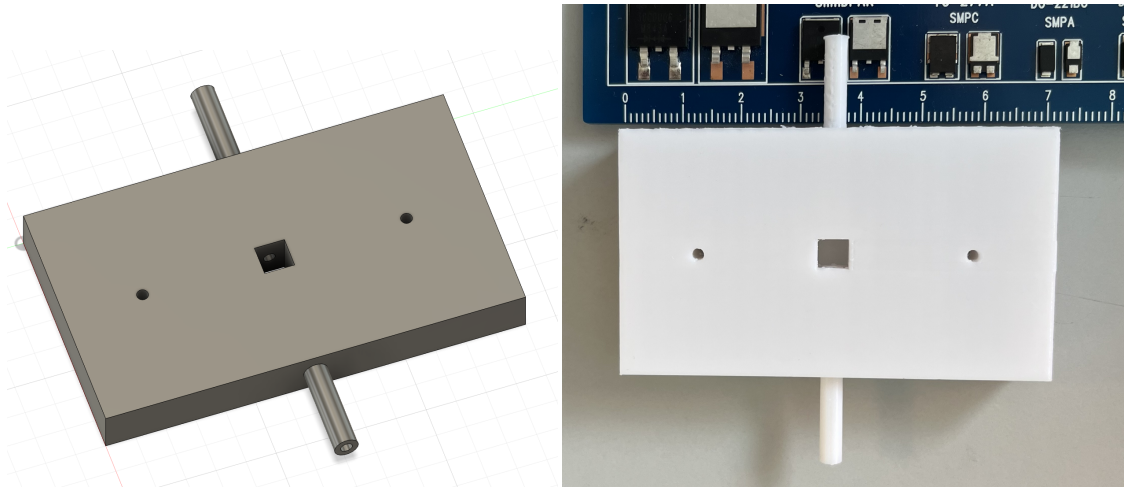


Figure 6.6: Model and final piece for the trivial wall design, 3D printed with bio-compatible PLA.

The hole for the inlet and outlet tubes have a diameter of 1.9mm, so that our tubes would easily fit and be relatively tight, then they would be sealed with a biocompatible sealant and solvent-free super glue. The middle chamber is  $5\text{mm}\times 5\text{mm}$  big and 8mm high, because we will be provided mostly with organoids that are 2 to 4 millimeters big. This whole piece will cover the PMMA bottom plate completely in order to not leave any adhesive surface free, so it is  $4\text{cm}\times 7\text{cm}$  wide as well. By doing so the alignment of the two pieces should be easier and more controllable.

## 6.3 Needle and tubing wall

Our second complete design is the upgrade from that in Figure 6.5 and still related the simulations in Figure 4.19. However we have now enlarged the surface to cover the double-sided tape and we introduced the holes for the bottom channel's inlet and outlet as in the previous section.



(a) Fusion 360 model seen from the top.

(b) 3D printed piece from the top.

Figure 6.7: Model and final piece for the complete lateral tube wall design, 3D printed with biocompatible PLA.

As we can see from Figure 6.7 we have also included the lateral tubes for the perfusion of the chamber and the design looks very clean. The dimensions for the chip are the same as those for the trivial wall design. However the lateral tubes have an external diameter of 4mm and an internal one of 2mm, and the whole structure is 15mm long from the chip's wall. This design will be slightly more complicated to work with because it requires a second pair of tubes, but it was interesting for us to challenge ourselves with it.

## Chapter 7

# Assembling, testing and sterilizing the device

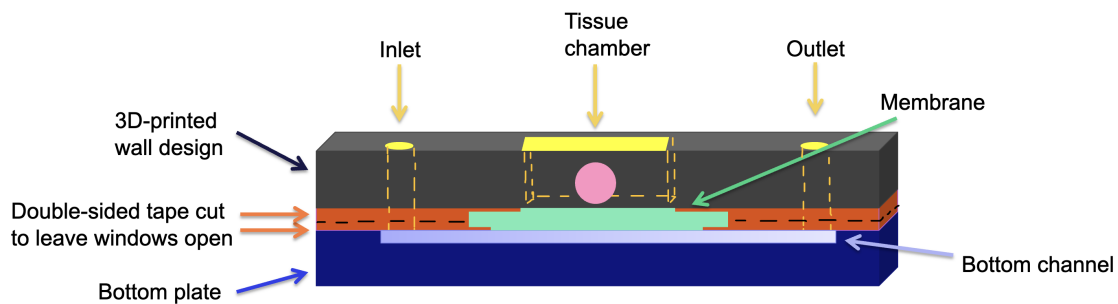


Figure 7.1: Cross section of the final chip with design descriptions to indicate the bonding steps.

The next step in the device fabrication is to attach each piece using double-sided tape, while including our membrane in the middle. The general idea for our device can be seen in Figure 7.1: on top of the bottom plate we place a piece of double-sided tape with the cut-out for the central chamber, the inlet and the outlet; after that the membrane will be positioned in the center and fixed with another piece of double-sided tape with a similar design to the previous one, but a smaller central square; finally the 3D-printed wall design will be attached on the top and the tubes will be glued in the inlet and outlet holes. By doing so, as we can see, the membrane is kept in place by the tape on both sides, while still being open for the diffusion of nutrients.

## 7.1 Step by step chip construction

### 7.1.1 Chip bonding

First we attach the first layer of double-sided tape to the bottom channel.

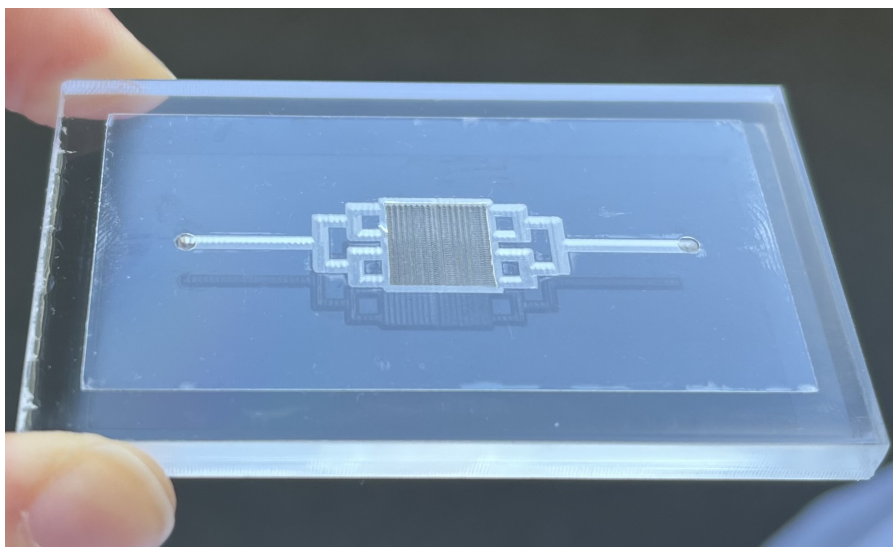


Figure 7.2: View on the bottom channel with the first piece of tape.

As seen in Figure 7.2, the tape covers most of the channels, but leaves two holes for the tubes and the open window for the central chamber. It was cut using the laser cutter with 8%-9% power and 50mm/s speed, because sometimes the higher power bowed the tape as it was being cut, misaligning the design. The holes have a diameter of 1.7mm, while the central square is 9mm×9mm big, slightly smaller than the bottom channel square (10mm×10mm), to have better membrane adhesion, while also not risking it attaching to the bottom and hindering the flow. Alignment and adhesion uniformity were our greatest concerns: the former is left to the ability of the technician, however the latter could be helped by wiping the surface with a wet paper towel and drying it. Finally, using a hard plastic to swipe the tape on with greater force and carefully not damaging the piece of tape, we could get fewer to no bubbles and great adhesion.

Afterwards we removed the second peel of the tape and attached a piece of membrane that will sit on top of the open window as seen in Figure 7.3. The membranes are Whatman® Cyclopore polycarbonate membranes with a pore size of 1.0 $\mu$ m, that come in circles of 47mm of diameter and have been cut up to fit our design. They have a high chemical resistance and good thermal stability, however a porosity value was not found when researched. The goal was placing it at least in the center square, but also making sure that it was not creased after positioning it. This is because the tape is highly adhesive and once it makes contact with the

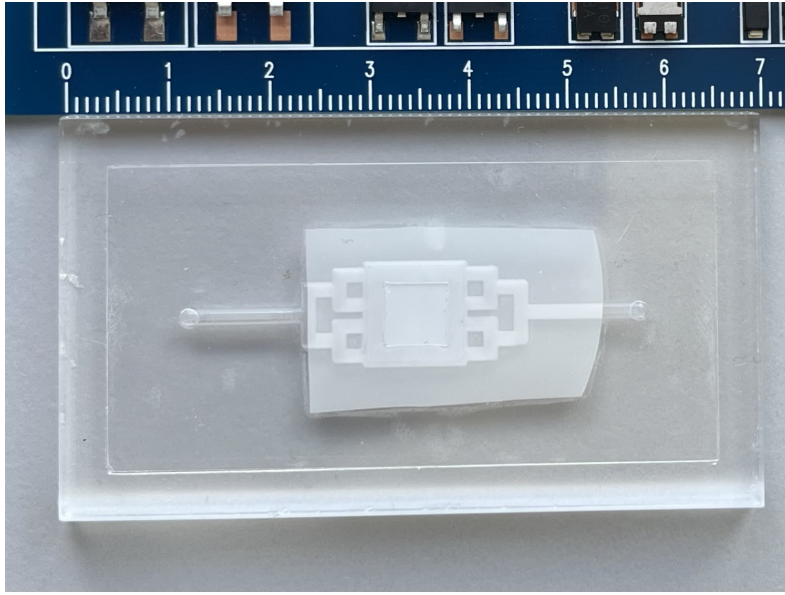
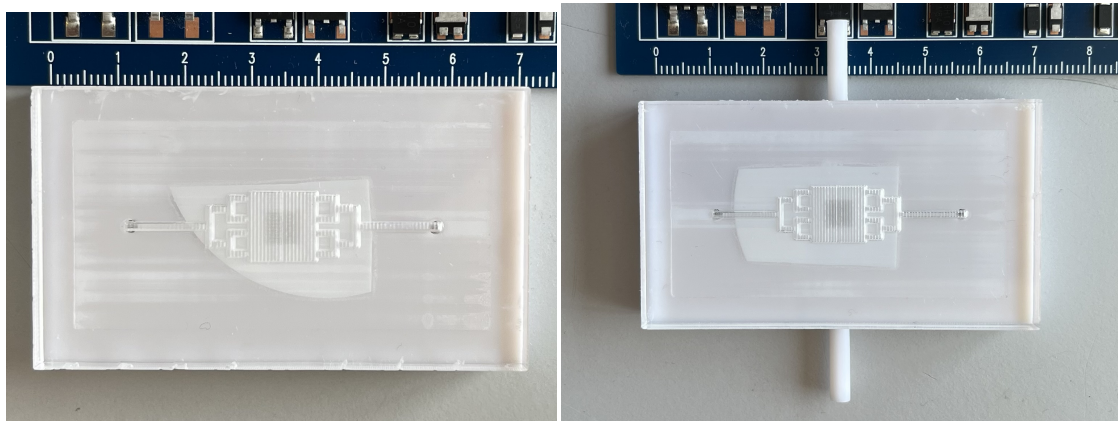


Figure 7.3: View on the bottom channel with a piece of filter paper in the middle.

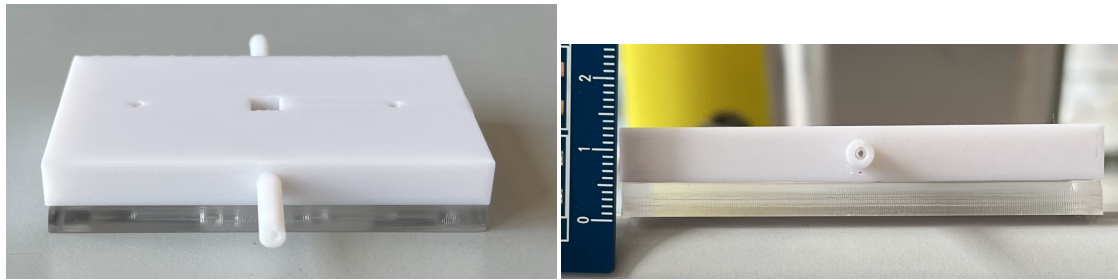
membrane it is not possible to remove it without damaging it. From this picture we can also see that the second layer of double-sided tape was laid down, however the design is slightly different. The center square is  $6\text{mm} \times 6\text{mm}$  big so that it is slightly bigger than the 3D printed chamber ( $5\text{mm} \times 5\text{mm}$ ), but not too much that it would risk leaking on the outer edges. We avoided making the membrane window smaller than the chamber floor because it would leave an adhesive surface which could damage the organoid.



(a) Normal wall design full chip.

(b) Needle wall design full chip.

Figure 7.4: Both wall designs bonded to the bottom channel seen from below to observe alignment.



(a) Final chip in perspective.

(b) Final chip from the side.

Figure 7.5: Full view of the final chip in the needle wall design for example.

Finally we ended up with these full chips with our two designs, where the alignment was done by removing the tape film and exploiting the bottom piece's transparency to match the holes in the two pieces, as seen in Figure 7.4. Some other perspectives are shown in Figure 7.5, where we see the chip in its correct position, with the 3D-printed chamber on top.

### 7.1.2 Tubings and flow splitting

At this point the only missing pieces were the tubes that needed to be inserted in each inlet and outlet, however for this step some considerations were to be taken into account and some troubles have been encountered. We had to consider that the chips would have been placed in an incubator for the organoid survival, so we wanted to minimise the number of tubes going from the outside to the inside and to have them be sturdy enough not to be crushed by the door. For this reason we had decided to use a flow splitter that will be sanitised and integrated inside of the incubator. It would have been connected with a long tube going to the syringe secured on the pump and it was fabricated using the PLA 3D printer. The initial goal was glueing the tubes directly to the inlets and outlets, however the tubes present in the lab were PTFE or Teflon tubes (1/16" outer diameter and 0.75mm inner diameter) which would not stick to our super glue. Therefore we implemented a less orthodox method of glueing pipette heads to these holes and then sticking the tubes inside, relying on their shared friction. To set them in place correctly, first a layer of silicone sealer was dispensed around the hole and secondly the super glue was layered on top of it. This was done for one main reason, aside from better chance of sealing the structure: if only a layer of glue was placed near the hole it would slide to the bottom and the results were two. Either the glue could directly block the channel and completely stop the flow of medium, or when we would introduce some isopropanol to sterilise the structure it could come in contact with the glue and react and create this white liquid that would then sediment in the channel.

The consequence of this second case would be that the flow would then be hindered

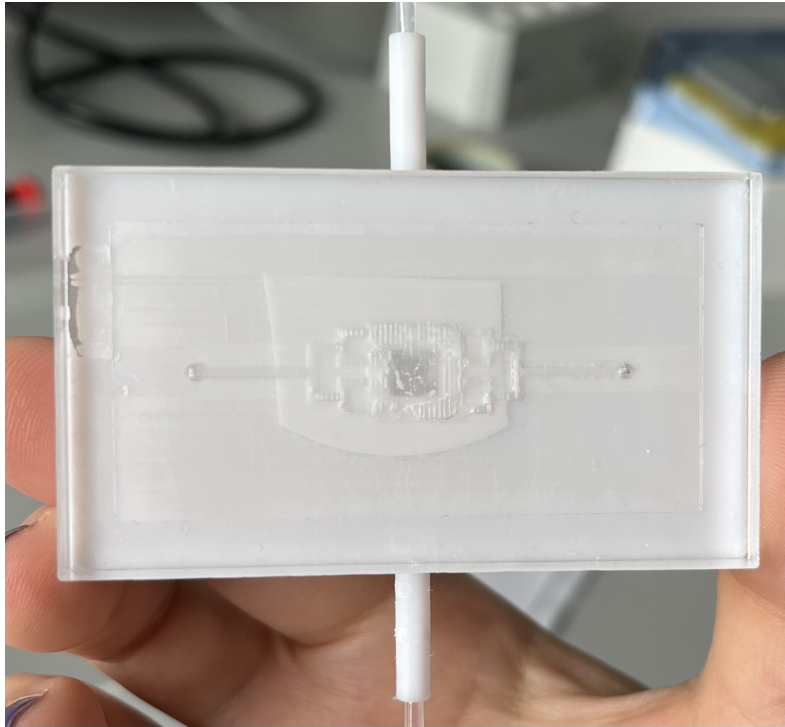


Figure 7.6: White residue scattered in the bottom channel after isopropanol and super glue reacted.

and it would not behave correctly in the channel, sometimes it would not flow at all. The aftermath of such reaction can be seen in Figure 7.6, where the chip was not able to transfer liquids from one side to the other of the bottom channel. Since this completely wastes materials and the printing process for the upper piece is very long, we avoided this probability completely by sanitizing the inner channel during the device assembly and avoiding introducing isopropanol once the glue was set.

In Figure 7.7 we can finally see the end result of our devices. The next step was to test them for leakage and overall performance before putting the organoids inside. For the aforementioned flow splitters we had ordered some that arrived too late, so we used a model granted by a lab coworker and we tested it. It originally was made to split the flow in four directions, but since we needed six outlets, we printed one more to subsequently clog two of the exits with the silicone sealer and the super glue. Since we had the same glue adhesion problem with the Teflon tubes, we also glued pipette heads to these structures and the result can be seen in Figure 7.8. They ran pretty smoothly, with only some asymmetries in the flow splitting that we overlooked for lack of an alternative.

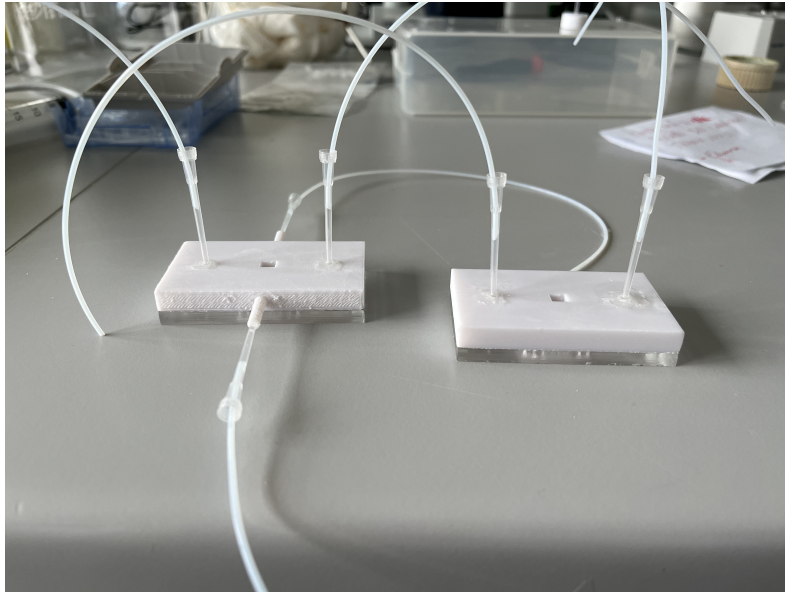


Figure 7.7: Complete chips in both designs.



(a) Flow splitter from the side.



(b) Flow splitter from the bottom.

Figure 7.8: Four way flow splitter with attached pipette heads.

### 7.1.3 Chamber sealing

The last step required in the assembly was finding a way to seal the top of the chamber once the organoids would have been inserted. Unfortunately since our

device would have been placed in an incubator we were limited by the fact that any open surface could grow unwanted organisms, so we had to close it. By doing so we cannot study our air-liquid interface device as simulated and read in the article, but we will just analyse it in what we previously defined as the growth stage with the organoid fully submerged in medium. Also, since we are constantly providing fluids to the chamber, we could also have had a risk of it overflowing so in any case a seal is required because we do not have an exhaust aside from the outlet.



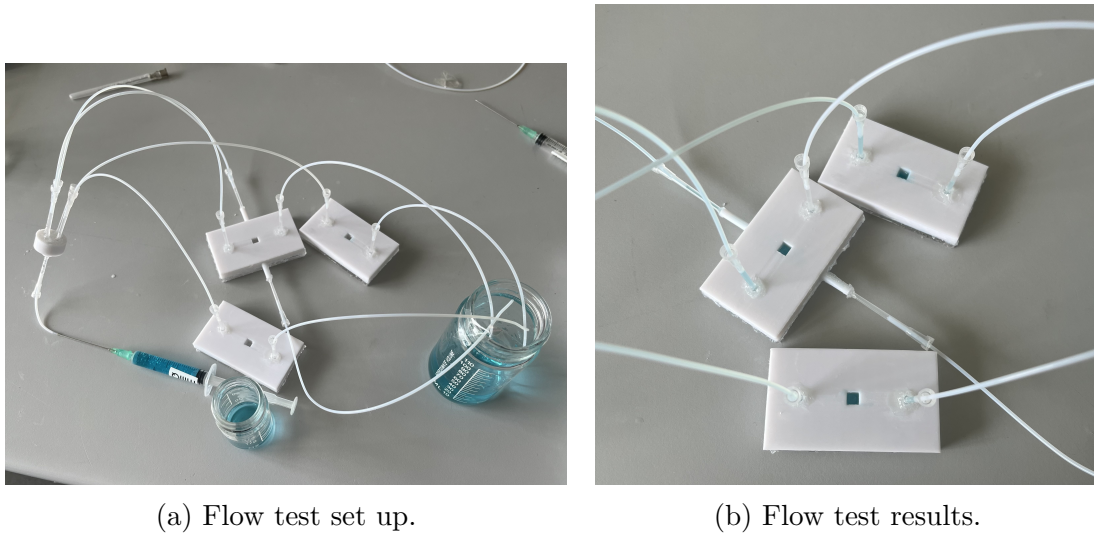
Figure 7.9: Sealing test to close the organoid chamber.

After a few tests the successful process was to place a silicone barrier around the chamber entrance and closing it with a piece of parafilm around the the device. Finally it was secured to the surface with two pieces of tape on both sides of the parafilm as can be seen in Figure 7.9.

## 7.2 Preliminary tests

Due to a lack of time we were able to only crudely test the devices by introducing Milli-Q water (or purified water) through Sterican® needles with external diameter 0.80mm that would tightly fit our tubes for a few days. The Milli-Q water was coloured with a light blue food colouring to follow the path of the liquid and check for structural problems, however as we will later see this dye was not strong enough for our tracking needs. The set up can be observed in Figure 7.10a.

Some lateral leakage was found coming from the space between the bottom and the top plate of the device, probably due to the double-sided tape not sticking correctly. Since better adhesion was difficult to achieve, we decided to seal the sides with silicone and super glue to at least limit the damages. From Figure 7.10b we can observe that the splitter worked correctly and that each inlet and chamber received nutrients. However we can faintly see that the output for the bottom chamber in the lateral perfusion device did not get any water. This means



(a) Flow test set up.

(b) Flow test results.

Figure 7.10: Flow test set up and results of three devices with the four-way flow splitter and dyed Milli-Q water.

that the liquid preferred going out through the output in the chamber, having convection through the membrane, probably due to a more favourable pressure difference even if it seemed quite unlikely. Also some overflowing from the chamber happened, which made the seal even more needed for when the organoids would be introduced. Lastly for the devices with the lateral tubes, it was found that the tube that was built surrounded by supports could present some leakages due to a forceful removal of such supports. This caused a hole in the outer shell of the print that had to be closed with silicone and super glue. Aside from these defects the tests seemed to run well enough and we were ready to sterilise the devices to finalise this fabrication process.

### 7.3 Sterilisation

As previously mentioned the inner channels in the device, both in the bottom plate and in the top chamber have been sterilised using isopropanol and drying it quickly before assembling. This is because PMMA is sensible to organic solvents, especially ethanol, which could crack and ruin its structure. The outside was cleaned using some isopropanol on a paper towel and dried again with another clean towel. For the other components (tubes, pipette heads and flow splitters) we used ethanol 70%, dipping them for a few minutes in a container in a fume hood and then flowing some of it inside using a syringe. They were then cleaned inside with Milli-Q water to remove any residue of ethanol. After these steps the devices were ready to be tested properly with the organoids at KU to finally get the experimental results.

## 7.4 Fabrication summary

Overall good solutions were found for each step of the process: the bottom channel depth was more or less close to our expected dimension and the roughness was manageable; the 3D printed piece required some precautions in the design and in the creation and removal of the supports, but it looked apt for our purposes. For what concerns the assembling, it is a very quick process with double-sided tape that simply requires a lot of precision, especially in aligning each separate piece, in sealing tubes and other holes present in the designs and in sterilising the PMMA quickly without any residue of solvent. After all of the preliminary tests with a hand held syringe, the device seemed to work as anticipated, aside from the unexpected water rising in the middle chamber and some occasional leakage from the side, which hopefully had been taken care of for good. We were aware of the limited time we had spent on these tests and that there was a chance of some problems arising in the experimental one at KU, but it was time to carry it out once and for all.



## Part IV

# Real organoid experiment and results



# Chapter 8

## Final setup and outcome

### 8.1 Setup

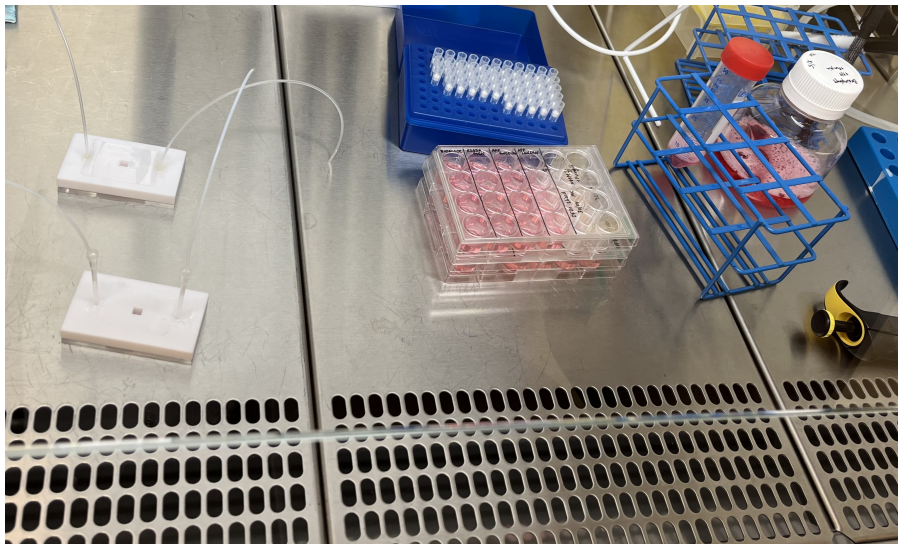


Figure 8.1: Loading the organoids in the chips through pipettes.

To begin the experiments the organoids have to be moved inside of the devices inside a fume hood as seen in Figure 8.1. It is done using a pipette and by doing so both the organoid and its medium will be inserted in the chamber, carefully not touching the walls and the membrane. This red medium is from Stemcell Technologies[15] and it is recommended for neuronal maturation. It is BrainPhys™ basal medium with some supplements for culturing human iPS-derived neuronal progenitor cells, where iPS stands for "induced pluripotent stem". We can see the organoid in Figure 8.2 in the simpler design and another was put in the lateral perfusion design. It has approximately a diameter of 2-2.5mm and perfectly fits our design. To have a more

complete analysis we loaded two other equivalent devices with only an organoid slice, which should technically have a higher survival chance than the full organoid, to compare them in the end.



Figure 8.2: Organoid inside of the central chamber of the chip. The pink colour is due to the medium colour.



(a) Syringes full of medium loaded in the syringe pump.



(b) Loaded devices, flow splitters and bottle to collect the output, all connected.

Figure 8.3: Set up inside and outside of the incubator, connected through a tube going from the syringes to the flow splitters. The pump used is a Harvard Apparatus syringe pump PHD 2000.

At this point we sealed the devices as shown in Figure 7.9 and inserted them in the incubator at 37°C. The total set up can be seen in Figure 8.3, where the syringe pump was placed directly below the incubator, so that we did not require long tubes. In Figure 8.3a we can see that the syringes would be set to the same infusion flow rate. Because we previously simulated a flow rate of  $2.1\mu\text{L}/\text{min}$  in the bottom channel and since at most our flow is divided in four outlets we have to set the total flow rate to  $8.4\mu\text{L}/\text{min}$ , assuming that the tubes are all the same.

Syringe 1: connected to the 4 outlet splitter

$$Q_{tot1} = Q_1 + Q_2 + Q_3 + Q_4 = 8.4\mu\text{L}/\text{min}$$

$$\Rightarrow Q_1 = Q_2 = Q_3 = Q_4 = 2.1\mu\text{L}/\text{min}$$

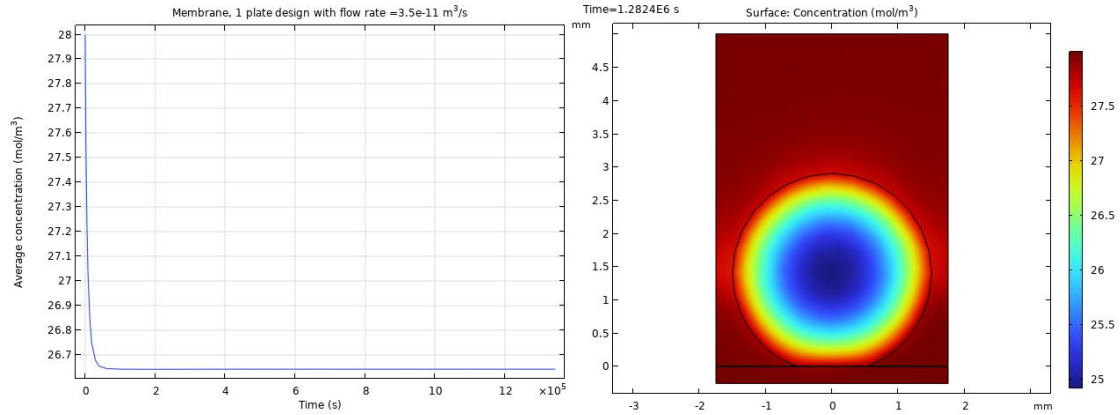
Syringe 2: connected to the 2 outlet splitter

$$Q_{tot2} = Q_5 + Q_6 = 8.4\mu\text{L}/\text{min}$$

$$\Rightarrow Q_5 = Q_6 = 4.2\mu\text{L}/\text{min}$$

(8.1)

where the numbered flow rates are the ones in the tubes directly connected to the devices' inlets. Since in the simulations we used a much higher flow rate for the lateral tube, we checked again with COMSOL to see if such a slow flow rate would make a difference.



(a) Average concentration in the organoid. (b) Concentration along the xz-cutplane.

Figure 8.4: Average concentration in the tissue and cutplane after 14 days in the lateral perfusion design with plate flow rate =  $3.5 \times 10^{-11} \text{m}^3/\text{s} = 2.1\mu\text{L}/\text{min}$  and needle flow rate =  $3.5 \times 10^{-11} \text{m}^3/\text{s} = 2.1\mu\text{L}/\text{min}$ .

We simulated for the required 14 days that our experiment should run for with the lowest possible flow rate and got the results in Figure 8.4. Compared to the graphs in Figure 4.19 where the lateral perfusion flow rate was  $60000\mu\text{L}/\text{min}$ , the average concentration only has a slightly lower value and the same goes for the cutplane

concentration, which means that we can run the experiment with these lower flow rates and still get optimal results.

In Figure 8.3b we can see that all the inputs are connected to a flow splitter and all the outputs lead to the central bottle for waste collection. This bottle was sterilised and closed with two layers of parafilm to better block the tubes going inside, while also perfectly sealing the inside so that no unwanted growth may happen. For the flow splitting, as explained in equation 9.3, three devices (2 with the simple design and 1 with the lateral perfusion one) were connected to syringe 1 and the second device with the lateral tubes was connected on its own to syringe 2. This decision was made despite the fact that the device on its own would have double the flow with respect to the others in both inlets because, during testing, it showed more resistance to getting the flow going. This is probably due to some contamination similar to that in Figure 7.6, and for this reason we not only wished that double the flow rate would make it work similarly to the others, but also that by separating it from them it would not affect the others' operation.

## 8.2 Results



Figure 8.5: Failed experiment with leakages and no waste collected in the output bottle after 2 days and a half of operation.

The experiment was set up and started with the required parameters described in the previous chapter, however the result after 2 days and a half can be seen in Figure 8.5. The device on its own seen in the bottom right and the device in the

top left are completely red due to the medium leaking, while the other two devices did not get any medium at all. This was a surprise since in the short term, as we were monitoring the devices in the first minutes of operations, they seemed to be working fine and the waste was being collected in the central bottle. We are not sure what the causes of such leakages were, but we can suggest some, and for this reason we will analyse them and we will try to look for solutions.



# Chapter 9

## Troubleshooting

To try to understand what problems may have arisen in the experiment, we propose some possible causes that will be addressed one by one after having tested again the devices used up to now.

### 9.1 Devices' tests

Of the two devices with the simpler design one of them worked as expected and presented no leakages, so we chose it for our next testing steps. The other one, that leaked and can be seen in the top left in Figure 8.5, presented a leakage at the pipette head connected to the output of the bottom channel. This may have caused a favourable pressure difference that attracted all the medium to this device and left the other two untouched, spilling everything out. The more complex device that leaked and can be seen in the bottom right in Figure 8.5, pushed all the liquid out of the central chamber and requires a pretty high flow rate to expel it just through the lateral output like the other one of its kind. Moreover for this one, as previously mentioned in section 8.1, there is a quite high resistance when pushing liquid only through the bottom channel.

### 9.2 Problems and possible solutions

Considering these faults a list of causes was drawn out and here they are summarised:

1. The loading of the organoid and the medium building up in the chamber may cause the membrane to buckle under the weight and obstruct the path in the bottom channel;
2. The combination of pipette head and tube may create a high hydraulic resistance that hinders the flow going from the channel inlet to the outlet, pushing

the liquid through the membrane and up the main chamber;

3. The sealing technique on the top of the chamber is not good enough;

and we will now analyse each point.

For point 1 we decided to fabricate a new device of the simplest design with a small pillar in the middle of the main chamber of the bottom channel to keep the membrane from possibly sagging. It would then have been tested with the equivalent device from those brought to KU to monitor any difference in operation.

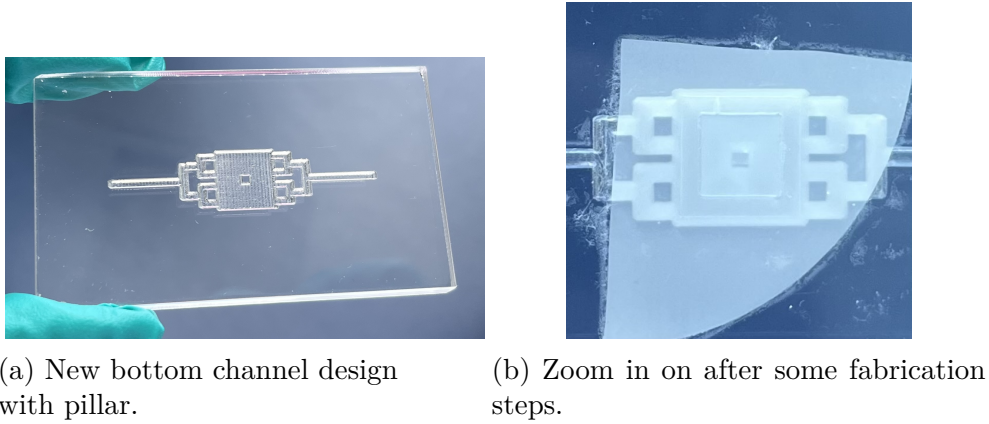


Figure 9.1: New design for the bottom channel and zoom in after the complete fabrication steps for the bottom half of the device.

From Figure 9.1 we can observe the new design, bare and after applying the two layers of double-sided tape with the membrane in between. In Figure 9.1b specifically it is clear that the pillar is supporting the membrane, that is already quite stretched. For this reason when fabricating it we designed it as a  $1.5\text{mm} \times 1.5\text{mm}$  square, otherwise it would be too sharp and it would risk damaging the membrane. After some tests we can conclude that also this new device has a lot of liquid going through the membrane and out from the main chamber, which leads us to deduce that this is not the cause for our malfunctioning. However we will keep testing the next points with both the old device and the new one with the pillar to keep an eye on possible changes.

To address point number 2 we decided to test it theoretically knowing that the hydraulic resistance for a channel of circular cross section is defined as

$$R_{hyd} = \frac{8\eta L}{\pi R^4} \quad (9.1)$$

where  $\eta$  is the liquid viscosity (  $1\text{mPa}\cdot\text{s}$  for water),  $L$  is the length of the channel and  $R$  is the inner radius of the channel. Since the pipette head itself contains different inner radii also different from the tube's radius, we can consider them as resistances

in series, so that the total hydraulic resistance is a sum of each segment's value. The tubes usually have a length of approximately 10cm and they all have an inner radius of 0.375mm, while the pipette heads have an effective length of 2cm and a radius that goes from 0.15mm to 0.8mm. The effective length is measured as the total length of the component minus the amount of length occupied by the tube.

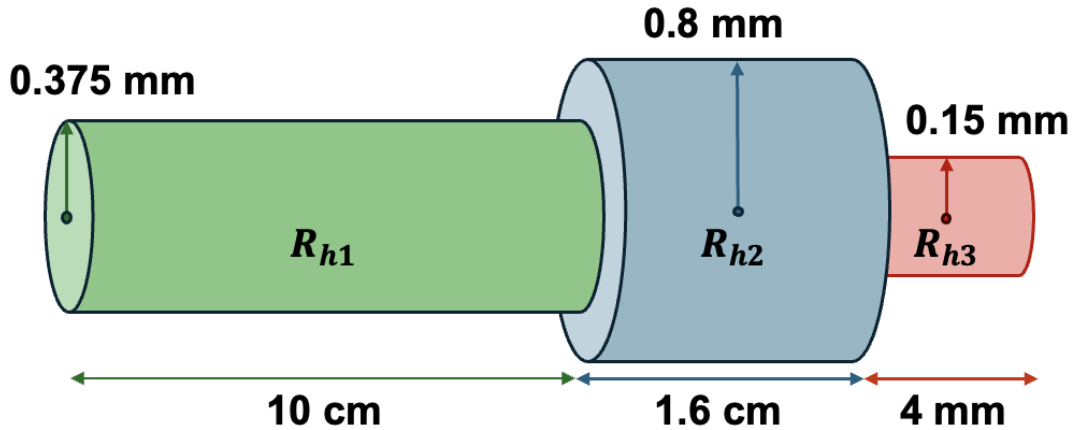


Figure 9.2: Approximation of the hydraulic resistances in the tube-pipette head system with quoted lengths and radii: the green cylinder is the tube, the blue cylinder is the first part of the pipette head, the red cylinder is the end of the pipette head.

To approximate our calculations we will consider what can be seen in Figure 9.2: the last 4mm of the pipette head has a radius of 0.15mm and the rest 1.6cm, closer to the tube, has a radius of 0.8mm. We can now find each individual hydraulic resistance and the consequent total one.

$$\begin{aligned}
 R_{h1} &= 1.29 \times 10^{10} \frac{Pa \cdot s}{m^3} \\
 R_{h2} &= 9.94 \times 10^7 \frac{Pa \cdot s}{m^3} \\
 R_{h3} &= 2.01 \times 10^{10} \frac{Pa \cdot s}{m^3} \\
 R_{tot} &= R_{h1} + R_{h2} + R_{h3} = 3.31 \times 10^{10} \frac{Pa \cdot s}{m^3}
 \end{aligned} \tag{9.2}$$

This total hydraulic resistance  $R_{tot}$  has a relatively low value, in fact if we check through the Hagen–Poiseuille equation we get:

$$\Delta P = R_{tot}Q = 1.16 \text{ Pa}$$

$$\text{with } R_{tot} = 3.31 \times 10^{10} \frac{\text{Pa} \cdot \text{s}}{\text{m}^3} \text{ and } Q = 3.5 \times 10^{-11} \frac{\text{m}^3}{\text{s}} \quad (9.3)$$

which is an extremely low pressure difference for our system. For this reason this cannot be the cause of the malfunctioning because going through the porous membrane must be more unfavourable in terms of pressure difference, even if there was only the tube.

For what concerns point 3, we decided to try a new sealing technique that consisted in changing the order in which we placed the previous components.

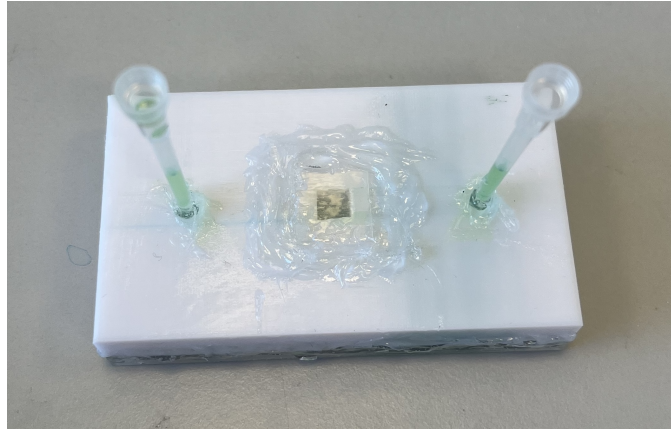
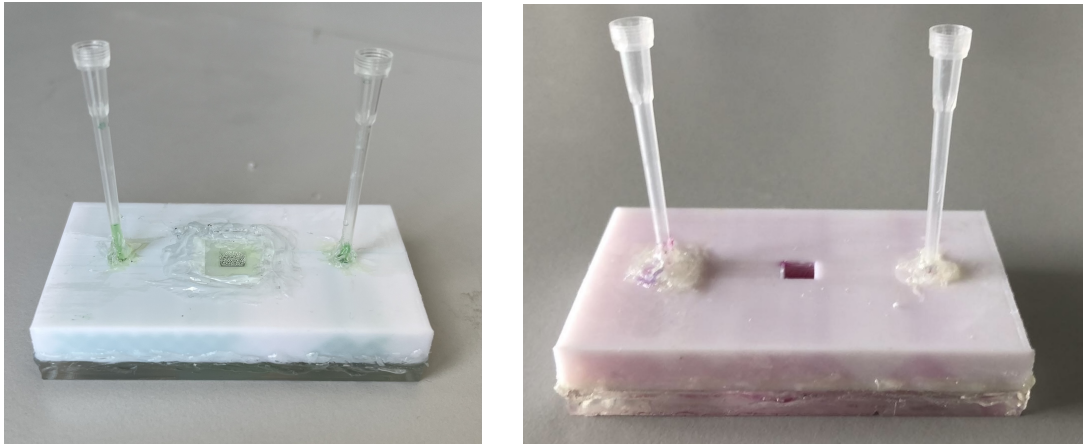


Figure 9.3: New sealing technique: we place a piece of parafilm slightly bigger than hole on top of it, we stick some tape over it and then seal it with silicone on the edges.

We can see the new process explained in Figure 9.3: by placing the parafilm on top of the hole we would shield the tape from getting too much liquid and losing adhesion, the tape would keep it in place and the silicone would completely seal the two pieces in place. After some tests this technique seems to be holding great and will be used again in the future when needed, but most importantly we noticed an important detail, that can already be observed in Figure 9.3 on the right side of the device.

After changing the softer blue dye with a stronger green one we were able to clearly see, as in Figure 9.4a, that the 3D printed piece of the device was absorbing the water. This happened throughout an entire night where the device was fed water at a flow rate of  $2.1 \mu\text{L}/\text{min}$ , the bottle had collected no fluid, but there were also no leakages. What we previously dismissed as just staining on the surface due to external contact with the dyed liquid, turned out to be actual water going through the internal structure of the component. After this realization we were able to see



(a) Absorbed green dyed water inside of the 3D printed piece of the device.

(b) Absorbed red medium inside of the 3D printed piece of the device.

Figure 9.4: The 3D printed piece absorbs any liquid going through the device, either through the inlet and outlet holes or the chamber.

that the same had happened with the devices at KU that now appeared red also on the sides (see Figure 9.4b); in fact they had ended up expelling no medium in the waste bottle. The reason for this might be some defects on the surface of the 3D printed piece, especially in the critical features like the inlet and outlet holes or in the central chamber, since those seem to be the most affected regions. As a consequence, due to the low infill density, liquid may infiltrate through the defects and fill up the internal structure, causing the chamber to fill up more than it should with the fluid coming from the inside without any control. The print defects may be due to a resolution problem of the nozzle or to how the supports are removed after the print, which in the case of this design would only concern the main chamber due to how these supports are built in the printing process (explained previously in Chapter 6). We finally proposed one last solution to avoid this absorption problem: fabricating also the top piece through laser cut PMMA.

### 9.3 Fully PMMA device

While fabricating these pieces we have to take into consideration that since the laser cutter will enlarge a structure by melting around it as it is cutting through it, we need to downsize the inlet and outlet diameters from 1.9mm to 1.8mm, otherwise the pipette head would be too loose and risk detaching. The center chamber is kept as a 5mm×5mm square, since its dimension is less critical. The piece of PMMA was 5mm thick which is good enough for us now, even if the previous 3D printed one was 8mm high, but in the future it will be something to keep under control

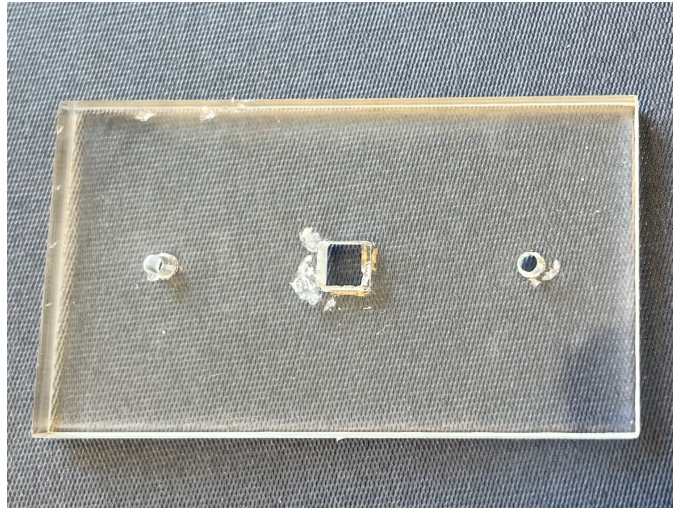


Figure 9.5: Example of laser damage caused by too many cuts at a too high laser power on the bottom of a piece of PMMA, especially close to the central square.

should we need higher walls. We also need to find a balance between cutting speed, power and number of times we cut not to damage the piece as it happened with the device in Figure 9.5, otherwise this could cause leakages or incorrect adhesion. For this reason we summarised the settings chosen for each part of the design in Table 9.1, where we can see that the square chamber has one less pass and is faster in order to cause less damage. The outer rectangle and the inlet and outlet instead were found to require that same settings.

Design element	Speed (mm/s)	Min/Max power (%)	N° of cuts
Inlet/Outlet	50	80	8
Square chamber	65	80	7
Outer rectangle	50	80	8

Table 9.1: Laser power, speed and cuts repetitions settings for the new PMMA piece for the top element of the device.

By using these values we get optimal results for the piece and we make sure to use the smoother side for the tape bonding. The rest of the fabrication steps follow those in Chapter 7, to better compare the devices, as well as all the sealing steps for precaution. The great thing about having a fully transparent device is that we will be able to follow the dyed water throughout the channels and closely observe possible defects. We set the system up similarly to how it was at KU with the syringe pump (Figure 8.3a), but we will now only be testing two simple design devices (one with the pillar in the main chamber and one without) separately, so

that we do not have to use the flow splitters which were found to be not perfect and consistent enough for troubleshooting. The two syringes would pump green dyed water in the devices at  $8.4\mu\text{L}/\text{min}$ , since time was running out and we wanted to be sure that we would get visible results overnight. We placed them in a box and on top of some paper towel so that we would have been able to easily observe leakages that may have happened during the night and prevent them from staining the lab table.

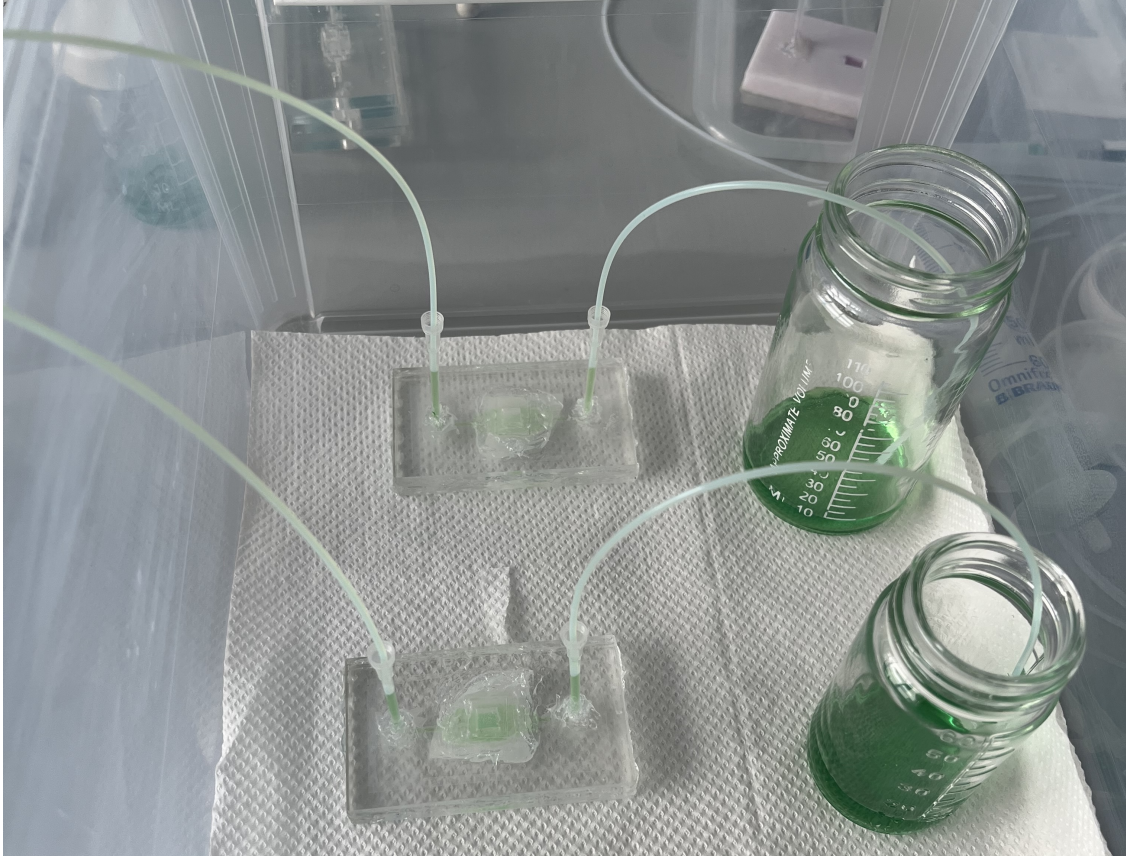
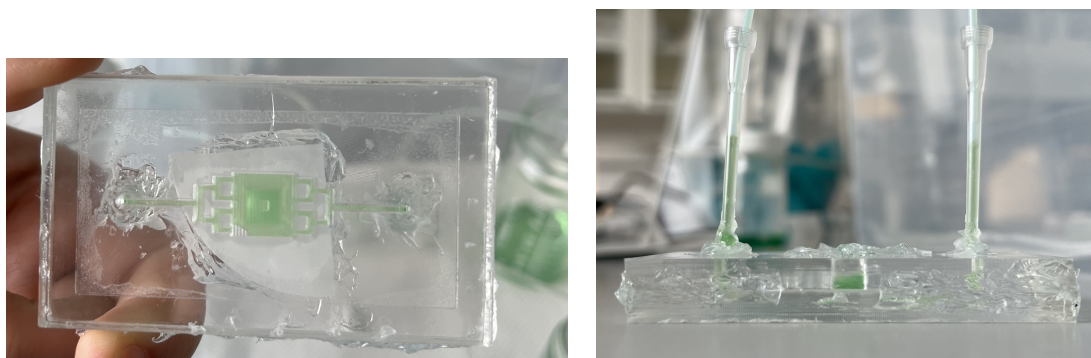


Figure 9.6: Final successful test with the device fully made of PMMA, on top is the normal design and below is the one with the pillar in the main chamber. We can see the inlet tubes coming directly from the two syringes, one per device, and the outlet tubes ending up in a collection bottle.

In Figure 9.6 we can observe the end of our final experiment that lasted approximately 18 hours and, as shown in the picture, worked perfectly and as expected: both the bottles collected almost 10 mL of Milli-Q water as they should have ( $Vol = Q \cdot time = 8.4\mu\text{L}/\text{min} \cdot 18h \cdot 60\text{min}/h = 9.072\text{mL}$ ), and we can see no leakages on the paper towel. This means that all of the precautions taken for sealing the devices on the sides with silicone and on the top as we showed in Figure 9.3 are

not actually needed when the device works as expected. However we should not forget that in our case some chamber sealing was required due to the usage of the incubator.



(a) Bottom channel after the final test.

(b) Chamber filling after the final test.

Figure 9.7: Details of the final test: bottom channel distribution of the water and main chamber filling seen from the side.

Looking at Figure 9.7a we can see how the channel worked almost perfectly, with only the bottom left corner of the chamber not filled correctly, probably due to surface tension. However this can be helped with slightly higher flow rates in the beginning to help spreading the liquid homogeneously and then bringing it back to the correct value, since we know that higher flow rates are not a problem. This was also confirmed analysing the liquid height in the main chamber by removing some of the silicone on the side: in Figure 9.7b it can be observed how the liquid did not rise up in the chamber as before and did not even reach half of the height of the chamber. Keep in mind that the picture was taken with the easiest perspective to observe the liquid on camera and in reality it was lower than it seems, also showing a clear meniscus distribution. The height was approximately the same for the two devices, but the pillar one was slightly higher probably due to the fact that the pillar itself takes up some of the available volume in the bottom channel chamber. However since they ended up working more or less the same this promptly confirms that this pillar design is not needed anymore. More importantly we also confirmed that ramping up the flow rate would not increase the height of the liquid in the chamber and, with a  $100\mu\text{L}/\text{min}$  flow rate, nothing changed, confirming what we said previously about establishing an initial flow and then settling to the correct one after the chamber was perfused completely. With these last two pictures and results we can conclude that leakages from the sides were probably due to the surface roughness of the 3D printed piece, which caused the tape to not adhere correctly; while the leakage from the middle chamber was probably due to the absorbed liquid travelling in the piece and filling it up through the surface defects.

# Chapter 10

## Conclusions

It was argued throughout this thesis that using a dynamic medium in organ-on-a-chip systems, through the introduction of flow in the reservoirs, is the next natural step to the devices present nowadays in order to combat the lack of vascularization and prevent the formation of necrotic cores in the long term. It was demonstrated via multiple COMSOL simulations and a variety of designs, which led to approximated, yet promising results. Most notably we have shown that such design choice will lead to the stabilisation of the average nutrients concentration in the organoids and quite high core concentrations, especially through the help of tubes, needles and multiple reservoirs. Through the fabrication process we have rigorously followed the planned methods, both with laser cutting and 3D printing, after some initial characterisation and tests, progressively reaching our final models. In particular we have shown the step by step assembly of the device, making sure to properly explain each choice: the resolution and roughness were at acceptable levels for the bottom channel, but not quite for the 3D printed piece; for the bonding of the two pieces, double sided tape ended up being a great choice by itself, especially for lending itself to laser ablation; the flow splitters and the tubes posed some obstacles that were ingeniously overcome, as well as the need for a chamber seal and sterilisation. The first tests conducted were admittedly rushed and not as thorough as we would have needed, only because the time window in which we could do the experimental tests was closing in more and more as the organoids would not survive long enough to wait for us. This led to us attributing the leakages we observed and the fact that water was rising from the main chamber to either a sealing mistake on our side or a lack of adhesion of the tape, which lastly brought us to overdo the sealing on each device to overcompensate and finally to the main oversight. From the troubleshooting after the failed test at KU with the live organoids, it emerged that the main, and probably only, problem of our devices was the 3D printed piece absorbing all of the water and mishandling the flow, causing it to not go through the bottom channel and spill either outside of the whole device or inside the chamber. This was confirmed by a final and successful test with two fully PMMA devices, where none

of the previous issues arose, instead they ran smoothly and exactly as expected. Even though this was discovered right at the end of our experiments and we did not have the chance of testing it with real live organoids as we wanted to initially, it is still relevant to note that despite the many drawbacks we were able to find our footing again and get to the bottom of the problem. This project challenged the existing designs and aimed at building something new and potentially better for the landscape of organ-on-a-chip systems, especially for brain organoids, and finally reports many auspicious findings. This thesis is a strong foundation for the claims and objectives we made in the beginning and it is a great starting point for future work, since from this point onwards the research has a lot of data and practical information.

## Part V

# Project plan and self-evaluation



---

## Project plan

Organ on chip technologies have been gaining a lot of attention as they allow research on how organs work and respond to external stimuli, i.e. chemicals, mechanical or electrical forces, radiation etc, in vitro. In terms of personalised medicine, this is one of the most promising technologies, as it allows the testing of e.g. several drugs on the patient's cells before administering to the patient, thus increasing the chances of success. However, in vitro devices do not necessarily have the functionality of the natural environment. It is e.g. not easy to grow organs while maintaining blood flow through the tissue, or deliver nutrients to the tissue in the way as in the body. Microfluidic devices offer several possibilities in this respect. Nutrients can be delivered to the tissues/organs by diffusion, mimicking the blood supply, and maintaining the cell communication by not removing signaling molecules by convective forces. In this project the student is going to design and fabricate a system able to maintain and/or grow brain organoids in-vitro. The organoids will be initially grown in the lab and moved to the device and their growth and survival will be monitored by standard methods and compared to organoids grown with standard state-of-the-art systems. The learning objectives of the project will be to: 1) Identify current lab-on-a-chip solution for brain organoids and their advantages and disadvantages through a literature review 2) Design and fabricate a system that can host a brain organoid and provide nutrients to it 3) Investigate how system parameters affect the survival and function of the organoids 4) Learn how to work in a highly interdisciplinary research area 5) Become familiar with different soft fabrication techniques, e.g. laser ablation, pdms casting and 3D printing.

## Self-evaluation

During the project I was able to find interesting and relevant literature and I came up with good ideas for the designs to try and simulate. Through the help of my group supervisors and their expertise, I realised many simulations that were able to approximately describe the operation of my future devices. The results were promising and predicted a system able to keep the organoids at a high constant average concentration for as long as the flow was applied. Consequently I fabricated the devices with laser cutting and 3D printing, after a characterisation analysis I carried on with the stylus profilometer and the first prints. However when the systems were put to the test at KU some problems started emerging that had not been seen in the previous tests. After some days of troubleshooting I was able to find the main cause of the failure: the 3D printed piece was absorbing the majority of the liquids and the rest was pushed out through the main chamber, causing leakages and an overall system malfunction. Thankfully I still managed to fabricate two last devices completely made of acrylic that finally ended up working as expected in the beginning, and took less time to manufacture. Truthfully if we

---

had had more time to test the devices before inserting the organoids, we probably would have been able to find this design flaw a lot earlier. Alas, due to external time constraints, we managed to do our best and overall get an interesting overview of different aspects to take into consideration in the future, in order to avoid the many obstacles that arose during this thesis. I am very proud of my work, including both the victories and the hurdles met along the way. I am positive that this project can lead to new discoveries and that my contribution was just the beginning.

# Bibliography

- [1] S. Y. Tan, X. Feng, L. K. W. Cheng, A. R. Wu, *Vascularised human brain organoid on-chip*, Lab on a chip, **2023**, 23, 2693-2709
- [2] T. Lokai, B. Albin, K. Qubbaj, A. P. Tiwari, P. Adhikari, I. H. Yang, *A review on current brain organoid technologies from a biomedical engineering perspective*, Experimental Neurology, **2023**, 367, 114461
- [3] X. Qian, H. Song, G. Ming, *Brain organoids: advances, applications and challenges*, The Company of Biologists Ltd | Development, **2019**, 146
- [4] *Brain organoid modeling to study neural development and disease*, BioLamina, **2022**, URL: <https://biolamina.com/wp-content/uploads/2022/06/AN-019-01-Brain-organoids-with-Biosilk-Biolaminin.pdf>
- [5] H. Castiglione, P.-A. Vigneron, C. Baquerre, F. Yates, J. Rontard, T. Honegger, *Human Brain Organoids-on-Chip: Advances, Challenges, and Perspectives for Preclinical Applications*, Pharmaceutics, **2022**, 14, 2301.
- [6] A.-N. Cho, Y. Jin, Y. An, J. Kim, Y. S. Choi, J. S. Lee, J. Kim, W.-Y. Choi, D.-J. Koo, W. Yu, G.-E. Chang, D.-Y. Kim, S.-H. Jo, J. Kim, S.-Y. Kim, Y.-G. Kim, J. Y. Kim, N. Choi, E. Cheong, Y.-J. Kim, H.-S. Je, H.-C Kang, S.-W. Cho, *Microfluidic device with brain extracellular matrix promotes structural and functional maturation of human brain organoids*, Nature Communications, **2021**, 12:4730.
- [7] Z. Ao, H. Cai, D. J. Havert, Z. Wu, Z. Gong, J. M. Beggs, K. Mackie, F. Guo, *One-Stop Microfluidic Assembly of Human Brain Organoids To Model Prenatal Cannabis Exposure*, Analytical Chemistry, **2020**, 92, 4630-4638.
- [8] *How it Works: Co2 Laser Cutters*, AP Lazer, **2020**, URL: <https://aplazer.com/how-it-works-co2-laser-cutters/#>
- [9] *All You Need to Know About PLA for 3D Printing*, 3Dnatives, **2023**, URL: <https://www.3dnatives.com/en/pla-3d-printing-guide-190820194/>
- [10] C. Nicholson, *Sheet and void porous media models for brain interstitial space*, The Royal Society Publishing, **2023**, 20, 205
- [11] M. Ermis, S. Calamak, G. C. Kocal, S. Guven, N. G. Durmus, I. Rizvi, T. Hasan, N. Hasirci, V. Hasirci, U. Demirci, *Handbook of Nanomaterials for Cancer Theranostics, Chapter 15 - Hydrogels as a New Platform to Recapitulate the Tumor Microenvironment*, Elsevier, **2018**, 463-494

- [12] A. Friedrichs, J. Bohnet, V. Korger, S. Adler, M. Schubert-Zsilavec, M. Abdel-Tawab, *Dose accuracy and injection force of different insulin glargine pens*, Journal of Diabetes Science and Technology, **2013**, 7(5):1346-1353.
- [13] M. Dimaki, P. Shah, D. Kwasny, J. Moresco, W. E. Svendsen, *Microfluidic Systems for Cell Growth and Cell Migration Studies*, COMSOL Conference in Stuttgart, **2011**.
- [14] Y. Yang, W. Zhan *Role of Tissue Hydraulic Permeability in Convection-Enhanced Delivery of Nanoparticle-Encapsulated Chemotherapy Drugs to Brain Tumour*, Pharmaceutical Research, **2022**, 39:877–892.
- [15] *BrainPhys™ Neuronal Medium N2-A & SM1 Kit*, Stemcell Technologies, URL: <https://www.stemcell.com/brainphys-neuronal-medium-n2-a-sm1-kit.html>
- [16] L. F. de Oliveira, D. M. Filho, B. L. Marques, G. F. Maciel, R. C. Parreira, J. R. do Carmo Neto, P. E. F. Da Silva, R. O. Guerra, M. V. da Silva, H. da Costa Santiago, A. Birbrair, A. H. Kihara, V. J. Dias da Silva, T. Glaser, R. R. Resende, H. Ulrich, *Organoids as a novel tool in modelling infectious diseases*, Seminars in Cell and Developmental Biology, **2023**, 144:87-96.
- [17] G. Saorin, I. Caligiuri, F. Rizzolio, *Microfluidic organoids-on-a-chip: The future of human models*, Seminars in Cell and Developmental Biology, **2023**, 144:41-54.
- [18] D. Patel, S. Shetty, C. Acha, I. E. Morales Pantoja, A. Zhao, D. George, D. H. Gracias, *Microinstrumentation for Brain Organoids*, Advanced Healthcare Materials, **2024**, 2302456.
- [19] Y. Zhu, X. Zhang, L. Sun, Y. Wang, Y. Zhao, *Engineering Human Brain Assembloids by Microfluidics*, Advanced Materials, **2023**, 35, 2210083.
- [20] T. K. Matsui, Y. Tsuru, K. Hasegawa, K. Kuwako, *Vascularization of human brain organoids*, Stem Cells, **2021**, 39:1017-1024.
- [21] F. Yu, W. Hunziker, D. Choudhury, *Engineering Microfluidic Organoid-on-a-Chip Platforms*, Micromachines, **2019**, 10, 165.